2008

Bioluminescence-Based High Precision Bacterial Growth Rate Measurements and Their Potential Application in Quantifying Deleterious Effects of High Mutation Rates

Sri Ram

BIOLUMINESCENCE-BASED HIGH PRECISION BACTERIAL GROWTH RATE MEASUREMENTS AND THEIR POTENTIAL APPLICATION IN QUANTIFYING DELETERIOUS EFFECTS OF HIGH MUTATION RATES

A Thesis Presented to the Faculty of

The Rockefeller University

in Partial Fulfillment of the Requirements for

The degree of Doctor of Philosophy

by

Sri Ram

June 2008

BIOLUMINESCENCE-BASED HIGH PRECISION BACTERIAL GROWTH RATE MEASUREMENTS AND THEIR POTENTIAL APPLICATION IN QUANTIFYING DELETERIOUS EFFECTS OF HIGH MUTATION RATES

Sri Ram, Ph. D.
The Rockefeller University 2008

The genomic mutation rate of wild-type *Escherichia coli* is 3×10^{-3} per generation, a value that is shared by many DNA-based microbes and viruses. A majority of clinical isolates of *E. coli* also have a mutation rate that is close to the wild-type value. These findings raise the possibility that the observed mutation rate is constrained by some universal evolutionary forces. In many laboratory settings, however, strains with high mutation rate (mutator strains) have been shown to outcompete otherwise isogenic wild-type cells. These results have been explained by positing that mutators offer a short-term benefit in the form of increased probability of generation of beneficial mutations. Yet, given that a majority of non-neutral mutations are deleterious, there is a long-term cost associated with high mutation rates. This thesis explores the idea that one form of the long-term cost involves the fixation of deleterious mutations when rare beneficial mutations sweep through large asexual populations. Our simulations suggest that this is indeed the case at high mutation rates (~200-fold higher than the wild-type mutation rate), but the deleterious effects are expected to be quite small (~1%). Detection of such effects requires the measurement of mean fitness of large populations with high precision and high frequency. Towards this end, we constructed an apparatus that combines bioluminescence based growth rate measurements with techniques for long-term microbial culture for recording of growth rate dynamics of luminescent *Escherichia coli*. After a comparison of several culture media, we found that the reproducibility of growth

rate measurements is the best in LB. In LB, growth rates can be measured every 65 min (~3.5 generations) and with an overall precision of ~2.7%. Instrumental errors are estimated to contribute only 0.3% to the overall precision. We show that the apparatus can be used to detect small changes in growth rates by measuring the sensitivity of growth rate to temperature changes as small as 0.3°C. We also show that precision can be maintained in long-term measurements of growth rates. We are now poised to evaluate the deleterious effects of high mutation rates in our apparatus.

To Amma, Appa, Rajesh, Becky, and Leela

for their love and support during my Ph.D.

Acknowledgements

I would like to begin by thanking the people who were instrumental in making my admission to The Rockefeller University possible. Without timely help and advice from Drs. R. Gurunath, Andrej Šali, and John Kuriyan, I would never have been in the Rockefeller graduate program.

At Rockefeller, I have had the privilege of pursuing my thesis under the guidance of Dr. Stanislas Leibler. It is a telling comment on my naiveté and ignorance at the time of joining Rockefeller that I was not aware of Stan's research. Indeed, had he not spoken about his research in the "Seminars in Modern Biology" course, I might never have spoken to him about joining his lab. Yet, at the completion of my thesis, I cannot imagine a better advisor to facilitate my transition from computer science to biology. I am particularly grateful to Stan for the broad training that I have received under his guidance; I was exposed to a wide range of ideas during my graduate education and it is unlikely that I could have received the same exposure in any other lab. Stan's approach to biology has always been creative, imaginative, and insightful and this reflects in the open-mindedness and the diversity that characterizes our lab. Stan introduced me to the phenomenon of mutators, and I have been fascinated by the problem ever since. He gave me the freedom to pursue the problem independently and the independence has helped me mature as a scientist. Thanks, Stan, for your support and patience. If I ever head a lab, I will strive to create the intellectual environment that existed in the Leibler lab.

Along with the freedom that I enjoyed in the lab, I was also fortunate to have a very supportive thesis committee. I am deeply indebted to Drs. Brian Chait, Andrew Murray, and Shai Shaham for their advice, feedback, and encouragement over the course of my Ph.D. I do not think that I could have performed the research that I did without their appreciation and understanding. I would also like to express my gratitude to Dr. Saeed Tavazoie, who served as the external examiner for my thesis defense.

Among the many privileges of working in the Leibler lab is that one gets to interact with an immensely talented set of colleagues with a diverse background. I am especially grateful to Remy Chait and Jack Merrin for introducing me to microfluidic fabrication and helping me with various machining projects, and to John Chuang, Giovanni Sena, Calin Guet and Doeke Hekstra for teaching me whatever little molecular biology that I know. I enjoyed many fruitful discussions with Doeke, Edo Kussel, Clément Nizak, and Wenying Shou, and their insights and advice proved very useful. I also wish to thank Wenying Shou and José Vilar for giving me the opportunity to contribute to their investigation of synthetic cooperation in yeast.

In the last seven years, I have experienced several highs and lows, both within the lab and outside. It was invaluable to have the love and support of my friends and family in helping me through this phase of my life. I dedicate this thesis to my parents, my brother Rajesh, his wife Becky and my delightful little niece, Leela. My parents have always supported my education, although I am not sure what they would have thought if I decided to do a second Ph.D. like my brother. While they were understandably anxious

about my well-being and the progress of my thesis, they never let their concerns weigh on me. It was always reassuring to talk to them on the phone, and they were very understanding when I had to put off my trips to India because of visa issues. Amma, appa, I wish I could have made more trips to India. Rajesh and Becky were only a short (and thanks to Messrs Fung Wah and company, inexpensive) bus ride away and ever willing to provide me a break from New York when I needed one. I am also grateful to Becky's parents who invited me to their wonderful home in Concord for several Thanksgiving and Christmas dinners, helping me avoid the desolate environs of The Rockefeller University on those occasions.

If I had to make a list of people whose support I called upon the most during my Ph.D., Wenying and Revati would feature prominently. They often had the unfortunate task of cheering me up during my periods of despondency. Thanks to both of you for your patience and perseverance. To Wenying, I owe my introduction to vegetarian shaved noodles and flavored ice at Flushing, and the moniker of "Indian vegetarian colleague" in her restaurant reviews. I hold Revati responsible for the misplaced belief and pride in my modest cooking skills.

I have been very fortunate to have several welcome distractions outside of the lab, which also served as occasional reminders for the passion and enthusiasm with which science should be performed. Among the many things that I would miss when I leave New York City would be the weekly cricket matches in the Cornell gym. Guys, thanks for the endless hours of entertainment, the free dinners, and for all the health benefits that

resulted from the release of endorphins. For their company and for several moments of pure joy, I wish to thank my fellow IRFCA railfans in the New York region, especially Jaimin, who was ever willing to drive hundreds of miles on our railfanning quests, Jay and Anand, who hosted a couple of railfan meets, and Bharat and John who were always willing to share their knowledge of Indian and American railway history. Likewise, life would have been quite uneventful without discussions on the relative merits of commas, em dashes, and colons at the monthly meetings of *Natural Selections*. To all current and former members of the editorial board, thanks for all the fun. Finally, I also wish to thank Mary Abraham for introducing me to many cultural treasures of New York City; I would have been too lazy to explore them myself.

One of the little-known benefits of doing experimental science is that it allows one to use lab work as an excuse to wriggle out of any event. To my friends from IIT living in Jersey City who have become accustomed to hearing "I'm busy with lab work" from me, I offer my sincerest apologies. Nitin, Saurav, and Gaurav, this thesis is proof that I wasn't always lying! Thank you so much for being so understanding of my lab commitments, and for all those ski trips.

In the end, I would like to thank Kristen Cullen and Marta Delgado at the Dean's Office and Maria Lazzaro at the Office of Immigration and Academic Appointments for all their assistance. Their help made it easy to deal with the peculiar situations that arose with me having just one name.

Table of Contents

List of Figures

List of Tables

Chapter 1. Introduction

The population geneticist's view of evolution is one of population variation in traits being shaped by the forces of natural selection and genetic drift. This view has been developed through over 100 years of work in evolutionary biology, starting from the publication of Charles Darwin's classic book *On the Origin of Species by Means of Natural Selection* in 1859 (Darwin, 1859), the development of the mathematical theory of population genetics by Sewall Wright, J. B. S. Haldane, and R. A. Fisher (Fisher, 1930), and the formulation of the neutral theory of molecular evolution by Motoo Kimura (Kimura, 1983). Notwithstanding debates over the relative importance of selection and drift in shaping natural populations, the presence of genetic variation is essential for either mechanism to act.

Population variation in traits can be generated through various mechanisms including ecological ones such as migration and genetic ones such as spontaneous mutations, recombination, and the action of certain viruses and mobile genetic elements such as transposons. Spontaneous mutations play a fundamental role in the generation of novel variations and have been referred to as "engines to drive evolution" (Maki, 2002). While most of these variations would be deleterious, rare beneficial mutations facilitate the process of adaptation to new environments. This is especially true in pure asexual populations that grow by clonal expansion, since other means of generating genetic variation are essentially absent.

Given the importance of spontaneous mutations, it is natural to ask whether the rate of such mutations has any special significance. What are the constraints on spontaneous mutation rates? Can the value mutation rates in natural populations tell us something about these constraints? In this thesis, I explore the hypothesis that the process of adaptation itself might impose a constraint on the value of the mutation rate. Specifically, I ask whether adaptive processes involving rare beneficial mutations with substantial fitness advantage can result in the fixation of linked deleterious mutations. Furthermore, would the combined effects of the fixation of such deleterious mutations over long term, present an evolutionary constraint against high mutation rates?

1.1 Perspectives on Mutation Rates

1.1.1 Quantitative biology of mutation rates

The mutation rate of wild-type E. coli strains is estimated to be around 3×10^{-3} per genome per genome replication (Drake, 1991). Is this value typical, small or large? While a theoretical answer is still lacking, insights into this question can be obtained from the following comparisons:

(1) Genomic mutation rate of E. coli compared to other species: Drake and colleagues have shown that the genomic mutation rate of many DNA-based microbes and viruses, including *E. coli*, is the same and close to 3.4×10^{-3} per genomic replication (Drake *et al.*, 1998; Drake, 1999). The organisms they surveyed had genomic sizes ranging from 6.4 kilobases (Bacteriophage M13) to 42 Megabases (*Neurospora crassa*). This remarkable result suggests that the mutation rate of E. coli is typical. Furthermore, one can posit that the evolutionary

forces that shape mutation rates are fairly universal, i.e., not restricted to a particular organism or ecological niche.

(2) Distribution of mutation rates in clinical isolates of E. coli: Several groups have surveyed the distribution of mutation rates in collections of E. coli strains (Hall and Henderson-Begg, 2006). Baquero *et al.* found that the distribution of the mutation rates had a strong mode around the wild-type value (Baquero et al., 2004). These strains, the so-called normomutable strains, comprised around 60% of the collection. They also found that around 15% of the strains had a mutation rate which was lower than the modal value (hypomutators). The overwhelming majority of the hypermutating strains have less than 10-fold elevation in mutation rate and are classified as weak mutators (Baquero et al., 2004; Matic et al., 1997). Strong mutators are found with a frequency of around 1-2% (Baquero et al., 2004; LeClerc et al., 1996; Matic et al., 1997). Thus, one finds that a majority of isolates of E. coli have a mutation rate close to its typical value.

(3) Competition between high mutation rate and wild-type strains: Competition experiments between high mutating strains of E. coli (mutators) and otherwise isogenic wild-type strains have demonstrated that mutator strains have an advantage, at least in the short term (see section 1.3.2). On the other hand, theoretical work suggests that the eventual outcome of such experiments should be the reduction of mutator strains to a minority fraction (see section 1.3.3). Nevertheless, available experimental data suggests that in the absence of severe

population bottlenecks, strong mutator strains can be grown for thousands of generations without any detectable loss in fitness (see section 1.3.2).

The three comparisons outlines above show that the answer to even such a basic question as the typical value of mutation rate is nuanced. While the majority of natural isolates have a mutation rate close to the typical value, several laboratory experiments have demonstrated scenarios where strong mutators have an advantage. How can we reconcile these laboratory experiments with the relative paucity of strong mutators in nature? Is there a cost to high mutation rates that existing laboratory experiments have not been able to detect?

1.1.2 Mutation rate and adaptation to fluctuating environments

Mutations help in generating and maintaining genetic diversity in a population. In a constant environment, genetic diversity reduces mean fitness and therefore mutation rates should evolve to zero or to the lowest value permitted by physiological costs. In fluctuating environments, however, a non-zero mutation rate may have long-term adaptive value. The notion that the mutation rate may be selected to generate an optimal amount of genetic diversity is often referred to as second-order selection (Tenaillon et al., 2001). As such, second-order selection arguments are similar to ones examining the role of stochastic phenotypic switching as an adaptive strategy to counter fluctuating environmental conditions (Kussell and Leibler, 2005). Mutation can be viewed as a stochastic phenotypic switch, albeit with very low (and typically asymmetric) switching rate.

The idea that mutation rates can be optimized to maximize long-term fitness in fluctuating environments was first considered by Kimura (Kimura, 1967), who found, in essence, that the optimal mutation rate was equal to the average rate (per generation) at which new (fitter) alleles are substituted in the genome as a result of change of the environment. A similar result was obtained by Leigh (Leigh, 1970). Palmer and Lipsitch extended Leigh's analysis to include the effects of unconditionally deleterious mutations (mutations which are deleterious in all environments) and finite population size and showed that a slightly modified version of the Leigh's (and Kimura's) result was valid for a wide parameter range (Palmer and Lipsitch, 2006). On the other hand, André and Godelle have argued that in small populations, the optimal mutation rate as computed by Leigh's method does not represent a stable value and that rare populations with a mutation rate different from the optimal one can invade the population (André and Godelle, 2006).

That high mutation rates can be an adaptive strategy in fluctuating environments is best illustrated by the existence of "contingency loci," which are highly mutable loci in the genomes of pathogenic microorganisms and which play a role in evading host immune responses (Moxon et al., 1994). What is the disadvantage of having a global high mutation rate as opposed to restricting the high mutation rate to a few "contingency loci?" It has been argued that the restricted high mutation rate enables essential "housekeeping" genes to be replicated with greater fidelity and minimizes the acquisition of deleterious mutations. If that is the case, what are the fitness consequences of these deleterious mutations in a global high mutation rate strategy?

1.1.3 Clinical perspective

The observation of mutator strains of bacteria among clinical isolates has prompted questions regarding whether the evolution of high mutation rates has a role to play in the emergence of antibiotic resistance and whether mutators pose a threat to failure of antibiotic regimens (Blázquez, 2003; Chopra et al., 2003). Mutator strains have been shown to develop increased resistance to commonly used antibiotics (Miller et al., 2004; Örlén and Hughes, 2006). Weak hypermutators among natural isolates of *E.coli* also show an increased propensity towards multidrug resistance (Denamur et al., 2005). Such weak mutators are also overrepresented in *E. coli* isolates with extended-spectrum β-lactamases (Baquero et al., 2005). These findings, although mostly associative, suggest that high mutation rates among bacterial populations might be of consequence in clinical settings.

Nevertheless, the fact remains that there is only limited evidence demonstrating a direct link between mutators and the evolution of drug resistance (Blázquez, 2003). There are also doubts as to whether the phenomenon of mutators contributing to drug resistance is a general one or restricted to a few pathogens (Blázquez, 2003). It remains to be seen whether evolution of hypermutation is an epiphenomenon with regards to clinical progression of disease and potential therapeutic strategies.

1.2 Evolution of Asexual Populations

1.2.1 Theoretical work

In this section, I review some of the theoretical work on the evolution of asexual populations. Typically, these models study a population of size N with a beneficial mutation rate U_b and a deleterious mutation rate U_d. In most models, every beneficial mutation has a selection coefficient of s_b and every deleterious mutation has a selection coefficient of s_d. In some cases, selection coefficients of beneficial and deleterious mutations are drawn from some pre-specified distribution. Another assumption that is often made is that epistasis is absent, so that the relative fitness of a genotype with N_b beneficial mutations and N_d deleterious mutations would be $(1 + s_b)^{N_b}(1 - s_d)^{N_d}$.

When beneficial mutations are absent, large asexual populations ($N \to \infty$) achieve a mutation-selection equilibrium. For the particular case with deleterious mutations having equal fitness effects, Haigh showed that at equilibrium, the fraction (f_{N_d}) of individuals with N_d deleterious mutations follows a Poisson distribution with mean U_d/s_d (Haigh, 1978). In this case, the mean fitness of the population at equilibrium is e^{-U_d} and is independent of the fitness effects of deleterious mutations (s_d). For any finite N, however, there is steady accumulation of deleterious mutations, an effect known as Muller's ratchet. This effect is most pronounced for small populations and early theoretical work suggested that the speed of the ratchet depended primarily on the number of individuals with the least number of deleterious mutations (Haigh, 1978). More recent work, based on diffusion approximation to the ratchet, has shown that the rate of the ratchet can vary over an order of magnitude even if the expected number of

individuals with the least number of deleterious mutations is kept fixed (Gordo and Charlesworth, 2000).

The presence of beneficial mutations makes theoretical analysis more complex. When population size or beneficial mutation rate are small, beneficial mutations survive genetic drift and get fixed in the population independently, i.e., before other beneficial mutants are generated. In this regime, the rate of adaptation (rate of increase of population mean fitness) varies linearly with both population size and beneficial mutation rate (Desai and Fisher, 2007). When populations are large or beneficial mutations are not rare, the accumulation of beneficial mutations is impeded by two factors: (a) clonal interference, the possibility that the fixation of a particular beneficial mutation is prevented by the establishment of a clone with a more fit beneficial mutation (Gerrish and Lenski, 1998), and (b) the possibility that a lineage can acquire multiple beneficial mutations before any beneficial mutation gets fixed, and consequently there is competition between lineages with different number of beneficial mutations (Desai and Fisher, 2007). Clonal interference analyses usually neglect the effect of lineages with multiple beneficial mutations (Gerrish and Lenski, 1998; Orr, 2000; Wilke, 2004). On the other hand, theoretical studies on the effects of multiple mutations have been performed under the assumption that all mutations have an equal fitness effect and therefore clonal interference is not an issue. These analyses are performed using a semi-deterministic approximation: while the bulk of the population is treated deterministically, the most fit population, being rare, is described in a stochastic manner (Desai and Fisher, 2007; Rouzine *et al.*, 2003; Rouzine *et al.*, 2008; Tsimring *et al.*, 1996). The main result of both

clonal interference analyses and multiple mutation analyses is that the rate of adaptation no longer increases linearly with population size and mutation rate, but shows only a logarithmic or sub-logarithmic increase with increasing N and U_b.

When deleterious mutations are also taken into account, the probability of fixation of a beneficial mutation is reduced compared to a scenario when deleterious mutations are absent (Johnson and Barton, 2002; Orr, 2000). Moreover, the adaptation rate shows a maximum at a particular value of the total mutation rate, and this yields an optimal mutation rate. Orr showed that when beneficial mutations have a selection coefficient less than that of deleterious mutations ($s_b < \min\{s_d\}$), the optimal mutation rate is equal to the harmonic mean of the selection coefficients of the deleterious mutations (Orr, 2000). Johnson and Barton (Johnson and Barton, 2002) extended this analysis to the regime where $s_b \geq s_d$. While they found that an optimal mutation rate still existed, they could only compute it numerically.

One aspect that has not received sufficient consideration in the literature is whether the fixing of beneficial mutations can result in fixation of linked deleterious mutations in large populations. In the $s_b < s_d$ regime, Peck demonstrated that this is not possible although the proof does not consider the possibility of multiple beneficial mutations compensating for the effect of a deleterious mutation (Peck, 1994). On the other hand, Johnson and Barton showed that deleterious mutations can indeed be fixed if $s_b > s_d$, but the caveat with their analysis is that it considers neither clonal interference nor multiple beneficial mutations. Campos and De Oliviera have carried out extensive

simulations which take into account clonal interference but discount the possibility of multiple beneficial mutations (Campos and De Oliveira, 2004). They, however, did not look at the fixation of deleterious mutations as a result of linkage.

1.2.2 Laboratory evolution experiments

Laboratory evolution experiments, in conjunction with modern tools of molecular biology and genomics, can provide major insights about evolutionary phenomena (Elena and Lenski, 2003). These experiments involve monitoring of populations over periods ranging from 100 generations (Chao and Cox, 1983) to over 20,000 generations (Cooper et al., 2003). Given the long times involved, such experiments require the use of organisms with short generation times, and unicellular microorganisms and viruses are the common choice.

From the early experiments of Novick and Szilard in chemostats investigating spontaneous mutation rates (Novick and Szilard, 1950a) to relatively recent experiments of Lenski and colleagues involving propagation of *E. coli* over 20,000 generations by repeated serial dilutions (Lenski et al., 1991), laboratory evolution experiments have a rich history and a broad scope. Such experiments have unearthed several phenomena such as reproducible patterns of mutations or gene expression changes in replicate lineages (Cooper et al., 2003; Notley-McRobb et al., 2003), the emergence and fixation of strains with high mutation rates (Notley-McRobb et al., 2002a; Sniegowski et al., 1997), the generation of high phenotypic diversity even in constant and unstructured environments (Maharjan et al., 2006), and the high rate of beneficial mutations (Perfeito

et al., 2007). In general, laboratory evolution experiments may be classified into two groups, depending on the measurement being performed:

(1) Selection coefficient measurements: These experiments involve co-culturing of two or more populations which can be distinguished by some neutral or near-neutral markers. Changes in frequencies of these markers are indicative of selection events and the rate of such changes can be used to quantify the fitness difference (selection coefficient) between the marked populations. Typical markers that have been used include auxotrophic markers (de Visser and Rozen, 2006), microsatellite alleles (Imhof and Schlötterer, 2001), and fluorescent proteins (Hegreness et al., 2006). Selection coefficient measurements have been used to estimate the distribution of fitness effects of beneficial mutations (Imhof and Schlötterer, 2001) and to investigate clonal interference phenomena (de Visser *et al.*, 1999; de Visser and Rozen, 2006).

(2) Measurement of mean fitness trajectories: These experiments monitor the mean fitness of the population or the distribution of fitness of the population as a function of time. Fitness trajectories are usually recorded by competition between evolved strains and a common, ancestral reference strain at regular intervals (Desai et al., 2007; Lenski et al., 1991). Alternately, such trajectories can be obtained by monitoring environmental parameters as in the case of residual substrate concentration in nutrient-limited chemostats (Wick et al., 2002). Measurements of such trajectories have been used to estimate the deleterious mutation rate and the average effect of deleterious mutations

(Kibota and Lynch, 1996), to study the reproducibility of fitness trajectories at large population sizes (Wick et al., 2002), and to compare different models (clonal interference models and models tracking lineages with different number of beneficial mutations , see section 1.2.1) for asexual adaptation (Desai et al., 2007).

For measurement of mean fitness trajectories, there are three main requirements: the ability to monitor populations over long periods of time and the feasibility of measuring fitness both frequently and precisely. Frequent measurements can reveal phenomena that coarser measurements do not resolve such as the presence of discrete jumps in fitness or correlates of fitness (Lenski and Travisano, 1994). Precise measurements, on the other hand, are necessary for small fitness differences to be resolved. Small fitness differences have to be measured in several contexts, for instance, the mutation load suffered by a *mutS* mutator strain well-adapted to its environment was estimated to be around 1% by Boe *et al.* (Boe *et al.*, 2000). In Chapter 4, I describe the development of an apparatus for long-term, high-precision and high frequency measurements of bacterial growth rates.

1.3 Mutators

1.3.1 DNA repair and mutator strains

The spontaneous mutation rate in all organisms is governed by a combination of proofreading and DNA repair mechanisms. Disruption of these mechanisms leads to an increase in the mutation rate, referred to as a mutator phenotype (Cox, 1976; Miller, 1996). Beginning with the isolation of the *mutT1* allele in the 1950s by Treffers and colleagues (Treffers et al., 1954), several mutator alleles have been characterized in *E.*

coli (Horst et al., 1999; Miller, 1998). These include: *mutD* (*dnaQ*), the proofreading subunit of DNA polymerase III; *mutH*, *mutL*, *mutS,* and *uvrD* involved in methyl-directed mismatch repair; and *mutT*, *mutY,* and *mutM* comprising the GO system for oxidative repair (Miller, 1996; Miller, 1998).

Mutator alleles are characterized by their strength and by the spectrum of mutations that are enhanced in cells bearing them. A *mutT*-mutator shows increased rate of G:C→T:A transversions, while mismatch repair deficient strains have an elevated rate of transitions and frameshifts (Miller, 1996). The strength of the mutator phenotype refers to the factor by which mutation rates are elevated with respect to the wild-type. Based on mutation rate estimates derived from measurements of number of spontaneous rifampicin-resistant mutants, the strength of the *mutT* mutator is about 25-fold, while that of the *mutS* mutator is around 80-fold (Garibyan et al., 2003).

As described in section 1.1.1, *E. coli* mutator strains are found among natural isolates. Wild-type cells can also mutate to give rise to mutators. It is estimated that in a large culture of wild-type cells with population in excess of 10^{10} cells, about 1 in 10^5 cells are mutators (Boe *et al.*, 2000; Miller *et al.*, 1999). This mutator subpopulation can be easily enriched by subjecting the population to a sequence of strong selections such as antibiotic treatment or auxotrophic reversion (Mao et al., 1997; Miller et al., 1999).

Mutators arising from mutations in DNA repair genes are usually constitutive, heritable and global (i.e., the mutation rate is high for the entire genome). In contrast, there exist

mutator phenotypes which are non-heritable and transient (Humayun, 1998; Sundin and Weigand, 2007) as well as heritable local mutators, where only a specific region of the genome shows an elevated mutation rate (Metzgar and Wills, 2000). The prototypical system where the mutator phenotype can be transiently induced is the SOS response, which involves induction of error-prone polymerases in response to DNA damage (Nohmi, 2006). SOS-polymerases also appear to play a significant role in the generation of the wild-type Growth Advantage in Stationary Phase (GASP) phenotype (Yeiser et al., 2002). Examples of heritable local mutators include the so-called "contingency loci," which play a role in helping pathogenic bacteria evade host immune responses (Moxon et al., 1994).

1.3.2 Laboratory phenomena associated with mutators

Competition experiments between mutator and wild-type strains have shown that mutators have a short term advantage (Nestmann and Hill, 1973; Tröbner and Piechocki, 1984a). In a series of experiments in glucose-limited chemostats, Cox and colleagues demonstrated that *mutT*-mutator strains outcompete their wild-type counterparts provided that they are present above a certain ratio in the population (Chao and Cox, 1983; Cox and Gibson, 1974; Gibson et al., 1970). The early experiments were inconclusive as to whether this reflected an intrinsic advantage of the *mutT* defect or whether the mutators won by generating beneficial mutations. Later experiments with finer sampling revealed that mutators take over the population following a characteristic lag period and only if they are present above a certain ratio. More recently, it has been shown that the transition (between mutators winning and wild-type winning) does not occur at a threshold ratio, but rather at a threshold mutator population size (Le Chat et al., 2006). The threshold

mutator population size corresponds to the one where the expected number of beneficial mutants in the mutator subpopulation is one. These observations suggested that mutators took over by hitchhiking with beneficial mutations rather than because of an intrinsic fitness advantage.

In some cases, however, competition experiments between mutators and wild-type have demonstrated a fitness disadvantage for the mutator. Tröbner and Piechocki showed that the *dam* mutators lose to wild-type cells at all starting ratios (Tröbner and Piechocki, 1985). However, the loss is probably due to the pleiotropic effects of the allele, rather than because of mutation load. In a separate report, Tröbner and Piechocki also showed that the mutation rate of a *mutT* mutator decreased as a result of acquisition of compensating mutations, when the strain was cultured in a chemostat for 2,200 generations (Tröbner and Piechocki, 1984b). They interpreted their results as suggesting that high mutation rates are selected against once populations are well-adapted. An instance of mutators losing out to wild-type strains has been documented in an animal model as well. Daurel *et al*. showed that a *mutL* variant of *Staphylococcus aureus* suffered a fitness disadvantage when competed with an otherwise isogenic wild-type strain in the rat model of osteomyelitis of the tibia (Daurel et al., 2007).

Even when mutator strains have not been deliberately introduced (as in competition experiments), cells with higher mutation rate have been observed to take over populations in long-term cultures. Mutator strains took over 3 out of 12 independent populations that were maintained for over 10000 generations by serial dilutions (Sniegowski et al., 1997).

Similarly, in 6 out of 11 independent glucose-limited chemostat populations, strains with elevated mutation rates were found to comprise between 30-100% of the population within 150 generations (Notley-McRobb et al., 2002a). A detailed analysis of both experiments yielded puzzling results (Notley-McRobb et al., 2002b; Shaver et al., 2002). In the first experiment, in one of the three populations where mutators were observed, mutators increased in frequency from 0% to 42% without any detectable increase in the average fitness (Shaver et al., 2002). Direct effects of the allele were measured to be negligible and could not be responsible for such an increase. In the second experiment, two of the populations that were analyzed in detail revealed that the mutator allele was first enriched and then eliminated (Notley-McRobb et al., 2002b). At the end of the enrichment phase, all isolates that were tested had a high mutation rate. However, in both populations, the mutators were eliminated within 150 generations. Mutation load, reversion of the mutator allele to the wild-type allele and antimutator mutations were ruled out as possible causes for the elimination. The emergence of mutators has also been observed in mouse models (Giraud et al., 2001). In 2 of 26 germ-free mice inoculated with a wild-type strain of *E. coli*, mutator bacteria formed a dominant fraction of the total *E.coli* population within 42 days. Furthermore, when mutators and wild-type bacteria were co-inoculated at ratios greater than 1/5000, the mutator/wild-type population ratio increased by over 2 orders of magnitude within 40 days.

Given the emergence of mutators in many laboratory conditions, one has to explain their rarity in nature by the long-term cost of an elevated mutation rate. Some measurements have been made to elucidate this long-term cost. Using cycles of single-cell bottlenecks,

Kibota and Lynch estimated that the genomic deleterious mutation rate for wild-type cells is at least 2×10^{-4} per replication with an average decrease of at most 1.2% in fitness per deleterious mutation (Kibota and Lynch, 1996). They observed a 2% loss in fitness over 300 cycles of single-cell bottlenecks (about 7500 generations). A similar protocol carried out with *mutS*-mutator yielded more dramatic results in much fewer cycles (Funchain et al., 2000). 100 lineages were passed through single-cell bottlenecks. After 90 cycles of single-cell bottlenecks (about 2400 generations), 5 lineages died out, while the remaining 95 lineages had growth rates ranging from 52% to 92% of the starting strain. Furthermore, all of these lineages accumulated mutations in biosynthetic pathways as assayed by inability to grow on various sugars and inability to form colonies on minimal media plates.

However, experiments with single-cell bottlenecks reveal only one half of the story. In these experiments, it is equally easy to fix deleterious mutations with small and large fitness effects. A different picture emerges when large populations are considered. For example, Boe *et al.* estimated that the reduction in fitness of a *mutS*-mutator on account of deleterious mutations was around 1% in experiments with large populations (Boe *et al.*, 2000). Furthermore, the authors suggested that this figure is an upper limit as the effect of the marker used to distinguish mutators from wild-type cells was not determined. More strikingly, in one of the twelve populations in the long-term cultures mentioned above (Sniegowski et al., 1997), mutators have survived over 8000 generations without any discernible effect on viability or fitness when compared to populations where mutators did not take over the population. It is therefore an open

question whether there is any significant disadvantage to having a high mutation rate as long as population sizes remain large.

1.3.3 Theoretical work on mutators

The emergence of mutators in laboratory systems (see section 1.3.2) provided the motivation for theoretical investigation of the phenomenon of hitchhiking of mutator genes with beneficial mutations. Using simulations, Taddei *et al.* showed that intermediate strength mutators could get fixed in large populations by hitchhiking (Taddei et al., 1997). The effect of various parameters like population size and the height and steepness of the fitness peak on the probability of fixing mutators of different strengths has also been studied (Tenaillon et al., 1999).

In models with finite number of beneficial mutations, the presence of a constant genetic landscape and the non-zero probability of back-mutation from a mutator state to the wild-type state ensure that the eventual outcome is the establishment of a mutation-indirect selection (MIS) equilibrium (Kessler and Levine, 1998). At the MIS equilibrium, mutators form the minority population (typically, the mutator frequency is around $10^{-5} - 10^{-4}$). Tenaillon *et al*. provided an approximate expression for the MIS equilibrium fraction of mutators by ignoring the distribution of deleterious mutations in the wild-type and mutator subpopulations and treating them as a two populations at the classical mutation-selection (MS) equilibrium (Tenaillon et al., 1999). Since the mean fitness at MS equilibrium does not depend on the selection coefficient against deleterious mutations (cf. section 1.2.1), the approximation of Tenaillon *et al*. suggests that the mutator fraction at MIS equilibrium is independent of deleterious effects of mutations as

well. The MIS, however, differs from the MS equilibrium in one respect. In the MS equilibrium scenario, deleterious effects of mutations are manifested as soon as they are acquired (this follows from the definition of a deleterious mutation). In contrast, mutation from a wild-type state to a mutator state does not result in immediate reduction in fitness. The deleterious effects of the mutator state are not direct, but follow from the increased generation of deleterious mutations in subsequent generations. Consequently, there is a delay in manifesting deleterious effects of the mutator state (André and Godelle, 2006) and the approximation of Tenaillon *et al*. underestimates the equilibrium fraction of mutators (Johnson, 1999). A better approximation has been developed by Johnson (Johnson, 1999), who found that the mutator fraction at MIS varies inversely with the strength of selection against deleterious mutations.

Another aspect of mutators that has been studied theoretically is the effect of environmental change in mutator frequency (Tanaka et al., 2003; Travis and Travis, 2002). This has been studied in the context of antagonistic pleiotropy, viz., a situation where mutations which are beneficial in the current environment are deleterious in subsequent environments. If environmental fluctuations are too fast, there is no advantage to be gained in acquiring beneficial mutations, as these will prove deleterious in short time. In this case, a higher mutation rate proves disadvantageous as it leads to generation of beneficial mutations at higher rate. On the other hand, if environmental fluctuations are so slow that the population spends bulk of the time at MIS equilibrium, mutators would be the minority population for most of the time. At intermediate frequencies of

environmental fluctuations, however, mutators can be present at appreciable frequency (Travis and Travis, 2002).

1.4 Microbial Growth and Measurement of Growth Rates

Recording of growth curves is a classical quantitative measurement in microbiology and has many applications in the study of bacterial physiology and evolution. Indeed, in his classic review on the growth of bacterial cultures, Jacques Monod referred to such measurements as the "basic method of Microbiology" (Monod, 1949). Traditionally, a typical bacterial growth curve comprises several phases, including a lag phase, where the organism adapts to a new environment; an exponential phase, which can be viewed as steady state growth; and a stationary phase, which usually reflects the exhaustion of one or more nutrients from the medium. Monod characterized the exponential phase as "the only phase of the growth cycle when the properties of the cells can be considered constant, and can be described by a numeric value, the exponential growth rate" (Monod, 1949). The exponential phase represents an ideal regime for laboratory evolution experiments and the precise measurement of growth rate is a crucial requirement for such investigations.

1.4.1 Measurement of Growth Rates

Consider an exponentially growing microbial population whose population at time t is given by $N(t) = N(0)e^{\lambda t}$, where λ is the exponential growth rate. For any measurement of the growth rate performed over a measurement duration τ, the precision of measurement is determined by two factors: (a) the intrinsic measurement precision of the

technique, which is the precision in measurement of $N(t)$, and (b) growth rate reproducibility, which is the variance of λ over the measurement duration τ. The growth rate may vary over the measurement period either as a result of environmental fluctuations or because of changes in internal physiological states. In general, there are two methods for improving measurement precision:

(1) Increasing measurement duration τ. The intrinsic precision in growth rate measurement, roughly speaking, is given by $\Delta\lambda = \frac{1}{\tau}\left(\frac{\Delta N(\tau)}{N(\tau)} + \frac{\Delta N(0)}{N(0)}\right)$. As a result, for a given intrinsic precision in population size measurement, a longer measurement period improves the intrinsic precision in growth rate measurement. Moreover, as the growth rate that is measured (λ_{meas}) is actually the time average of the fluctuating growth rate over the measurement period, i.e., $\lambda_{meas} = \frac{1}{\tau}\int_0^\tau \lambda dt$, a longer measurement time would average out fluctuations in λ over a wider frequency range, resulting in better growth rate reproducibility. Increasing the measurement duration would, of course, impose constraints on how often growth rates can be measured.

(2) Relative measurements, i.e., measurement of growth rate relative to a reference strain whose growth rate is λ_{ref}. These techniques actually measure the difference $\lambda - \lambda_{ref}$, and exploit the fact that fluctuations in λ and λ_{ref} are likely to be highly correlated. As a result, the variance of $\lambda - \lambda_{ref}$ can be lower than the variance of λ itself. In long-term evolution experiments, relative measurements of mean growth rates would require setting up

completions between evolved populations and the reference strain. This would require sampling of cultures and also impose constraints on how often fitness measurements can be made.

Relative measurements of growth rate have been performed by measuring population sizes using a variety of techniques including plate counting (Desai et al., 2007), optical density readings (Dekel and Alon, 2005), or flow cytometry (Desai et al., 2007). As described, however, these techniques have long measurement durations ranging from several hours to a day. The alternative to relative measurements is to use absolute methods of evaluating population sizes. Absolute measurements have been performed using optical density (Kibota and Lynch, 1996) and bioluminescence (Kishony and Leibler, 2003). Absolute measurements using optical density have low intrinsic precision, while bioluminescence measurements have no such issues. However, the measurement duration in the experiments of Kishony and Leibler was long (~10 generations or ~3 hours in rich media). Nevertheless, bioluminescence measurements may be ideal for long-term, high-precision recording of growth rates, especially if the measurement duration can be reduced to facilitate high-temporal resolution as well.

Bioluminescence has found numerous biotechnological and biological applications (Meighen, 1993; Roda et al., 2004) because of its high sensitivity and the ease of measurement of luminescence signals through automated means. Bacterial bioluminescence results from oxidation of reduced flavin mononucleotide ($FMNH_2$) and a long-chain fatty aldehyde catalyzed by bacterial luciferase (Meighen, 1993). The lux operon, which comprises five structural genes (luxCDABE), forms a self-sufficient

bioluminescence module. Cloning of the five lux genes into non-luminescent bacteria makes them luminescent without the need for additional substrates. More importantly, in the exponential phase of growth, the expression of the lux operon from a constitutive promoter in *Escherichia coli* yields a quantitative signal proportional to the cell population (Kishony and Leibler, 2003; Marincs, 2000). The advantages of bioluminescence measurements are their feasibility even at low cell densities (unlike optical density measurements), low background and high dynamic range, and the absence of requirement for an external light source for measurement (unlike OD or fluorescence). In Chapter 4, we demonstrate that these advantages permit long-term, high-precision recording of growth rates with good temporal resolution.

1.4.2 Long-term culturing techniques

Laboratory evolution experiments, such as those described in section 1.2.2, require populations of organisms to be maintained over periods ranging from 100 to over 10,000 generations. To maintain microbial cultures over such long periods, two kinds of culturing techniques have been adopted, viz., repeated serial dilutions and continuous culture devices.

Repeated serial dilutions involve cycles of growth and dilution. Dilutions are performed periodically, typically once a day, and are performed by transfer of a small fraction of the current culture to a second culture with fresh medium. Such dilutions can be performed manually (Desai et al., 2007; Lenski et al., 1991) or automatically (Hegreness et al., 2006). While serial dilutions are an elegant solution to the problem of maintaining cultures over long times, one typically dilutes culture around 100-fold or more in each

cycle to minimize the frequency of dilutions. Consequently, during the growth phase of the cycle, the density of the culture may vary over 100-fold, and thus the population may experience culture conditions that are not constant throughout the growth phase. This is especially true if cultures are allowed to reach stationary phase, but also true of exponential phase cultures in rich media, where exponential growth proceeds through a sequence of physiological states distinguished by their gene expression profiles (Baev et al., 2006).

In order to achieve greater control over culture conditions, one typically uses continuous culture devices such as chemostats and turbidostats. The chemostat was invented almost 60 years ago as a means for quantitative study of bacterial physiology and evolution (Monod, 1950; Novick and Szilard, 1950b). The chief advantage of the chemostat was the ability to establish user-defined, steady-state culture conditions with high reproducibility (Hoskisson and Hobbs, 2005). Chemostats are typically operated under conditions where a single nutrient limits the growth rate of the cultured microorganism (Tempest, 1970). While chemostats may provide constant environments over the short-term, they also select for mutants that have increased affinity for the limiting nutrient resulting in a decrease in its concentration (Dykhuizen and Hartl, 1983). The main problem with chemostats is that the measure of fitness of the population is the concentration of the limiting nutrient in the medium (Wick et al., 2002). Such concentration measurements are inherently more difficult to perform than population size measurements.

Chemostats, are operated at a fixed dilution rate, which sets the concentration of the limiting nutrient. Turbidostats (Munson, 1970), and other similar devices such as permittistats (Markx et al., 1991), differ from chemostats in that the rate of dilution is adjusted constantly to keep population size. The population size is monitored through culture turbidity (turbidostats) or dielectric constant (permittistats). In principle, the culture dilution rate required to maintain steady state provides a measure of population growth rate. This idea was demonstrated by Anderson, who built a device for continuous recording of growth rates using turbidity measurements (Anderson, 1953). The main disadvantage of both turbidostats and permittistats is that they require dense cultures for population measurements to be made, and thus are restricted in the density range that they can be used for.

While continuous culture devices suffer from several technical problems, including the adherence of microorganisms to walls of the culture vessel, they have proven to be quite useful in laboratory evolution experiments (see section 1.2.2). Moreover, recent advances such as the development of microchemostats (Balagadde et al., 2005) and a renewed interest in the use of continuous culture devices (Hoskisson and Hobbs, 2005) may result in a greater adoption of such techniques.

Chapter 2. Materials and Methods

2.1 Bioluminescence-based High Precision Measurement of Growth Rates

Description of apparatus

The setup is depicted in Figure 1 and has a 250 ml, four-necked glass flask (Kimble Kontes) at its core. The central neck of the culture vessel was covered with a borosilicate optical window (Edmund Optics) and a photomultiplier tube (PMT) module (Hamamatsu H5783) was positioned above the window to measure light emitted by the bacteria. The other necks were used to supply fresh medium, remove spent culture, and to fix an air vent (Cole Parmer) that allowed diffusion of air without compromising sterility of the culture. Inoculation of the medium was carried out through an inoculation port which consisted of a threaded cap with a PTFE-silicone septum (National Scientific) secured on a side-neck on the vessel. To minimize temperature fluctuations, the culture vessel was placed within an open-top transparent container (Nalgene) that was connected to a circulating water bath (VWR Scientific). A magnetic stirrer (Thermolyne) located underneath the vessel was used to gently stir (< 50 rpm) the culture. The stirrer, culture vessel and PMT were enclosed in a dark, cardboard box that blocked external light and facilitated measurement of bacterial luminescence.

For long-term cultures, two peristaltic pumps (Rainin RP-1) were used to supply fresh medium and remove spent culture which were stored in 5-liter glass bottles (Kimble Kontes). Pumping flow rates were maintained by measuring the rate of fresh medium

supplied and the rate of spent culture removed using precision balances (A & D Company Limited, GX-6000 and GX-6100, precision of 0.1 g and 0.01 g respectively) and adjusting pump speeds accordingly. For peristaltic pump tubing, we used Pharmed® BPT tubing, while Dow Corning® Pharma-65 tubing was used in the rest of the apparatus. To minimize the risk of contamination during replacement of media/waste reservoirs, they were connected using quick-disconnect fittings (Colder Products Company). Other tubing connections were made with polypropylene barbed fittings. All fittings were secured using Barblock® retainers (Barblock Corporation).

The current output signal of the PMT module was transduced to a voltage signal by means of a 1 MΩ resistor and then measured using a digital multimeter (Agilent 34401A) operated in the DC Voltage mode with an integration time of 100 power line cycles. A GPIB port was used to interface the digital multimeter with a personal computer, while serial ports were used to communicate with the pumps and balances. Regulation of devices and logging of data were performed using a custom program written in C and compiled using Microsoft Visual C++. The program used the Agilent VISA library (Agilent Technologies) for communicating with the external devices.

Bacterial strains

Unless otherwise indicated, all batch cultures and long-term culture experiments described in Chapter 4 were performed with the non-adherent *Escherichia coli* strain NS2 transformed with the luminescence plasmid pCSλ (Kishony and Leibler, 2003).

Some experiments were performed with wild-type MG1655 strain (Figure 9) or the non-adherent HEHA16 strain (Figure 12B) (Kjargaard et al., 2000).

Strain NS2 was constructed in collaboration with Doeke Hekstra and with advice from Dr. John Chuang. It was derived from the wild-type MG1655 strain by engineering deletions in the *fimA* and the *flu* genes sequentially. Deletions were made by P1 transduction of the FRT-flanked kanamycin resistance cassette from the corresponding deletion mutant in the Keio Collection (Baba et al., 2006) and selecting for kanamycin-resistant transductants. Strains JW4277 and JW1982 were used to prepare P1 lysates for generating the *fimA* and *flu* deletions respectively. The kanamycin resistance gene was flipped out by first transforming the transductants with the plasmid pCP20 (Cherepanov and Wackernagel, 1995), which has ampicillin and chloramphenicol resistance markers, a temperature sensitive origin of replication and temperature-inducible FLP expression. After transformation, induction of FLP expression and cessation of replication of pCP20 were carried out by incubation at 42˚C. Removal of the kanamycin-resistance cassette and curing of pCP20 were verified by restoration of sensitivity to kanamycin, ampicillin and chloramphenicol. All genetic manipulations were performed using standard techniques (Miller, 1992).

Media, inoculation, and culture conditions

LB broth with 30 μg/ml kanamycin was used in most of the experiments described in Chapter 4. This medium was prepared by dissolving 25g of LB granules (EMD Chemicals) per liter of distilled water, adding 30 mg of kanamycin monosulfate (Sigma).

Other media used include: glucose and lactose minimal medium (Figure6) which had 10mM KH_2PO_4, 15mM $(NH_4)_2SO_4$, 0.5 mg/l $FeSO_4.7H_2O$ (pH adjusted to 7.0 with these three components), 1mM $MgSO_4.7H_2O$, 30 mg/l kanamycin monosulfate and either 0.105% glucose of 0.1% lactose; and LB with 25 μg/ml Chloramphenicol for the culture of HEHA16 (Figure 12B). Medium was usually sterilized by means of a 0.2μm SFCA filter (Nalgene), with the exception of LB used for culture of MG1655 and HEHA16 strains, which was sterilized by autoclaving. In all cases, antibiotics were added for maintenance of the luminescence plasmid. All experiments were performed at 38.3˚C, except for those described in Figures 9 and 12B which were performed at 37.2˚C, and those described in Figure 8, where the culture temperatures are indicated. Batch cultures were usually performed in 125 ml of the medium, whereas long-term cultures used 125.0 g of medium in the culture vessel.

For both batch cultures and long-term cultures, a small sample of glycerol stock of the strain to be cultured was streaked out on an LB agar plate with appropriate antibiotic and incubated at 35.5˚C or 37.0˚C. After 12 hours incubation, 10 colonies were randomly picked and inoculated in 0.65 ml of the culture medium. The inoculated medium was diluted 100-fold and 0.5 ml of the 100-fold diluted medium was used to inoculate the culture vessel. This procedure ensured that the initial inoculum was $5-10\times10^5$ cfu. Six hours prior to inoculation, the culture vessel with the medium was placed in the water bath and the PMT was switched on. This pre-inoculation phase was required for the temperature of the setup to equilibrate and for estimation of the background signal. While

batch cultures were allowed to go to stationary phase after inoculation, long-term cultures were performed using the indicated dilution protocol (Figures 10, 13A).

Data processing

The background signal, B, corresponds to the signal generated by the dark current of the PMT, and was typically taken to be the mean luminescence signal during the last 0.5 hours of the pre-inoculation phase (see above). The background signal was subtracted from the raw signal recorded by the multimeter, $L_{raw}(i)$, to yield the transformed signal, $L_{tr}(i) = L_{raw}(i) - B$. The index i denotes the i^{th} reading after inoculation.

Growth curves (Figures 6A, 6C, 6E, 7A, 7C, 8A, 8C88) plot $L_{tr}(i)$ (on a logarithmic scale) as a function of $t(i)$, the time at which the i^{th} reading was recorded. For plotting slope curves (Figures 6B, 6D, 6F, 7B, 8B88), the $L_{tr}(i)$ time series was divided into overlapping blocks of $N_S = 250$ points, with consecutive blocks separated by $N_{Slide} = 25$ points. For the I^{th} block, whose index i varies from $I \cdot N_{Slide}$ to $I \cdot N_{Slide} + N_S - 1$, $X(i) = \ln\left(L_{tr}(i)\right)$ was fitted to a linear function of $t(i)$ using least squares regression. The slope obtained from the regression, λ_{Blk}, represents the growth rate in that block. We then plot $\ln(2)/\lambda_{Blk}$ (the generation time in the block) as a function of the geometric mean of the luminescence signal in that block, $L_{Blk} = \exp\left(\sum_{i=I \cdot N_{Slide}}^{I \cdot N_{Slide} + N_S - 1} X(i) \Big/ N_S \right)$ by varying I from 0 to $\left\lfloor \left(N_{Tot} - N_S + 1\right)/N_{Slide} \right\rfloor$, where N_{Tot} is the total number of data points recorded. For

Figures 7D and 8D, a single block consisting of all data points in the operating region ($2.65\ \text{mV} \le L_{tr}(i) \le 7.00\ \text{mV}$) was used to obtain the generation time.

In long-term cultures, parameters such as masses of input and output reservoirs, RPM of input and output pumps, and temperature of the water bath were recorded in addition to the luminescence signal of the culture. The luminescence recordings were used to plot Figures 9A, 9B, 12B, and 14A, while the pump speed data was used to plot Figure 9C. In Figure14A, input flow rates were computed as the negative of the slope obtained by a linear least squares fit of the mass of the input reservoir to the time of recording of the mass during each period where pump RPMs where not changed. Vertical changes in input flow rate in Figure 14A are a result of changes in pump RPMs. For Figure 14B, data recorded in each no-dilution phase was used to calculate the growth rate (λ_{ND}) in that phase by performing linear least squares regression of $X(i) = \ln(L_{tr}(i))$ against $t(i)$ followed by plotting of $\ln(2)/\lambda_{ND}$ against the arithmetic mean of the time of recording of the data points.

Mock runs for measuring culture mass and temperature stability

For measuring culture mass stability (Figure 11) and temperature stability (Figures 12A, 13B), mock runs were set up with the indicated dilution protocols. In these mock runs, distilled water was used instead of culture medium, and no bacteria were grown. The control software was reconfigured to behave as if an ideal bacterial strain was growing exponentially with a doubling time of around 18 minutes. For recording culture mass, the stirrer in Figure 1 was replaced by a precision balance (A & D Company Limited, GF-

200, precision of 1 mg). Temperature recordings of the culture and the surrounding water bath were made using two independent thermistor probes (Omega Engineering) with the stirrer in place. The voltage output of the thermistor circuit was calibrated against a mercury thermometer (Figure 2) and digitized using a digital multimeter. The thermistor voltage varied linearly with temperature in the range used for calibration with a sensitivity of 10.5 mV/°C (Figure 2). Under measurement conditions, the digital multimeter had an accuracy of better than 0.35 mV, thus the thermistor probe could be used to perform temperature measurements with an accuracy of ~0.03°C.

2.2 Synthetic Cooperation System in Yeast

Construction of CoSMO components

Yeast strains of desired genotypes were obtained through genetic crosses. The complete genotype for WY811 ($R^{\leftarrow A}_{\rightarrow L}$) is *MAT***a** *ste3Δ::kanMX4 ade8Δ0 LYS21^{op} trp1-289::pRS404(TRP)-ADHp-DsRed.T4* and that for WY833 ($Y^{\leftarrow L}_{\rightarrow A}$) is *MAT***a** *ste3Δ::kanMX4 ADE4^{op} lys2Δ0 trp1-289::pRS404(*TRP*)-ADHp-venus-YFP*.

lys2Δ and *ade8Δ* mutations were derived from BY4743 (Euroscarf Y20000) (Brachmann et al., 1998) and SY9913 (Tomlin et al., 2001), respectively. Yeast cells of the same mating type do not mate. *ste3Δ::KanMX4* (Euroscarf Y05028) cells lack Ste3, the receptor for a-mating factor (Hagen et al., 1986). Thus, in the rare occasion where a cell of *MAT***a** *ste3Δ* genotype switches mating type to *MAT*$\boldsymbol{\alpha}$ *ste3Δ*, it still cannot mate.

ADE4^{op} mutant is the *PUR6* allele of *ADE4* (Armitt and Woods, 1970). *LYS21*^{op} was isolated in an MNNG (1-methyl-3-nitro-1-nitrosoguanidine, Sigma-Aldrich) mutagenesis screen as a mutation that was resistant to the lysine analog thialysine (L-4-thialysine hydrochloride, Sigma-Aldrich) and that also cross-fed *lys*$^{\Delta}$ cells (Gray and Bhattacharjee, 1976). One lysine-releasing mutation was dominant, showed tight linkage to *LYS21* (20/20 tetrads), and was therefore assigned *LYS21*^{op}. Both *ADE4*^{op} and *LYS21*^{op} mutations were backcrossed into the S288C background five times.

To introduce fluorescent protein markers, WSB37 and WSB41were constructed after ligating three DNA fragments: the *TRP1*- integrating plasmid pRS404 (ATCC) digested with SacI and XhoI, a SacI-HindIII fragment harboring the ADH promoter from pKW431 (Stade et al., 1997), and a HindIII-XhoI PCR fragment containing either Venus-YFP amplified from pDH6 (http://depts.washington.edu/~yeastrc/) or RGS-His6-DsRed.T4 amplified from pQE81-L-DsRed.T4 (Bevis and Glick, 2002). The resulting plasmids were linearized with XbaI and transformed into a yeast strain harboring *trp1-289*. Among *TRP*$^{+}$ transformants, a stable integrant was selected such that all its progeny cells expressed the expected fluorescent protein even when grown in non-selective media containing tryptophane.

Measurement of metabolite concentration using a bioassay

A series of SD media (Guthrie and Fink, 1991) supplemented with various amounts of metabolite adenine (lysine) and inoculated with a test strain auxotrophic for adenine (lysine) were grown to saturation (~20 hours). A linear regression of saturation OD600

values against concentrations of the metabolite was performed (correlation coefficient >0.99). To measure the metabolite concentration in a culture, the culture was filtered through a 0.2-micron filter and the supernatant was supplemented with 1/10 volume of 10×SD and inoculated with the appropriate test strain. The metabolite concentration was obtained from the saturation OD600 value through interpolation.

Measurement of population dynamics using flowing cytometry

For every round of measurement on FACS Calibur (with 488nm and 633nm lasers, BD Biosciences), the flow rate *k* of the instrument (μl/sec) was determined using a dilution series of a bead stock. Specifically, the concentration of a 6-micron bead stock (~2×10^6/ml, Duke, Cat #35-2) was measured using a hemacytometer. The bead stock was diluted 25-, 10-, 5-, and 2.5-fold to a standard 0.5ml-series of bead samples and processed by Calibur for 65 sec. The cumulative event counts at 5.2, 10.0, 15.2, 20.0, 25.2, and 30.0 sec were plotted against time and the event rate (events/sec) for each bead sample was deduced from the slope. Event rates (events/sec) were plotted against bead densities (beads/μl) for the standard series and the linear regression line was forced through the origin. The slope *k* was the flow rate of Calibur (μl/sec). The correlation coefficients of all linear regressions were greater than 0.999.

To measure the population composition of a culture, a sample was diluted into H_2O to OD_{600} ~0.01 and briefly sonicated. *S*, the event rate of the sample (events/sec), was determined as described above for bead samples. The total cell density is *S/k* (events/μl). Clusters of DsRed-positive, YFP-positive, and dark cells were clearly segregated (Figure

3), and the percentages of each cluster were calculated using FlowJo software (Tree Star). Dark cells accumulated during starvation and are considered dead because more than 99% (sample size > 5000) had lost colony-forming ability in a fluorescence-activated cell sorting (FACS) analysis. Fluorescent cells are considered alive because all of them retain the ability to exclude the nucleic acid dye propidium iodide (sample size>150).

2.3 Construction of Non-adherent Mutator Strains

In order to record mean fitness trajectories of strong mutators (cf. section 3.3), luminescent, non-adherent mutator strains are required so that they can be used in our apparatus for long-term culture (see Chapter 4). Mutators can, in principle, be constructed in a manner analogous to our construction of the non-adherent NS2 strain (section 2.1). However, the procedure involves several steps where single colonies have to be picked. Each such step introduces a single cell bottleneck and may result in accumulation of deleterious mutations in the strong mutators. Thus, we modify our strategy as follows:

(1) Create a plasmid where FLP recombinase is driven by an inducible promoter, and which also contains a wild-type copy of the mutator gene to be deleted. This copy should complement a chromosomal deletion.

(2) Transform the plasmid obtained in step (1) into the NS2 pCSλ strain.

(3) Create a strain where the mutator gene of interest has been replaced by FRT-flanked antibiotic resistance cassette (Datsenko and Wanner, 2000).

(4) P1 transduct the FRT-flanked antibiotic resistance cassette from the strain produced in step (3) into the transformants obtained in step (2). Induce expression

of FLP recombinase to flip out the chromosomal antibiotic resistance gene from the transductants.

(5) Selectively cure the plasmid created in step (1) and transformed in step (2) to obtain the desired strain.

Although this procedure also involves several steps where single colonies have to be picked, most of them are performed with the mutator deletion complemented by a plasmid copy. The steps where single-cell bottlenecks would be present in the mutator state are step (3) and step (5). Overall, our goal is to make six derivatives of the non-adherent NS2 strain: *ΔmutT*, *ΔmutS*, *ΔmutL*, *ΔmutY*, *ΔmutM*, and *ΔmutY ΔmutM*.

Creation of plasmid with inducible FLP expression and complementing mutator gene

The plasmid which is normally used to express FLP recombinase in an inducible fashion is pCP20 (Cherepanov and Wackernagel, 1995). The expression of FLP recombinase from this plasmid is quite leaky, and subsequently it is not possible to isolate antibiotic resistant transductants in step (4), presumably because the antibiotic resistance gene is flipped out by the basal FLP recombinase. We therefore chose to use a derivative of pInvRecA (Sektas et al., 1999), a plasmid with a temperature sensitive origin of replication and FRT recombinase expression driven by the inducible *tetA* promoter. Antibiotic resistant colonies can indeed by obtained after transduction of strains harboring pInvRecA with a lysate prepared from a strain having a chromosomal FRT-flanked antibiotic cassette.

Unfortunately, pInvRecA itself has two FRT sequences, and there is a possibility of pInvRecA integrating into the chromosome of NS2 since the strain has FRT scars left by the process of deleting the genes required to make it non-adherent. We therefore constructed pIndFLP, a derivative of pInvRecA without the FRT sequences.

pIndFLP was constructed by digesting pInvRecA with AatII, treating the singly cut plasmid with calf intestinal phosphatase, and then performing a restriction digest with XhoI. The larger band obtained by this process formed one of the ligation fragments for the construction of pIndFLP. The other ligation fragment was obtained by PCR amplification using pInvRecA as template, and with the following primers: 5'-AGCTATCTCGAGCCGATCCCCAATTCCTGGCA-3' and 5'-ATCTCAATGGTTC GTTCTCA-3'. Note that the first primer has a XhoI restriction site. The PCR product was ligated into pCR-Blunt-II TOPO vector (Invitrogen) and the resulting plasmid was transformed, mini-prepped and then cut with XhoI and AatII to obtain the second ligation fragment for pIndFLP. The two fragments were then ligated by overnight incubation with T4 DNA ligase at 16°C. The construct was verified both by restriction digests and DNA sequencing.

The next step involved introduction of mutator genes into pIndFLP to create pIndFLP-mut plasmids. pIndFLP was cut sequentially first with NheI and then with XhoI to generate one of the ligation fragments. Between the two restriction digest steps, the intermediate construct was treated with calf intestinal phosphatase. Mutator inserts were

Construct Name	Gene Amplified	Primer Sequences
pIndFLP-mutS	*mutS*	GTGAGA**CTCGAG**CGATGAGATGACGCACGGTTA CGTTGT**GCTAGC**GGCGATAGTGATGGGCATTGAT
pIndFLP-mutL	*mutL*	ATTCAA**CTCGAG**GCTCTGGGTCATCAGGGTAA TCCGAT**GCTAGC**CCAACCTTGCTCTGCCGCCT
pIndFLP-mutT	*mutT*	GACCAA**CTCGAG**GGAACAACAGCGTCGTATGGAA ATGACG**GCTAGC**CTCGGAGAATGGGCTGCTGAA
pIndFLP-mutY	*mutY*	GCTCAT**CTCGAG**GGTTTAGTCGCTTGTGAAAGTGTT CTGGCA**GCTAGC**GTATCTTTGACCCAGGCTTC
pIndFLP-mutM	*mutM*	CCTGGA**CTCGAG**CTGCTAAAGGTATGCGTGTAA CGTCTT**GCTAGC**CGCCGATTACCGTAGTTTCT
pIndFLP-mutYM	*mutY*	GCTCAT**CTCGAG**GGTTTAGTCGCTTGTGAAAGTGTT CTGGCA**GGTACC**GTATCTTTGACCCAGGCTTC
	mutM	CCTGGA**GGTACC**CTGCTAAAGGTATGCGTGTAA CGTCTT**GCTAGC**CGCCGATTACCGTAGTTTCT

Table 1. Primers used for the construction of pIndFLP-mut plasmids.
Restrictions sites are indicated in bold

generated by PCR amplification of a chromosomal DNA prep of MG1655 (prepared using DNAeasy Kit, Qiagen) with primers indicated in Table 1. The primers were designed with a XhoI or a NheI site, with the exception of the ones used for constructing pIndFLP-mutYM. These primers have a KpnI site instead of the NheI or XhoI site (Table 1). The PCR product was ligated into pCR-Blunt-II TOPO vector (Invitrogen) and the resulting plasmid was transformed, mini-prepped and then cut with XhoI and NheI to obtain the second ligation fragment for pIndFLP-mut. The two fragments were then ligated by overnight incubation with T4 DNA ligase at 16°C. To construct pIndFLP-mutYM plasmid, a similar procedure was used, except that it involved ligation of three

fragments: the original XhoI-NheI pIndFLP fragment, a *mutY* fragment with XhoI and KpnI overhangs (constructed essentially as above except that the plasmid obtained after TOPO cloning was cut with XhoI and KpnI) and a *mutM* fragment with KpnI and NheI overhangs (constructed essentially as above except that the plasmid obtained after TOPO cloning was cut with KpnI and NheI). All six constructs were verified by restriction digests.

We are currently in the process of testing whether the pIndFLP-mut plasmids complement mutator deletions by measuring the mutation rate of mutator strains with and without the plasmid. Once this is done, we can proceed with step (4). It has been verified that pIndFLP can be selectively cured (step 5) from derivatives of NS2 harboring both pCSλ and pIndFLP with an efficiency of ~20% by incubating the strain with the two plasmids on an LB + 30 μg/ml kanamycin plate at 42°C. Therefore, step (5) should be feasible with pIndFLP-mut plasmids as well.

Figure 1. Design of a bioluminescence based apparatus for precise measurement of growth rates. (A) Schematic illustration of the setup when used for batch cultures. A four-necked glass flask is at the core of the apparatus. A photomultiplier tube (PMT) module is used to measure bioluminescence, while a water bath maintains the temperature of the culture, which is stirred by a magnetic stirrer at the bottom. (B) A photograph of the setup showing the culture vessel, the open-top container used as a water bath, the PMT module and the inoculation port. (C) Schematic illustration of the setup when used for long-term culture. Peristaltic pumps are used to supply fresh medium and withdraw spent culture, and precision balances are used for tight control of the pumping flow rates. The light measurement apparatus is the same as in the batch culture setup. In panels A and C, the digital multimeter used to digitize the voltage readings and the personal computer used to record data and control the operation of the apparatus are not shown.

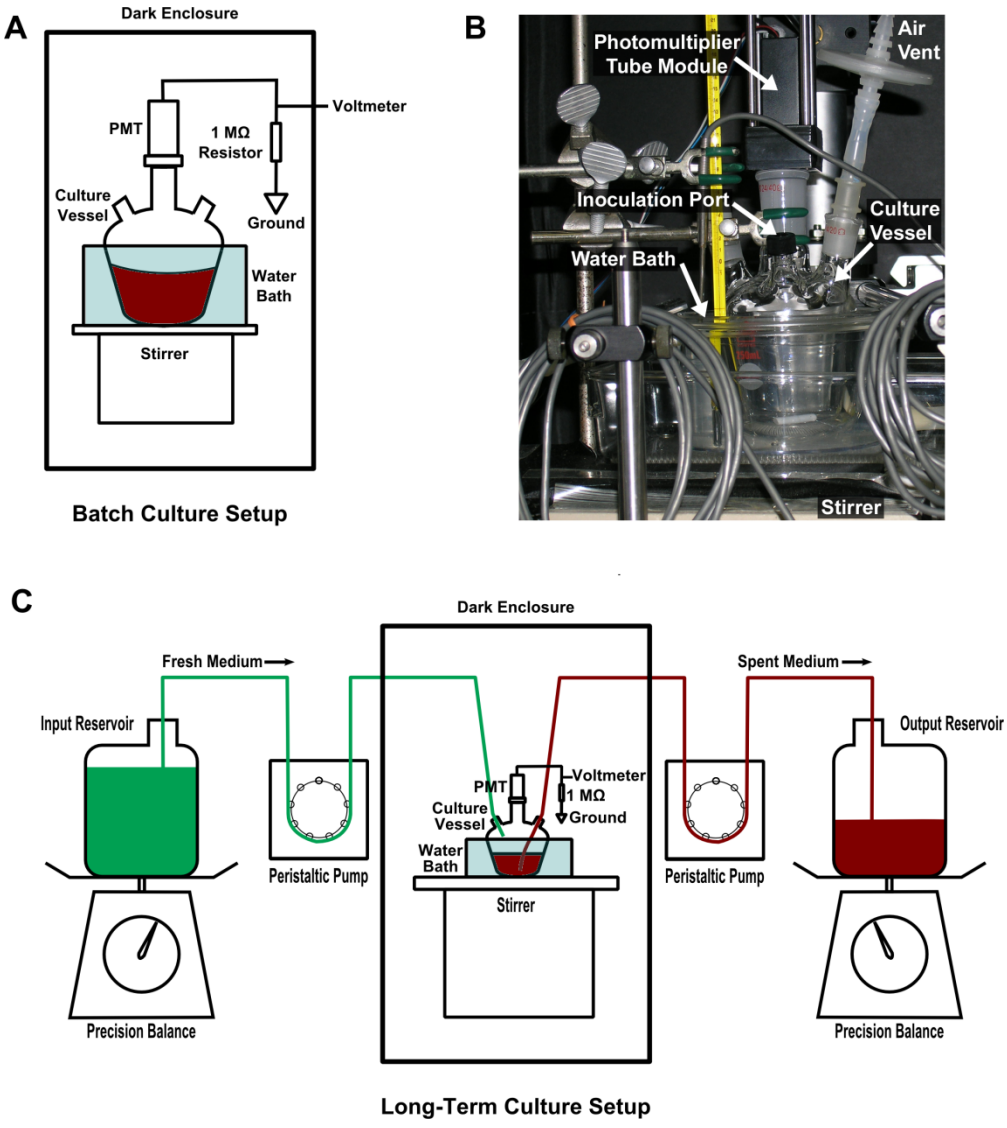

Figure 1. Design of a bioluminescence based apparatus for precise measurement of growth rates.

Figure 2. Calibration of thermistor probes for temperature measurement.

Thermistor probes used for temperature measurements were calibrated against a mercury thermometer by placing the probe and the thermometer in a water bath whose temperature is varied as indicated. The voltage output of the thermistor circuit is plotted against the water bath temperature as measured by the mercury thermometer. Circles depict actual measurements, while the dashed black line is the least squares linear fit. Also indicated are the slope of the line (10.5 mV/°C) and the linear correlation coefficient ($r = 0.999$), which quantify the sensitivity and linearity of the thermistor probe in the calibration temperature range.

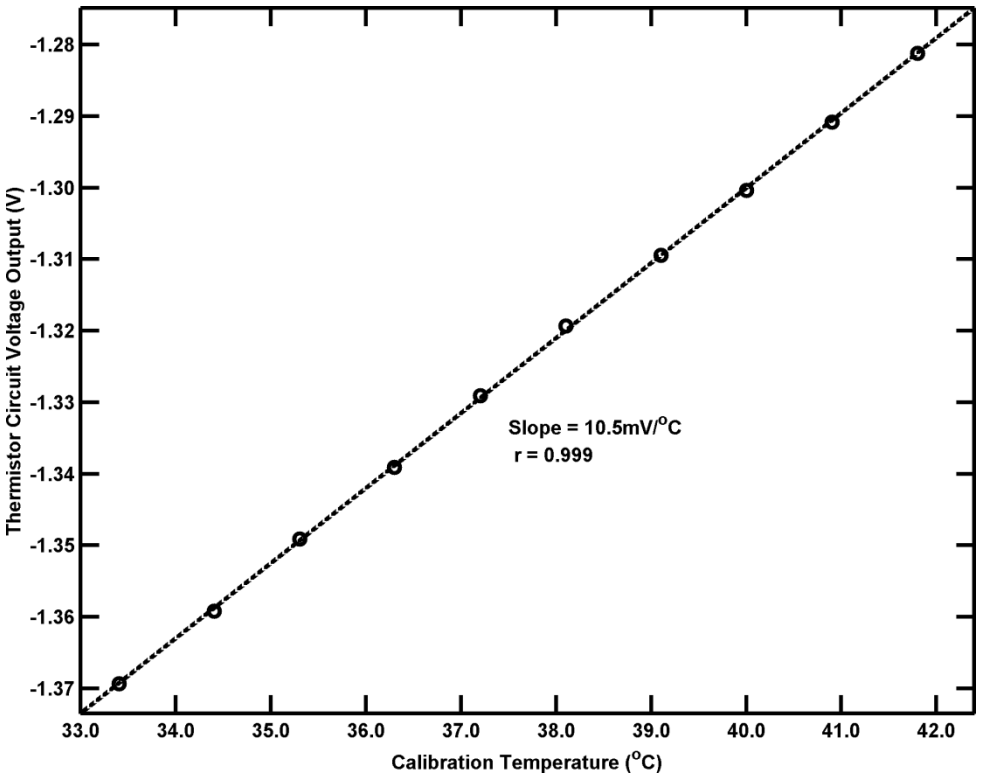

Figure 2. Calibration of thermistor probes for temperature measurement.

Figure 3. Characterization of CoSMO components using flow cytometry.

Exponentially-growing $R_{\rightarrow L}^{\leftarrow A}$ (left) and $Y_{\rightarrow A}^{\leftarrow L}$ (right) cells were washed free of supplements at time zero. Percentages of red-fluorescent (R), yellow-fluorescent (Y), and dark (Dark) cells were measured at 0 hour (top) and 97 hour (bottom), and their values are indicated.

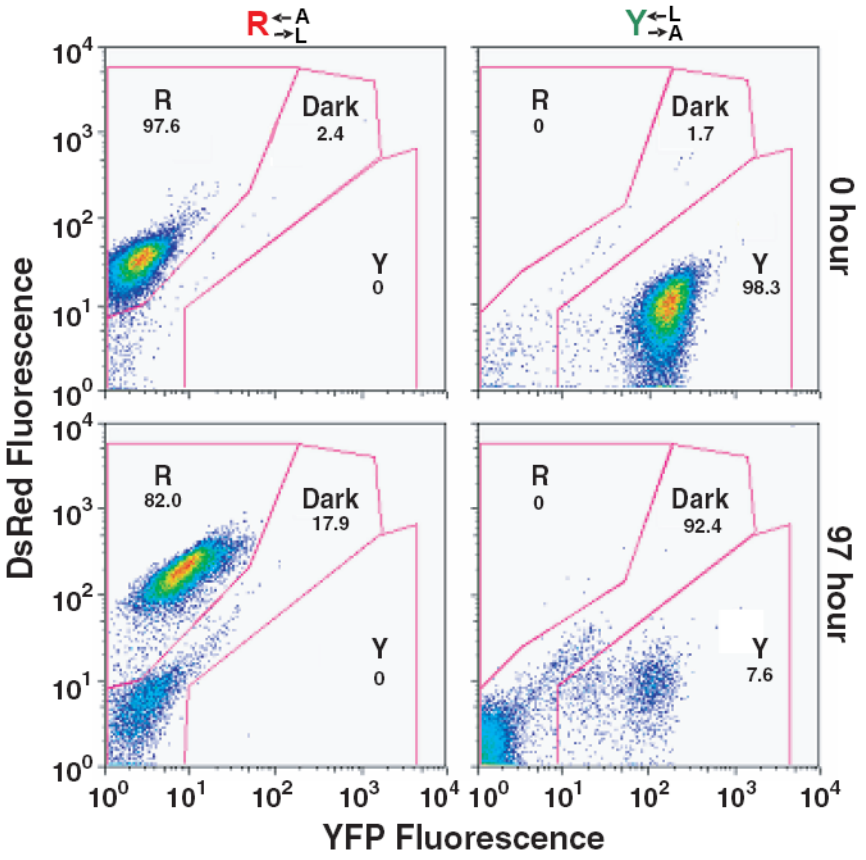

Figure 3. Characterization of CoSMO components using flow cytometry.

Chapter 3. Quantifying Mutation Accumulation in Large Asexual Populations

3.1 Motivation

The mutation rate of wild-type *E. coli* strains is estimated to be around 3×10^{-3} per genome per genome replication (Drake, 1991). More strikingly, as reviewed in section 1.1.1, this genomic mutation rate is typical of many DNA-based microbes and viruses. One also finds that a majority of clinical isolates of *E. coli* have a mutation rate close to the wild-type rate (cf. section 1.1.1). Taken together, these facts highlight the possibility that the mutation rate of *E. coli* is determined by some universal evolutionary constraints. What could these constraints be?

One way to understand the significance of the wild-type mutation rate is to ask what happens if the mutation rate is increased by 10-fold or 100-fold. If the wild-type mutation rate is special, one would expect to see some deleterious effects of high mutation rate. Many laboratory experiments (section 1.3.2), however, appear to contradict this expectation in that strains with high mutation rate (mutators) outcompete their wild-type counterparts. Theoretical work suggests that this should only be a transient phenomenon, and that eventually the wild-type mutation rate should be restored (section 1.3.3). In other words, mutators have a *long-term* cost, which results in their eventual downfall. What is the nature of this *long-term* cost? Can it explain the significance of the wild-type mutation rate?

There exist three hypotheses regarding the long-term cost of mutators:

(1) Lower equilibrium fitness. As discussed in section 1.2.1, the mean fitness of an asexual population at mutation-selection equilibrium is given by e^{-U_d}, where U_d is the genomic deleterious mutation rate. Thus, a mutator strain would have lower equilibrium fitness than a wild-type strain, and would be outcompeted (rather, a mutation-indirect selection equilibrium will be established with mutators in the minority, cf. 1.3.3).

(2) Mutation accumulation (MA). The gradual accumulation, through genetic drift, of mutations which are neutral in a given environment but are deleterious in others. This effect would be more pronounced in populations with high mutation rates.

(3) Antagonistic Pleiotropy (AP). Mutations that are beneficial in a given environment are deleterious in subsequent environments. Acquiring such mutations may provide a short-term benefit in the current environment, but will prove detrimental in the long-term.

While mutators have lower equilibrium fitness, it may take a long time for the equilibrium to establish (Johnson, 1999). As a result, the other two hypotheses are more likely to have a greater impact. MA has been demonstrated by subjecting populations to single-cell bottlenecks, in which case Muller's Ratchet becomes operational, and deleterious mutations can be accumulated rapidly (Funchain et al., 2000; Kibota and Lynch, 1996). AP has been demonstrated in the case of phage resistance mutants which

are outcompeted by their phage sensitive ancestral strain in the absence of phage (Lenski, 1988), as well as in a long-term evolution experiment in glucose minimal media lasting over 20,000 generations (Cooper and Lenski, 2000). It should be noted, however, that MA and AP are not mutually exclusive (Cooper and Lenski, 2000).

One explanation for the apparent competitive advantage of mutators in laboratory situations (cf. section 1.3.2) is that such experiments have been done with large populations and in a constant environment where MA and AP, as described above, may not operate. Is there a *long-term* cost to having a high mutation rate under these conditions? This question acquires particular importance if high mutation rate is viewed as an adaptive strategy (cf. section 1.1.2). Much theoretical work has been focused on the relationship between mutation rate and the speed of adaptation, i.e., the rate of increase of mean fitness of a population (cf. section 1.2.1). An alternate consideration would be to examine whether high mutation rate strategies are *perfect*. In particular, would a high mutation rate strategy lead the population to the top of a fitness peak, or would such a strategy necessarily result in accumulation of deleterious mutations on the way? The latter case would be an instance of MA, but the mechanism of accumulation would be linkage to beneficial mutations, and not genetic drift. In other words, if high mutation rate strategies are *imperfect*, there is a *long-term* cost in the form of accumulation of deleterious mutations during adaptation to novel environments.

In this chapter, we use simple simulations to explore the effects of MA in large asexual populations when rare beneficial mutations that confer high fitness advantage are present.

The goal of these simulations is to provide estimates of the deleterious fitness effects of MA and to give an idea of the precision, frequency, and duration of experimental measurements required to observe such effects. It should be emphasized that there is little experimental evidence for *long-term* costs of high mutation rates in large asexual populations (cf. section 1.3.2).

3.2 Details of Simulations

We model an asexual population of constant size N with discrete generations. The genotype of an individual is characterized by three numbers, viz., (1) N_d, the number of deleterious mutations in the genome, (2) N_b, the number of beneficial mutations with small fitness advantage, and (3) N_{rare}, the number of rare beneficial mutations with large fitness advantage. All deleterious mutations have the same effect, s_d. Likewise, the selection coefficients of small beneficial and rare beneficial mutations are s_b and s_{rare} respectively. Epistasis is assumed to be absent, thus the relative fitness of an individual is $w = (1 + s_{rare})^{N_{rare}}(1 + s_b)^{N_b}(1 - s_d)^{N_d}$.

We define M to be the mutator strength, the ratio of the mutation rate of the current population to the wild-type populaiton. $M = 1$ for a wild-type population, and $M > 1$ for mutator populations. Deleterious, small beneficial and large beneficial mutations are generated by independent Poisson processes with means MU_d, MU_b, and MU_{rare} respectively. Each generation consists of three steps:

(1) Selection, where the population of each genotype is multiplied by its fitness, i.e.,

$N_{sel}^{i}(t+1) = \lfloor w_i N^i(t) \rfloor$, where $N^i(t)$ is the population of the i^{th} genotype at the t^{th} generation, w_i is the fitness of that genotype, and $N_{sel}^{i}(t+1)$ is the population of that genotype after the selection phase.

(2) Mutation, where the number of individuals of genotype i that mutate to a genotype j is given by a binomial random variable with parameters $N_{sel}^{i}(t+1)$ and mutation probability p_{ij}. p_{ij} is consistent with deleterious, small beneficial, and rare beneficial mutations arising from independent Poisson processes. After this step, the population of the i^{th} genotype is denoted by $N_{mut}^{i}(t+1)$.

(3) Random sampling to maintain population size, where the population of the i^{th} genotype is given by a binomial random variable with parameters $N_{mut}^{i}(t+1)$ and $N/\sum_i N_{mut}^{i}(t+1)$. At this stage, we obtain $N^i(t+1)$.

In our simulations, $N_d \leq 15$, $N_b \leq 10$ and $N_{rare} \leq 4$. Thus, the relative fitness of the most fit genotype would be $w_{max} = (1+s_{rare})^4(1+s_b)^{10}$. To speed up our simulations, we only consider single and double mutations for step (2) above, and only single rare beneficial mutations. More precisely, there are seven possibilities for an individual in step (2): it can acquire (i) no mutations, (ii) one rare beneficial mutation, (iii) one small beneficial mutation, (iv) one deleterious mutation, (v) two small beneficial mutations, (vi) two deleterious mutations, or (viii) one small beneficial and one deleterious mutation.

In all cases, $U_d = 2 \times 10^{-4}$ per genome per generation, which is the lower limit determined by Kibota and Lynch (Kibota and Lynch, 1996), and $s_d = 0.01$, a value based on the results of Kibota and Lynch (Kibota and Lynch, 1996). Rare beneficial mutations have the following parameters: $s_{rare} = 0.1$ and $U_{rare} = 10^{-9}$ per genome per generation. The rare beneficial mutation rate corresponds to a target size of one base pair in the entire genome. For small beneficial mutations, $s_b = 0.01$, and $U_b = 10^{-5}$ per genome per generation The values of selection coefficients and mutation rates of beneficial mutations have been modeled on the results of Perfeito *et al.*, who looked at the distribution of beneficial mutations in long-term cultures in LB medium (Perfeito et al., 2007).

3.3 Mutation Accumulation in Large Populations

Consider a large asexual population which is at a fitness peak, i.e., there are no beneficial mutations which can improve the mean fitness of the population ($U_b = U_{rare} = 0$). As discussed in section 1.2.1, in such cases, a mutation selection balance is established in which the mean fitness depends only on the fitness of the most fit genotype in the population and the deleterious mutation rate. In the particular case of the model presented in section 3.2, the equilibrium distribution is given by $f_{N_d} = \frac{1}{N_d!} e^{-MU_d/s_d} \left(\frac{MU_d}{s_d}\right)^{N_d}$ where f_{N_d} is the fraction of individuals with N_d deleterious mutations and the most fit genotype has a relative fitness of 1 (Haigh, 1978). In Figure 4, the distribution of deleterious mutations is depicted for some values of mutator strength M. As expected, the population harbors greater number of deleterious mutations with increasing M. In fact, for sufficiently high mutation rates ($M > s_d/U_d$), the mode of the distribution (i.e., the

value of N_d which maximizes f_{N_d}) no longer corresponds to the fraction of the population with zero deleterious mutations.

In the presence of beneficial mutations, however, the mean fitness of the population keeps increasing till all such mutations have been acquired and a new mutation-selection balance is established. If beneficial mutations with large fitness effects are present, these will rapidly sweep through the population once they are generated. Since such mutations are expected to be rare, the fraction of the population which generates them is likely to be small. When the beneficial mutation becomes fixed, the entire population would be composed of the progeny of these small number of chance mutants. Thus, even though the total population can be large, sweeps of beneficial mutations with large fitness effects can constitute a population bottleneck.

Asexual populations can be forced to accumulate deleterious mutation by forcing them through small population bottlenecks (cf. section 1.3.2). Can the presence of beneficial mutations with large fitness effects also have similar consequences even when populations are large? We explored this question using simulation as described in section 3.2 (Figure 5). For each simulation run, we examined the mutation-selection equilibrium that is established after all beneficial mutations have been fixed and asked whether the most fit genotype in the population has zero or non-zero number of deleterious mutations. In the former case, we called the run *perfect* as the mean fitness of the population at equilibrium is as high as it can be. Figure 5A shows some representative mean fitness trajectories for three different values of mutator strength. When a run is *perfect*, the mean

fitness converges to $w_{max}e^{-MU_d}$, where w_{max} is the relative fitness of the most fit genotype (the genotype with all beneficial mutations but with zero deleterious ones). For $M = 1$, all simulation runs were *perfect*, whereas the fraction of *perfect* runs decreased to ~40% for $M = 200$ (Figure 5A inset). When looking at high mutation rate as an adaptive strategy, these results suggest that there is a *long-term* cost in the form of accumulation of deleterious mutations during adaptation to novel environments.

One of the motivations for the simulations was to give an idea of the precision, frequency, and duration of experimental measurements required to observe deleterious effects of high mutation rate. If one looks at simulation runs with $M = 200$, there are signatures of fixation of deleterious mutations within ~1000 generations (Figure 5B). The fact that the different mean fitness trajectories do not converge to the same level points to the accumulation of deleterious mutations. From an experimental point of view, deleterious effects would be most pronounced and manifested in the fewest number of generations if one used strong mutators ($M \sim 200$).

The detection of the deleterious effects, however, poses several experimental challenges. First, it should be emphasized that the fitness effects of deleterious mutation accumulation are quite small (~1%). The experimental recording of mean fitness trajectories as in Figure 5 would necessitate precise and frequent (~once/generation) fitness measurements over periods as long as ~1000 generations. Second, we have assumed that all rare beneficial mutations offer the same advantage; there is no variability in fitness trajectories on account of fixation of beneficial mutations with different effects.

In this context, it is pertinent to note that mutators in practice do not behave like ideal mutators and do not uniformly increase the mutation rate across the entire genome. All mutators have a spectrum, and tend to have elevated levels of certain specific kinds of mutations. In the case of very rare mutations, if the mutation that yields the fitness benefit is within the spectrum of the mutator, the beneficial mutation is acquired with the mutator rate, otherwise it is acquired only at the wild-type rate and there might be other beneficial mutations with large effect that are generated more frequently. Nevertheless, there is some evidence that in large populations ($10^{10} - 10^{11}$), mean fitness trajectories are quite reproducible, i.e., mutations of the same effect get fixed in the same order in independent experiments (Wick et al., 2002).

In spite of the difficulties mentioned above, there are some general merits in obtaining high precision, high frequency, mean fitness trajectories. First, they can be used to test whether the reproducibility of fitness trajectories in large populations breaks down when measurements are done with greater precision and frequency. Second, even if deleterious effects of high mutation rate are not resolved, mean fitness trajectories can aid in the development of empirical models for describing the adaptation process in large asexual populations. Finally, mean fitness trajectories with mutators of different strength can complement our knowledge of the short-term advantage of mutators, which is primarily based on competition-based experiments (cf. 1.3.2), and perhaps shed greater light on the hitchhiking of mutators with beneficial mutations.

3.4 Summary

We have used simulations to explore the possibility that deleterious mutations can be accumulated in large asexual populations. At high mutation rates ($M \sim 200$), at least one deleterious mutation was fixed in around 60% of the simulation runs. Although this phenomenon can be seen in simulations, it would be quite challenging to demonstrate it experimentally in view of the small effects involved. At the very least, it requires the ability to record mean fitness trajectories of large populations ($\sim 10^9$) with high precision (~1%), high frequency (~1 fitness measurement/generation) and over long times (~1000 generations).

Figure 4. Distribution of deleterious mutations at mutation-selection equilibrium. In the absence of beneficial mutations ($U_b = U_{rare} = 0$), populations achieve a mutation-selection equilibrium in which the fraction of the population harboring a given number of deleterious mutations remains fixed. For the case of $U_d = 2 \times 10^{-4}$ per genome per generation and $s_d = 0.01$, the fraction of population with N_d deleterious mutations $\left(f_{N_d}\right)$ is plotted as a function of N_d at indicated mutator strengths. Crosses mark the mode of the distribution for each mutator strength.

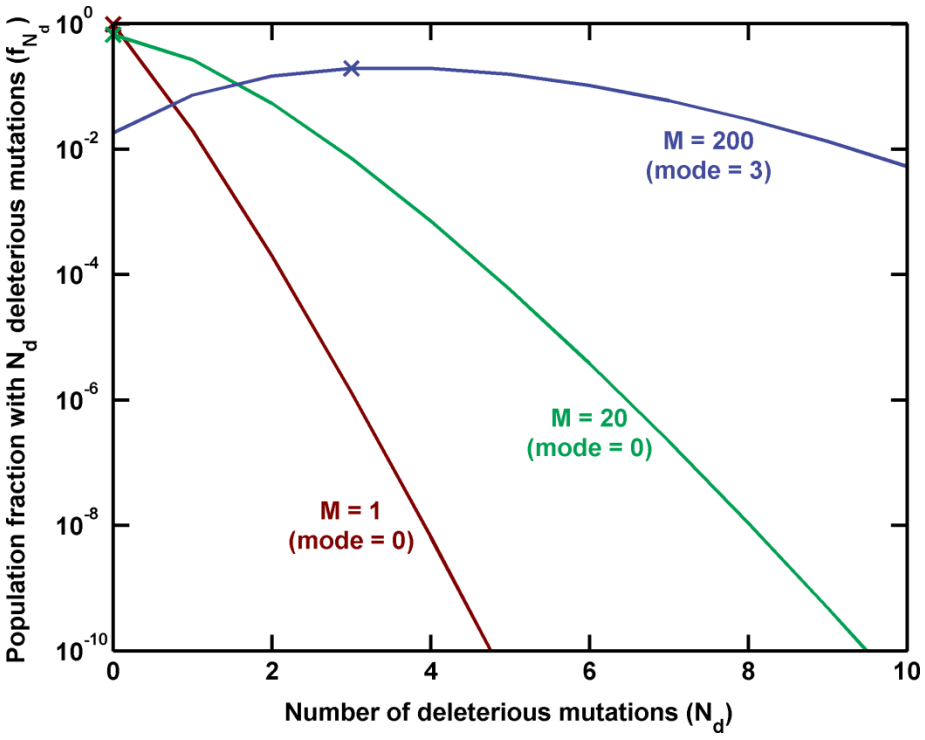

Figure 4. Distribution of deleterious mutations at mutation-selection equilibrium.

Figure 5. Mean fitness trajectories show fixation of deleterious mutations at high mutation rates. Simulations were performed with $N = 10^9$, $U_b = 10^{-5}$ per genome per generation, $s_b = 0.01$, and with indicated values of mutator strength (M). Rare beneficial mutations with $s_{rare} = 0.1$ and $U_{rare} = 10^{-9}$ were present in each simulation with their maximum number being four. U_d was set to 2×10^{-4} per genome per generation, with $s_d = 0.01$. At time zero, the population consisted entirely of individuals with zero deleterious mutations and zero beneficial mutations. 100 simulation runs were carried out for each value of M for a period of 3500 generations. (A) Mean fitness trajectories for five representative simulation runs for each value of M. The dashed horizontal line represents the mean fitness at mutation-selection equilibrium in the absence of fixation of deleterious mutations. For $M > 1$, the realized mean fitness at mutation-selection equilibrium is sometimes lower than the horizontal dashed line, implying that deleterious mutations were fixed in these runs. The inset displays the fraction of simulation runs in which no deleterious mutations were fixed (i.e. *perfect* runs) as a function of M. When $M = 200$, only ~40% of the runs are *perfect*. (B) Magnification of the representative mean fitness trajectories displayed in panel A for $M = 200$. The mean fitness during the first 1000 generations is plotted for each run.

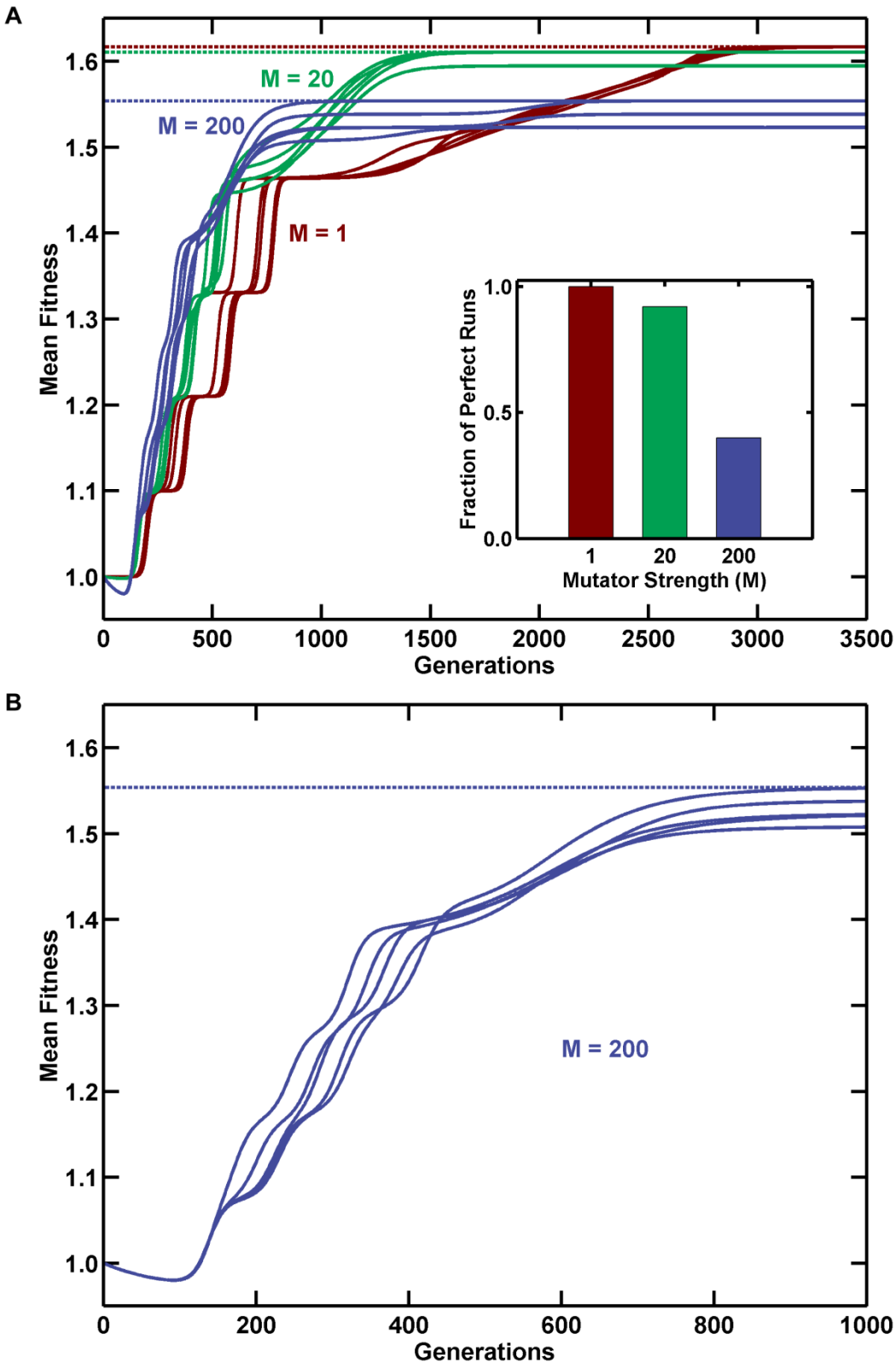

Figure 5. Mean fitness trajectories show fixation of deleterious mutations at high mutation rates.

Chapter 4. Bioluminescence-based High Precision Measurement of Growth Rates

4.1 Motivation

The long-term culture of microorganisms has proved to be a very useful tool for studying evolutionary phenomena in the laboratory (section 1.2.2). Many such laboratory evolution investigations involve measurement of mean fitness trajectories (or the distribution of fitness) of the population over the course of the experiment (Desai et al., 2007; Lenski et al., 1991). For such experiments, there are three main requirements: the ability to monitor populations over long periods of time from around 100 to over 10,000 generations (Chao and Cox, 1983; Lenski and Travisano, 1994), and the feasibility of measuring fitness both frequently and precisely. Development of an apparatus that can achieve these goals can therefore prove quite beneficial for laboratory evolution experiments.

In Chapter 3, we saw that detection of deleterious effects of high mutation rates in large asexual populations necessitated the measurement of mean fitness of large populations of bacteria ($\sim 10^9$) over a period of ~1000 generations with a precision of ~1%. The primary motivation of our work was to build a device that was capable of performing such measurements. Both frequency and precision of fitness observations have proven to be useful in independent contexts. For example, frequent measurements have resolved phenomena such as the presence of discrete jumps in fitness or correlates of fitness

(Lenski and Travisano, 1994). Precise measurements are required to resolve small fitness differences as in the case of the mutation load suffered by a *mutS* mutator strain well-adapted to its environment, estimated to be around 1% by Boe *et al.* (Boe *et al.*, 2000). Simultaneous high precision and high frequency measurements, however, can be quite challenging as the two considerations which are often at odds with each other (see section 1.4.1).

In section 1.4, exponential growth was presented as a paradigm that is ideally suited for the laboratory evolution experiments. The advantages of bioluminescence-based growth rate measurements were also presented there. Previous work in our laboratory had shown that bioluminescence-based measurements of growth rate could achieve a precision of 5% (Kishony and Leibler, 2003). However, as described, the measurement duration in the experiments of Kishony and Leibler was long (~10 generations or ~3 hours in rich media), a potential impediment for high frequency measurements. Nevertheless, this was a promising starting point for us to build an apparatus for long-term, high precision and high frequency recording of growth rates. This chapter details the steps taken to extend Kishony and Leibler's measurements to a long-term regime with improved precision and frequency.

4.2 Apparatus Design and Operational Concerns

The design of our apparatus is depicted in Figure 1 and described in detail in section 2.1. While sharing some features with previously described bioreactors and continuous culture devices for culturing luminescent organisms (Picart et al., 2004; Pooley et al.,

2004), the operation of our apparatus has been optimized for high frequency, high-precision growth rate measurements. In this section, some of the design choices for the apparatus as well as the procedure for operating the apparatus (cf. section 2.1) are explained.

Reproducibility of growth rate measurements is influenced by environmental factors such as temperature and pH. The growth rate of *E. coli* is sensitive to temperature, with the sensitivity being the least between 37°C and 42°C (Ingraham and Marr, 1996). For this reason, growth rates were measured in this temperature range. In addition, to minimize the effects of temperature fluctuations on growth rate measurements, a circulating water bath was used. The temperature stability of the water bath was determined to be 0.05°C which included a slight drift correlated with ambient temperature. The effects of adding pH buffers to the medium were also investigated, but no positive effects were found (data not shown).

Another concern for precise growth rate measurements is the potential for artifacts resulting from trace chemical contaminants. In our apparatus, leaching of chemicals from the tubing and spallation of peristaltic pump tubing could perturb the chemical composition of the culture medium. It has been reported that peroxide-cured silicone tubing can be toxic to plant cell cultures while platinum-cured silicone is biocompatible (Park et al., 2005). To minimize such effects, we chose low-spallation, long-life peristaltic pump tubing (Pharmed® BPT) and tubing with low extractable content for the rest of the set up (Dow Corning® Pharma-65). There could be some leaching of

chemicals from the Pharmed® BPT tubing, but our results indicate that this is not much of a concern (cf. section 4.4.3).

Growth rate reproducibility may also be limited by the intrinsic physiological state of the cells used to inoculate the culture. It is conceivable that the initial inocula differ in some physiological parameter which has a heritable effect on growth rates. One example of such a parameter could be the age of the old pole of a newly divided cell (Stewart et al., 2005). To buffer the effects of physiological heterogeneity, ten colonies were picked for the initial inoculum of our cultures (cf. section 2.1).

Mechanical aspects of the device can also introduce subtle artifacts. For instance, the placement of the PMT module above the culture vessel rendered the apparatus susceptible to glitches (sudden increases in luminescence signal) resulting from splashing of luminescent culture in the direction of the PMT sensor. Glitches were more pronounced in new glass vessels, and therefore vessels were "aged" before use by filling them with distilled water and subjecting them to vigorous stirring for about a week. Glitching was essentially eliminated by reducing the stirring speed in both batch and long-term cultures to less than 50 rpm and using 125 ml as culture volume.

While the factors mentioned above would tend to improve growth rate reproducibility, it was also desirable to achieve high intrinsic measurement precision (cf. section 1.4.1). Preliminary results in batch cultures revealed that the bioluminescence of the bacterial strain was sufficient to be measured by the analog PMT module without the need for

optics to increase the collection of light. To improve intrinsic measurement precision, the voltage generated by the current output of the PMT across a 1MΩ resistor was measured by the digital multimeter with its integration time set to its highest value (100 power line cycles). Although the long integration time made the duration between successive readings as long as 3.4 s, the sampling rate was more than adequate for measuring growth rates (typical generation times of ~18.5 min).

4.3 Batch Culture Results

4.3.1 Identification of medium with best growth rate reproducibility

We began our pursuit of high frequency, high precision growth rate measurements by exploring the possibility that higher growth rate reproducibility may be achieved in a culture medium other than the one used by Kishony and Leibler. We therefore measured the precision of growth rate measurements in different minimal media with glucose or lactose as the sole carbon source as well as the original medium used by Kishony and Leibler (a glucose minimal medium supplemented with casamino acids, methionine, and thiamine). In addition, we also tried LB (rich medium). Growth rate reproducibility was quantified by setting up multiple batch cultures in the same medium and evaluating the ratio of the difference between the maximum (λ_{max}) and minimum growth rate measurements (λ_{min}) to the minimum measurement, i.e., reproducibility $\equiv (\lambda_{max} - \lambda_{min})/\lambda_{min}$.

We found that reproducibility in minimal media ranged from 3.5% in Kishony and Leibler's medium to 9% in unsupplemented glucose minimal media, whereas it was

much better (<2%) in LB (Figure 6 and data not shown). Figure 6 is representative of the results we obtained in our search for the ideal culture medium. Multiple batch cultures of the non-adherent luminescent *E. coli* strain NS2 pCSλ (see section 2.1) were set up in the same medium at a temperature of 38.3°C. The growth curves obtained with glucose minimal medium, lactose minimal medium and LB are shown in Figures 6A, 6C, 6E respectively. In order to appreciate the variation in the growth curves, it is useful to plot the "slope curves," the derivative of the growth curve as a function of luminescence signal (Figures 6B, 6D, 6F and section 2.1). It is evident from Figure 6 that slope curves in LB are much flatter and more reproducible that those obtained in other media. We therefore chose LB as the medium for our experiments.

4.3.2 Identification of operating region for precise measurement of growth rates in LB

Having established LB as the medium of our choice, we wanted to further characterize the precision of growth rate measurements in LB. In particular, since LB broth is chemically undefined, we wanted to evaluate reproducibility across different lots of the medium. We set up batch cultures of NS2 pCSλ in different lots of LB at a temperature of 38.3°C. The resulting growth curves are shown in Figure 7A and the corresponding slope curves are shown in Figure 7B. Note that the slope curves in Figure 7B are over a broader region (0.1 mV to 70 mV) than those shown in Figure 6F (0.5 mV to 12 mV).

The typical slope curve is relatively flat until the luminescence signal reaches about 20 mV, and then shows a precipitous drop. Lot-to-lot variability is evident in Figure 7B as slope curves corresponding to batch cultures with the same lot of medium show a similar

trend. The variability, however, decreases as the average luminescence signal of the region of the growth curve used to measure growth rates increases.

For LB medium, we identified the region between 2.65 mV and 7.00 mV to be conducive towards precise growth rate measurements over long-term (Figure 7, dashed magenta lines). In this operating region, the average luminescence signal is high enough that effects of lot-to-lot variability are small (Figure 7D, total spread of ~1.1%), while it is low enough to avoid the region where slope curves drop sharply. In fact, growth curves within the operating region (Figure 7C) are well described as straight lines (linear correlation coefficient $r > 0.9998$). The operating region spans ~1.4 generations of growth and NS2 pCSλ takes ~26 minutes to traverse it. Thus, in the operating region, growth rates can be determined both quickly and precisely. It should be noted that our growth rate measurements are not limited by intrinsic measurement precision, i.e., the precision with which luminescence is measured. The estimated spread in growth rates on account of such errors is only 0.3% in the case of Figure 7D (Appendix B).

4.3.3 Temperature dependence of growth rates

In order to demonstrate the ability of the apparatus to detect subtle changes in growth rates, we examined the sensitivity of the growth rate to systematic changes in temperature. Batch cultures were set up in the same lot of medium at five different temperatures centered around the usual operating temperature of 38.3°C. The growth curves and the corresponding slope curves are shown in Figures 8A and 8B respectively. In the operating region (dashed magenta lines in Figure 8, growth curves in Figure 8C), we observe a strong negative correlation between the observed generation time and the

culture temperature (Figure 8D, $r = -0.993$). We find that the generation time decreases by ~1.3 minutes(~7.0%) over a temperature increase of 1.2°C, giving a temperature sensitivity of ~5.8%/°C. This is comparable to the temperature sensitivity of 6%/°C estimated from empirical square-root models of temperature dependence of growth rate of *E. coli* (Ratkowsky et al., 1982) and only slightly lower than the estimate of 7%/°C obtained by extrapolating Arrhenius-type models (Ingraham and Marr, 1996) that describe temperature dependence in the normal temperature range (21˚C to 37˚C, see Appendix A). Owing to this temperature sensitivity, a long-term growth rate measurement precision of around 1% would require a temperature stability of ~0.15°C.

4.4 Long-Term Culturing

Having established optimal growth conditions in batch cultures, we proceeded to optimize the set up for high frequency, high precision measurements of growth rates over long-term.

4.4.1 Requirement of non-adherent strains

Our first attempts at long-term culture showed that wild type *E. coli* strains such as MG1655 readily formed biofilms on the surface of the glass vessel at the liquid-air interface within a few hours of inoculation. For example, when the wild-type strain MG1655 was cultured using the luminostat protocol (described in section 4.4.2), the output pump failed to reduce the luminescence signal of the culture even when operating at maximum speed after five hours of the culture reaching the luminescence setpoint (Figure 9A and 9C). This suggested that cells were adhering to the vessel walls and could not be diluted out.

The adhesion property rendered wild-type strains unsuitable for long-term culture. However, we found that HEHA16, an *E. coli* strain lacking type 1 fimbriae and the autoaggregation mediating protein Ag43 (Kjargaard et al., 2000), behaved like a non-adherent strain and could be used for long-term culture. We also constructed a non-adherent variant of MG1655 as described in section 2.1. This strain, which we called NS2, can also be used for long-term culturing.

4.4.2 Optimization of the dilution protocol

In order to maintain cultures in the operating region (section 4.3.2), it is necessary to adopt some kind of dilution protocol to remove cells from the culture and to add fresh medium. In this section, we describe the process of development of the dilution protocol that was ultimately used in high frequency, high-precision measurements.

Luminostat protocol

The natural way to maintain cultures in the operating region is by continuously modulating the input and output flow rates so as to keep culture luminescence at a fixed setpoint. This is the idea behind the luminostat protocol which is schematically illustrated in Figure 10A (the luminescence profile in an actual experiment is shown in Figure 9B). The basic equation describing the population size in a luminostat is:

$$\frac{1}{L}\frac{dL}{dt} = \frac{1}{N}\frac{dN}{dt} = \left(\lambda - \frac{F_O}{m}\right) \qquad (1)$$

where N is the population size, L is the luminescence signal, λ is its growth rate, F_O is the output flow rate (mass per unit time) and m is the mass of the culture. In principle, the dilution rate in the luminostat protocol can be used as a continuous readout of the growth, since at constant luminescence, $\lambda = F_O/m$. This idea has been demonstrated in the case of turbidostats using optical density measurements instead of luminescence (Anderson, 1953).

Note that while F_O can be measured in our apparatus by means of the output precision balance (Figure 1), there is no way of measuring m directly in our apparatus. At the time of starting the experiment, m can be set to a known value. Subsequently, however, in order to record growth rates, one either has to assume that m is constant, or one has to estimate changes in m based on the measurements of input (F_I) and output flow rates. Assuming that mass of medium in the setup is conserved, changes in m $\left(\Delta m^{est}\right)$ are given by:

$$\Delta m^{est} = \left(F_I - F_O\right)\tau \tag{2}$$

where τ is the time interval over which the quantities F_I and F_O are measured. The estimated culture mass then becomes $m^{est} = m_0 + \Delta m^{est}$, where m_0 is either the initial known value of the culture mass or the previous mass estimate.

For the luminostat protocol to work, it is necessary that m^{est} be an accurate estimate of the culture mass. We set up mock runs using the luminostat protocol (see section 2.1) to evaluate whether this was indeed the case. Unfortunately, the difference between the actual culture mass (as measured by a precision balance) and m^{est}, referred to as

discrepancy, shows a steady negative drift (Figure 11). This result can be qualitatively understood by accounting for mass loss due to evaporation. Although the drift is slow, it renders the luminostat protocol unsuitable for high precision measurements over long times.

Rapid serial dilution protocol

The solution to the mass estimation problem is to measure growth rates in the absence of dilutions, i.e., with $F_O = 0$. In this case, equation 1 simplifies to $\frac{1}{L}\frac{dL}{dt} = \frac{1}{N}\frac{dN}{dt} = \lambda$, allowing measurement of growth rates without the need for mass estimates. For such measurements, the dilution protocol would consist of a growth phase, where the growth rates are measured in the absence of dilutions, and a dilution phase, where the cultures are diluted to maintain them in the operating region. To achieve the highest frequency of growth rate measurements, one would like to perform the dilutions at the maximum speed possible, and this leads to the rapid serial dilution protocol (Figure 10B). In this protocol, dilutions are performed by pumping out *M* grams (usually 40.0-55.0g) of culture at maximum speed, and then adding the same amount of fresh medium, again at maximum speed.

The problem with the rapid serial dilution protocol is that it induces large temperature fluctuations in the culture. The temperature inside the enclosing box (Figure 1) in our setup is higher than the ambient temperature as the stirrer is a source of heat, and the box is made of insulating material. Consequently, there is a temperature difference between the input reservoir (which is at ambient temperature) and the box temperature so that

supply of medium from the input reservoir increases the culture temperature (Figure 12A). In the case of the rapid serial dilution protocol, the temperature increases by as much as 0.3°C, which is unacceptable (cf. section 4.3.3). Either as a direct consequence of the temperature fluctuations or because of the rapidity of the dilutions, growth curves recorded with this protocol in the growth phase are not linear, but show reproducible kinks (Figure 12B). The kinks make the task of measuring growth rates difficult.

High precision dilution protocol

To devise a serial dilution protocol which did not have the problems associated with the rapid protocol presented above, we performed several mock runs with different dilution protocols and recorded the temperature fluctuations. At the same time, we also tried to improve the ventilation of the enclosing box and fine tuned several parameters including the temperature of the water bath (the main reason why cultures are performed at 38.3°C). We found that it is better to operate input and output pumps simultaneously, and to have a multi-phased dilution process (instead of a single, rapid dilution). The result of these optimizations was the development of the protocol that we used for long-term, high precision measurement of growth rates. This protocol is schematically illustrated in Figure 13A and the temperature fluctuations in it are shown in Figure 13B.

The protocol for high precision measurements has four dilution phases: (1) a fast-dilution phase where the signal is reduced from the high setpoint (7.00 mV) to the low setpoint (2.65 mV), (2) an intermediate-dilution phase, where the signal is further reduced to 2.00 mV, (3) a slow-dilution phase, where the signal is allowed to recover to the low setpoint,

and (4) a no-dilution phase (equivalent to the growth phase), which lasts until the signal reaches the high setpoint again. Dilutions were performed by adjusting input and output pump RPMs so that predicted flow rates in different phases would be as follows: fast-dilution, 12.5 g/min; intermediate-dilution, 7.5 g/min; slow-dilution, 1.88 g/min; and no-dilution, 0 g/min. One of the main considerations in the design of the protocol was to ensure that the slow-dilution phase lasted at least 10 minutes (the time constant for the equilibration of the temperature of culture in the absence of dilutions is around 3 minutes, 10 minutes ~ 3 time constants). During the dilution phases, both pumps were operating simultaneously, and so culture mass should remain the same. In practice, however, there were differences between the realized flow rates and the predicted flow rates. To correct for culture mass changes accruing from these differences, the input flow rate was modulated from the nominal value of 12.5g/min during the fast-dilution phase.

Figure 14A shows growth curves recorded using the optimized protocol. The growth curves during the no-dilution phase do not have any kinks.

4.4.3 High precision measurement of growth rates in long-term cultures

Long-term cultures of NS2 pCSλ were performed using the optimized dilution protocol described in the previous section. Figure 14B displays the observed generation time as a function of time after inoculation during such a culture. When a new media reservoir is put in place of an old one, there is often a transient period lasting one or two dilution cycles, where the observed generation time is substantially different from the generation time observations in the remaining dilution cycles with that reservoir. If such transient points are omitted from the evaluation of the spread of generation time observations, then

it is possible to achieve a precision of 2% over a period of ~75 generations (Figure 14B). Overall, if we pool all generation time measurements in the operating region in both batch cultures and long-term cultures (Figures 7D and 14B) and exclude transient long-term culture measurements, we find that they lie between 18.25 and 18.75 minutes (0.5 minute total spread), giving a precision of ~2.7%. The intrinsic measurement precision, on the other hand, for measurements in the operating region is only 0.3% (Appendix B), underscoring the fact that we are not limited by instrument precision in our measurements.

The optimized dilution protocol sets the time resolution of growth rate measurements. For cultures of NS2 pCSλ in LB medium, the average time between the end of one no-dilution phase (the phase in which growth rate is measured) and the beginning of the subsequent no-dilution phase is ~39 minutes. Given that each no-dilution phase lasts around 26 minutes, the dilution protocol results in a growth rate measurement resolution of ~65 minutes (~3.5 generations).

4.5 Summary

We have built a device capable of long-term recording of growth rates with high frequency (~3.5 generations) and high precision (~2.7%). We identified LB as the medium offering the most reproducible growth rate measurements and delineated a small region of the growth curve (operating region) in LB as most conducive to high precision measurements. Although we observed lot-to-lot variability in the measurement of growth rates with LB, we could achieve a precision of ~1.1% in the operating region. To achieve

similar levels of precision in long-term measurements, we developed an optimized serial dilution protocol that maintains cultures close to the operating region, while minimizing temperature fluctuations. Overall, we found that all growth rate measurements (batch and long-term cultures) performed in the operating region lie within a 30 second window (between 18.25 and 18.75 minutes) corresponding to a total spread of ~2.7%. The estimated spread from intrinsic measurement errors in this region, on the other hand, is only 0.3% (Appendix B), thus their contribution to the observed spread (2.7%) is small.

Figure 6. Growth curves and slope curves in batch cultures of NS2 pCSλ in different culture media. Batch cultures of NS2 pCSλ were set up in indicated media and growth curves (A, C, E) and corresponding slope curves (B, D, F) were plotted as described in section 2.1. Slope curve in panels B,D, and F were plotted for the region between the horizontal dashed gray lines (0.5 mV to 12 mV) in the growth curves. Batch cultures in glucose and lactose minimal media were performed with the same lot of medium, whereas different lots were used in the case of LB. Reproducibility is the best in LB cultures (see Figure 7).

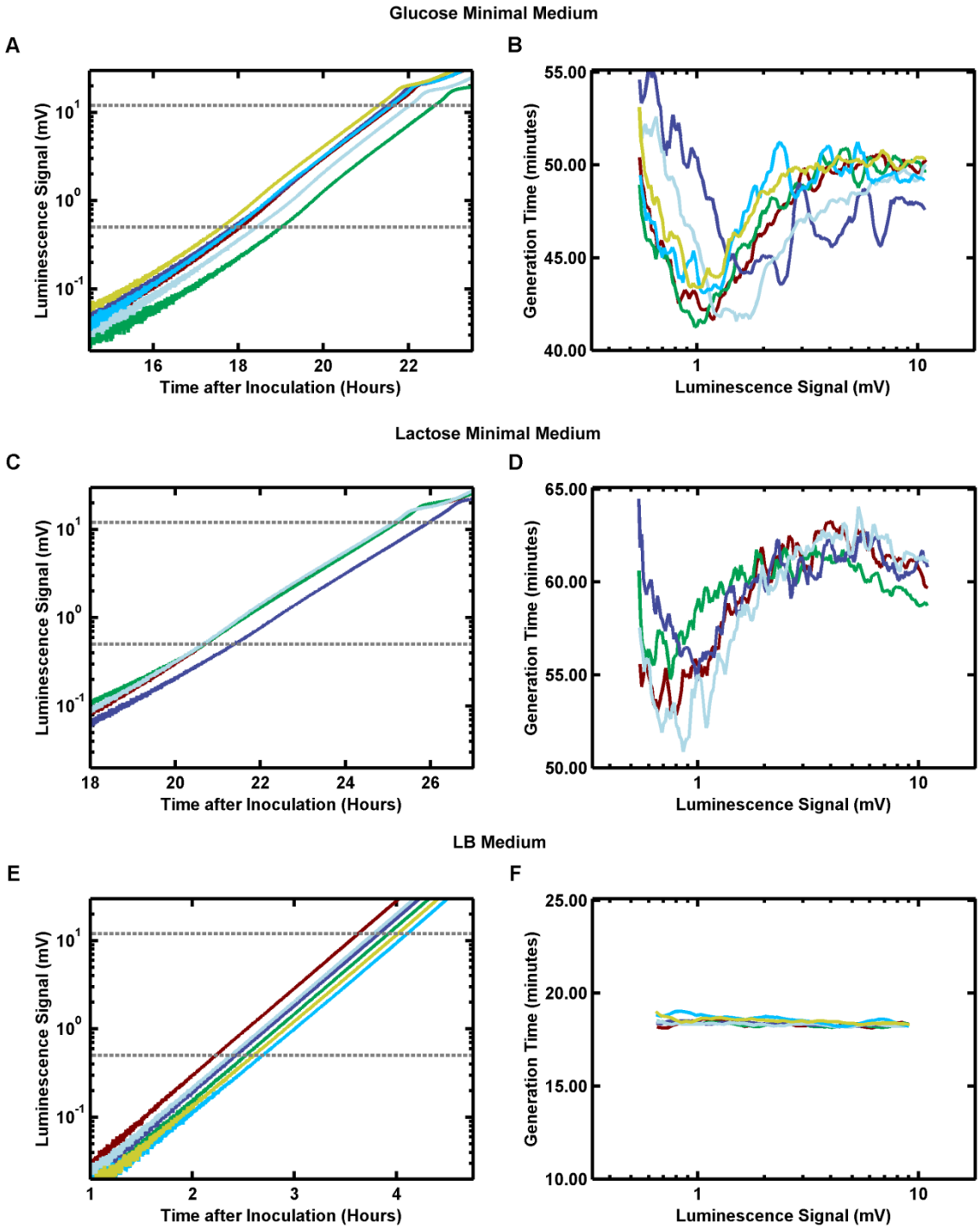

Figure 6. Growth curves and slope curves in batch cultures of NS2 pCSλ in different culture media.

Figure 7. Growth curves and slope curves in batch cultures of NS2 pCSλ in different lots of LB. Batch cultures of NS2 pCSλ were set up over a period of 8 days in different lots of the medium (Lot A, B, or C) and growth curves (A) and slope curves (B) were plotted as described in section 2.1. The slope curve in panel B was plotted for the region between the horizontal dashed gray lines (0.1 mV to 70 mV) in panel A. The operating region chosen for our setup in indicated by the dashed magenta lines (2.65 mV to 7.00 mV) and a magnification of the growth curves in the operating region is shown in panel C. In panel D, the generation time measurements in the operating region are plotted against the lot of the medium. The numbers (1-6) in panels C and D indicate the sequence in which batch cultures were set up. Error bars correspond to the estimated intrinsic measurement error ($\pm 2\sigma_{slp}$, equation 0 of Appendix B).

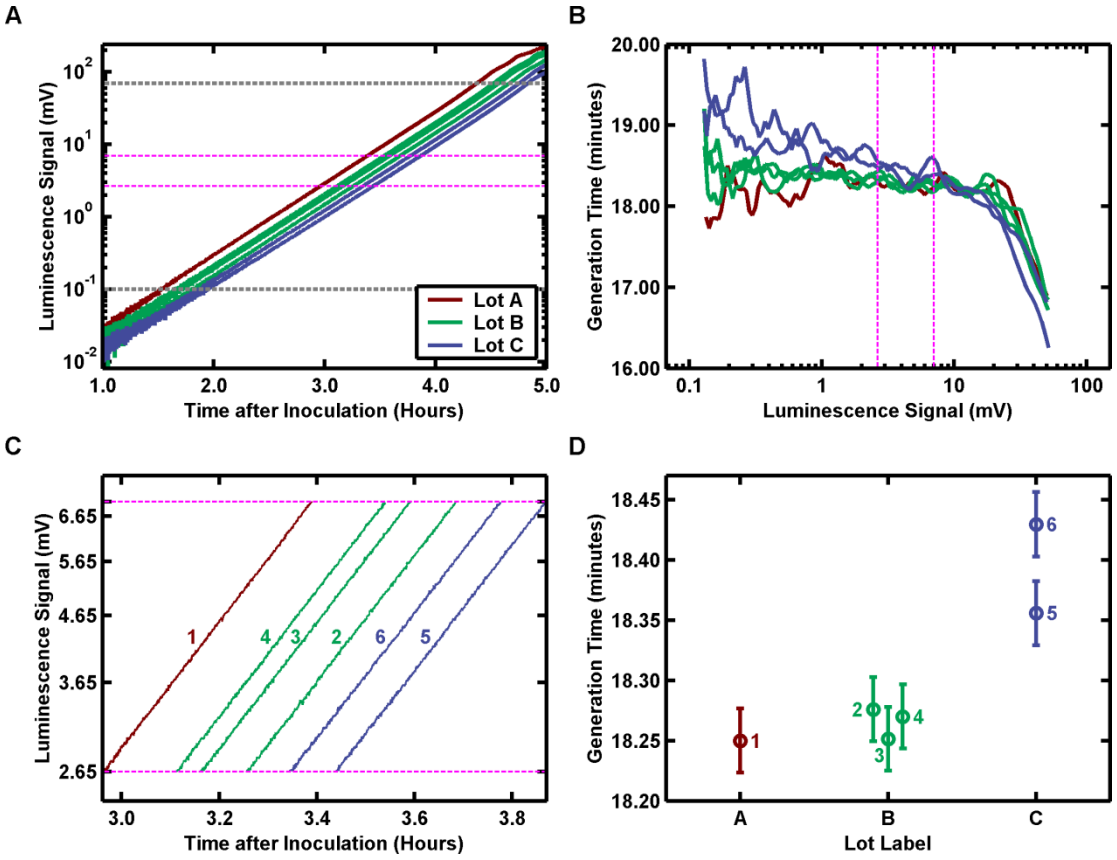

Figure 7. Growth curves and slope curves in batch cultures of NS2 pCSλ in different lots of LB.

Figure 8. Temperature dependence of growth curves and slope curves in batch cultures. Batch cultures of NS2 pCSλ were set up at indicated temperatures in the same lot of medium and growth curves (A) and slope curves (B) were plotted as described in section 2.1. The slope curve in panel B was plotted for the region between the horizontal dashed gray lines (0.1 mV to 70 mV) in panel A. Dashed magenta lines in panels A, B, and C indicate the operating region (2.65 mV to 7.00 mV) and a magnification of the growth curves in the operating region is shown in panel C. In panel D, the generation time measurements in the operating region are plotted as a function of temperature. The black dashed line depicts the least squares linear fit and the corresponding linear correlation coefficient is indicated. Error bars correspond to the estimated intrinsic measurement error ($\pm 2\sigma_{slp}$, equation 0 of Appendix B).

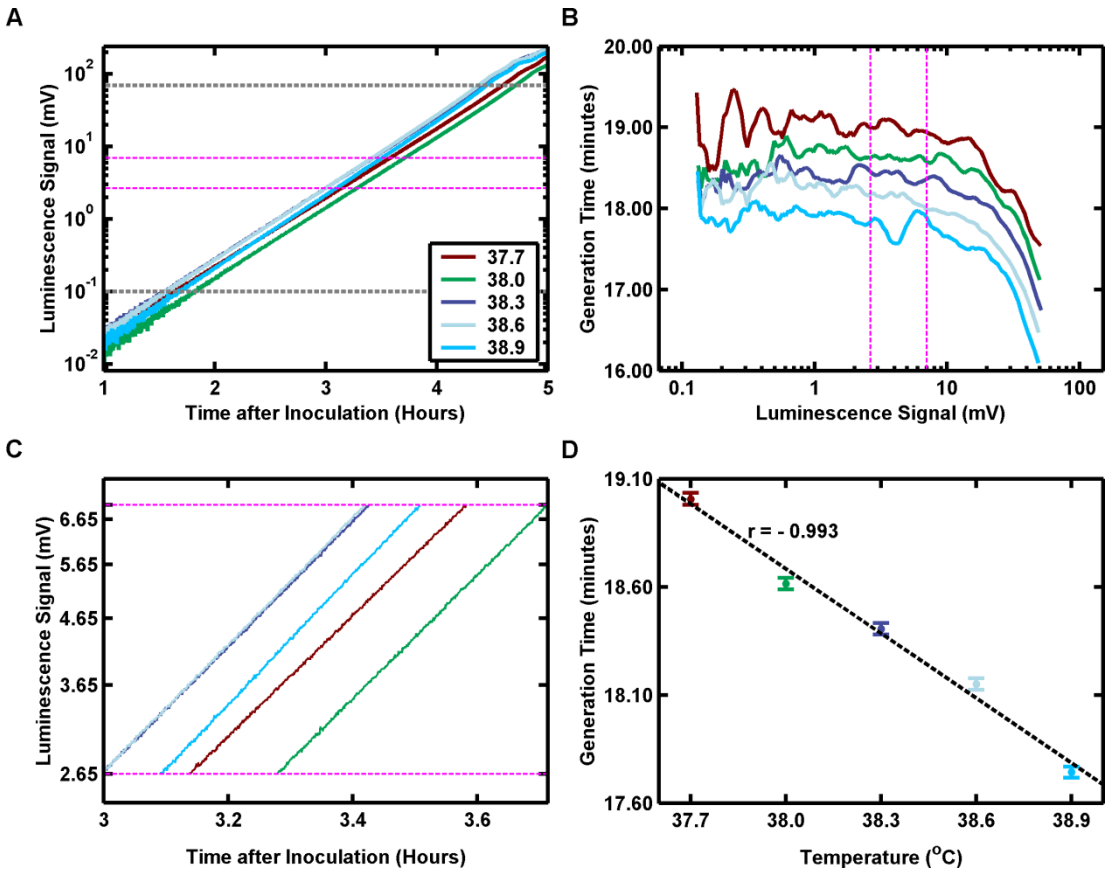

Figure 8. Temperature dependence of growth curves and slope curves in batch cultures.

Figure 9. Long-term cultures require the use of non-adherent strains. A long-term culture was set up with wild-type MG1655 strain transformed with luminescence plasmid pCSλ using the Luminostat protocol (Figure 10A). (A,B) Difference between culture luminescence and the luminescence setpoint, expressed as percentage of the setpoint. Panel B is a magnification of panel A during the first few hours where steady luminescence could be maintained.(C) Pump speed during the luminostat phase. Arrows indicate the time when the pump reached maximum speed. Culture luminescence continued to increase even when pumps were operating at maximum speed, suggesting that cells were adhering to the vessel walls and could not be diluted out.

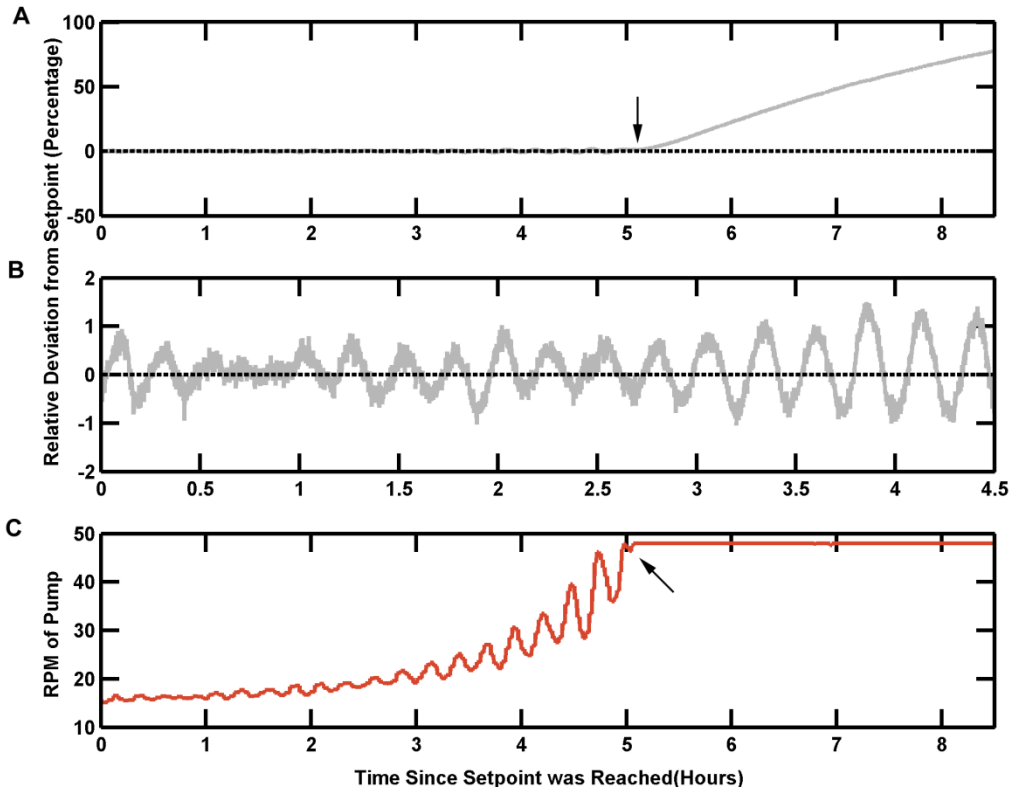

Figure 9. Long-term cultures require the use of non-adherent strains.

Figure 10. Schematic illustrations depicting dilution protocols for long-term cultures. (A) *Luminostat protocol*. The protocol consists of two phases, an initial phase where the culture is allowed to reach a luminescence setpoint, and a luminostat phase where the dilution rate of the pumps is continuously modified to keep the total luminescence constant. Both input and output pumps operate simultaneously and at the same flow rate. (B) *Rapid serial dilution protocol*. After an initial phase, the protocol consists of periodic dilution/growth cycles. In each cycle, the output pump first operated at maximum speed to remove M grams of culture. Next, the input pump flows in M grams of fresh medium at full speed. Finally, in the growth phase, the pumps are stationary, while the bacteria grow to reach the setpoint again. Growth rates are measured in the phase where there is no dilution.

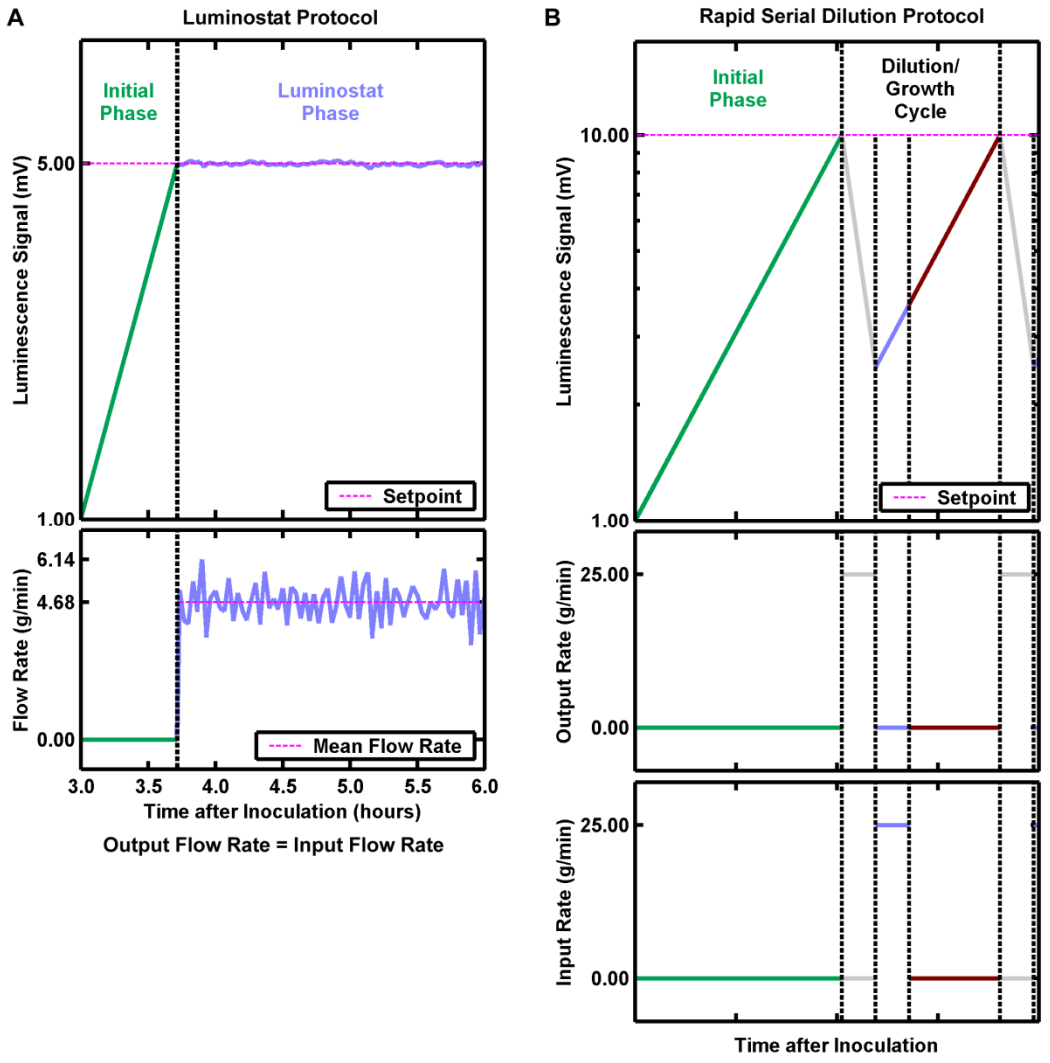

Figure 10. Schematic illustrations depicting dilution protocols for long-term cultures.

Figure 11. Discrepancy between estimated and actual mass of culture as a function of time during a mock run with the luminostat protocol (Figure 10**A).** A mock run was performed using the luminostat protocol with water as the fluid to assess the mass stability of the culture (section 2.1). The culture vessel was filled with 100.0g of water and the input and output pump speeds were modulated to maintain a constant flow rate. Culture mass was estimated by correcting for differences between measured input and output flow rates (section 4.4.2). Actual mass was measured by replacing the stirrer in Figure 1 with a precision balance. The difference between the estimated and the actual mass is referred to as discrepancy and shows a steady negative drift, possibly because of evaporative losses.

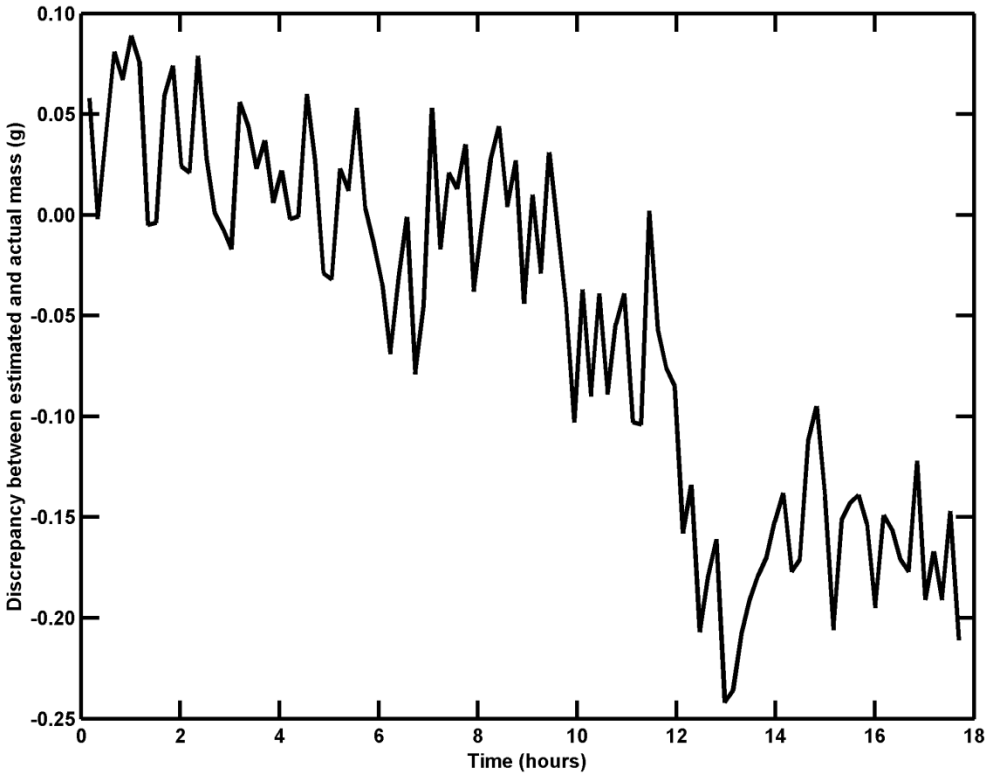

Figure 11. Discrepancy between estimated and actual mass of culture as a function of time during a mock run with the luminostat protocol (Figure 10A).

Figure 12. Temperature fluctuations and associated problems with rapid serial dilution protocol (Figure 10**B).** (A) Difference between the temperature of the culture and that of the surrounding water bath during one dilution/growth cycle. Data is color-coded as in Figure 10B. A rise of ~0.3°C occurs during the phase where the input pump supplies fresh medium. (B) Luminescence signal profile during a long-term culture with non-adherent HEHA16 strain using the rapid serial dilution protocol. The curves are not linear, instead, they show reproducible kinks (arrows).

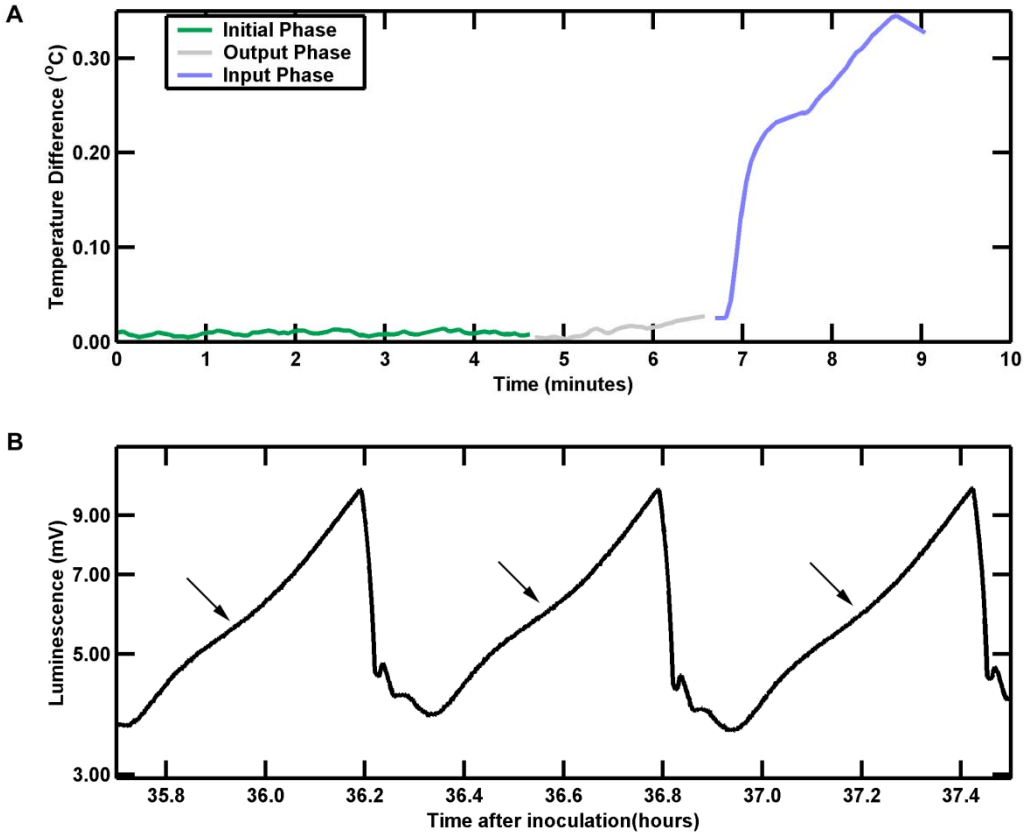

Figure 12. Temperature fluctuations and associated problems with rapid serial dilution protocol.

Figure 13. Dilution protocol for high precision growth rate measurements in long-term cultures. (A) Long-term cultures are subjected to a multi-phase dilution protocol. The typical luminescence signal profile during each phase is indicated in the top panel, while nominal values of pump flow rates are plotted in the bottom. After an initial phase (which begins right after inoculation), where the luminescence signal is allowed to reach the high setpoint (7.00 mV), a cyclic, four-phase dilution protocol is followed: (1) a fast-dilution phase where the signal is reduced from the high setpoint to the low setpoint (2.65 mV), (2) an intermediate-dilution phase, where the signal is further reduced to 2.00 mV, (3) a slow-dilution phase, where the signal is allowed to recover to the low setpoint, and (4) a no-dilution phase, which lasts till the signal reaches the high setpoint again. The nominal flow rates during the dilution phases are as follows: fast dilution, 12.5 g/min; intermediate dilution, 7.5 g/min; slow dilution, 1.88 g/min; and no dilution, 0 g/min. During the dilution phases, both pumps operate simultaneously with the indicated flow rates except that during the fast-dilution phase, the input rate is modulated to correct for small differences in input and output rates in previous phases and maintain culture mass. When required, replacement of media and waste reservoirs were performed in the no-dilution phase. (B) Temperature stability in the dilution protocol depicted in (A). Difference between the temperature of the culture and that of the surrounding water bath is plotted as a function of time and color coded as in (A). During the no-dilution phase, temperature remains stable to within 0.03°C.

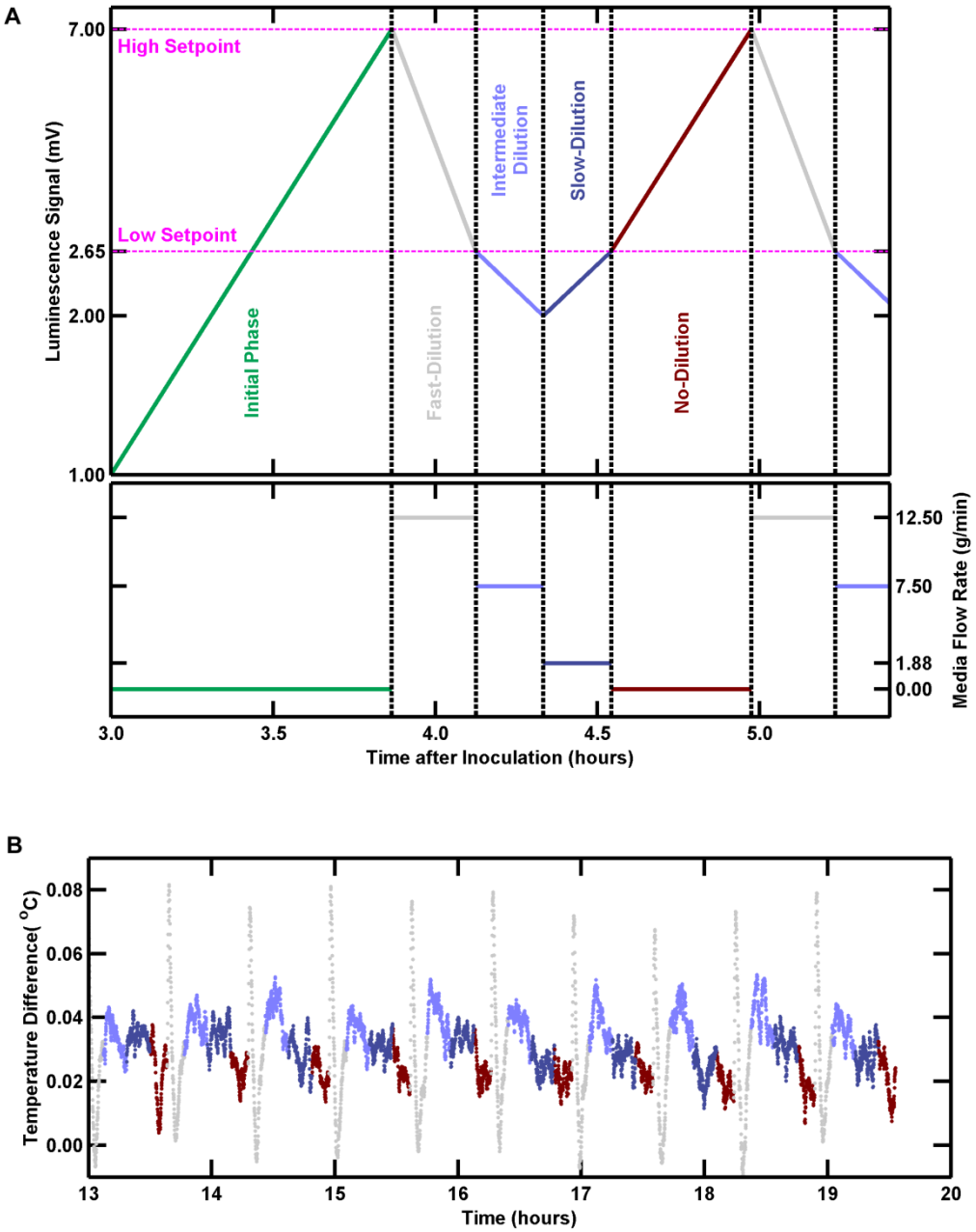

Figure 13. Dilution protocol for high precision growth rate measurements in long-term cultures.

Figure 14. High precision growth rate measurements in long-term culture. A long-term culture of NS2 pCSλ was set up in LB+30μg/ml kanamycin. (A) Transformed luminescence signal (L_{tr}, black) and the input flow rate of fresh medium (green) during a few hours of operation. Different phases of the dilution protocol are indicated as follows: initial phase (P_1), fast-dilution (P_2), intermediate-dilution (P_3), slow-dilution (P_4), and no-dilution (P_5, see section 4.4.2). Output flow rate is nearly identical to input flow rate in all phases except the fast-dilution phase, where input rate is modulated to correct for small differences in input and output rates in previous phases and maintain culture mass. Horizontal dashed magenta lines indicate the operating region (2.65 mV to 7.00 mV). (B) Growth rates computed during the no-dilution phase (phase P_5 in panel A) are plotted as a function of time (see section 2.1). The black vertical dashed line (16.2 hours after inoculation) represents the time when media and waste reservoirs were changed. Except for the first point after change of reservoirs, all growth rate measurements fall within a 2% band as indicated by the horizontal dashed maroon lines. Error bars correspond to the estimated intrinsic measurement error ($\pm 2\sigma_{slp}$, equation 0 of Appendix B).

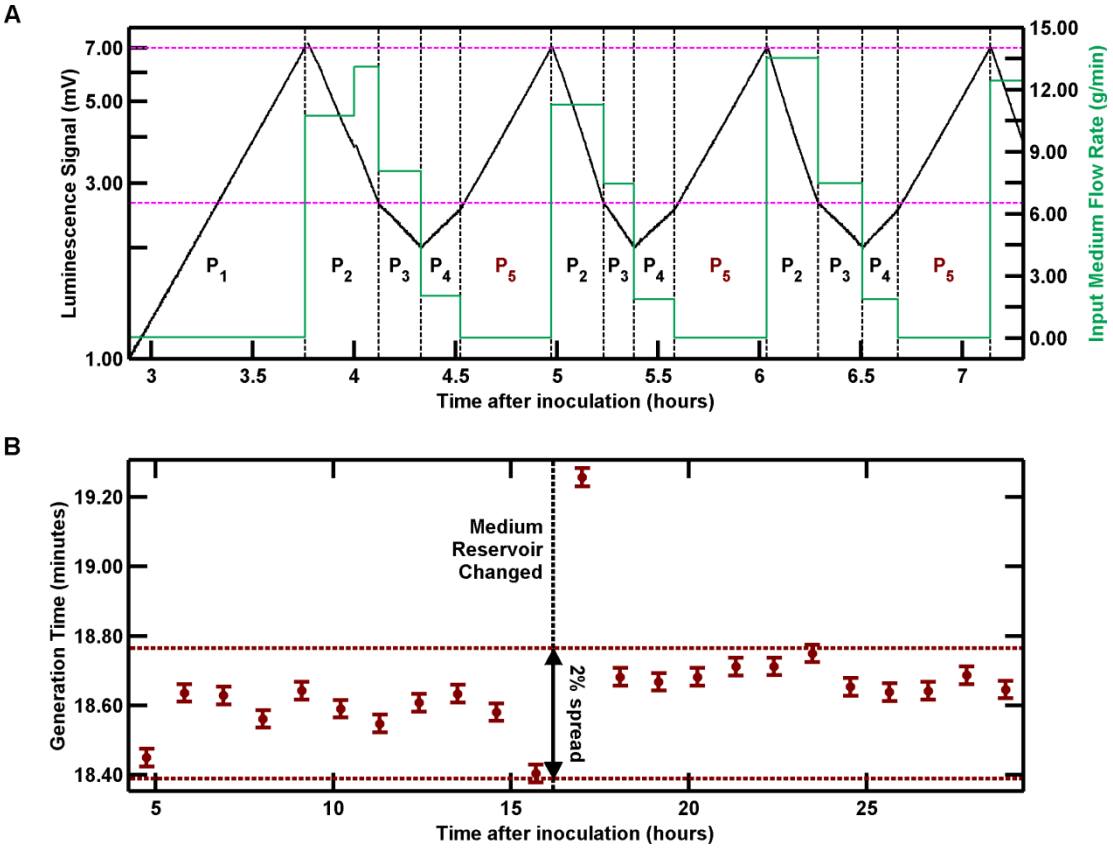

Figure 14. High precision growth rate measurements in long-term culture.

Chapter 5. A Synthetic Cooperation System in Yeast

This chapter contains work done in collaboration with Dr. Wenying Shou and Dr. José Vilar, and has been published before (Shou et al., 2007).

5.1 Motivation

In nature, cooperation emerges under diverse conditions and over varying scales ranging from the physiological, as in the emergence of cell-cell cooperation that facilitates tumor progression (Hanahan and Folkman, 1996), to the ecological, as in the evolution of mutualistic interactions between species (Bergstrom et al., 2002; Boucher, 1985). In some cases, the cooperative interaction is essential to the viability of the system (Bronstein and Hossaert-McKey, 1995; Cook and Rasplus, 2003; Pellmyr and Leebens-Mack, 1999; Rowan *et al.*, 1997; Wernegreen, 2002).

Cooperation is often viewed as a paradox, as one might expect that natural selection would favor selfish traits that maximize an organism's chances of survival. This naïve expectation prompted the development of a rich theoretical framework to explain the evolution of cooperative behavior (Lehmann and Keller, 2006; West et al., 2007). There, however, remains a disconnect between theoretical and empirical work on cooperation (Leimar and Hammerstein, 2006). While abstract theoretical models are useful to illustrate the basic paradox of cooperation and the scenarios in which it can arise, they are unlikely to shed light on constraints that emerge from the biology of cooperating entities. One way to address this issue is to develop a quantitative description of a particular

cooperative system and enumerate the constraints on the viability of the system. While such an approach may limit the generality of the conclusions, it can also uncover biologically relevant constraints that are often not considered by idealized theoretical models, especially if one chooses a system that is representative of a broad class such as that of metabolically coupled microbes (Dean-Raymond and Alexander, 1977; Nurmikko, 1956; Stams et al., 2006).

There are several challenges in performing quantitative measurements on natural cooperative systems. These include difficulties in measuring beneficial exchanges and population dynamics (Boucher, 1985) and in disengaging cooperation from non-cooperative interactions such as competition and inhibition (Rowan et al., 1997; Yeoh et al., 1968). To circumvent these difficulties, we decided to engineer a system with obligatory cooperation based on metabolite exchange. By designing the system so that it was easy to quantify population sizes, we were able to perform experiments that are difficult in natural systems. For example, we looked at how reliably viable cooperative communities could form under various initial conditions, and how well they could recover from population bottlenecks.

Prior to our work, there had been some reports documenting the emergence of cooperation in laboratory systems. Cooperation among cells of a single population had been shown to arise spontaneously under selective pressures (Rainey and Rainey, 2003), and cooperation between two populations had been attained either through mixing of organisms with natural capacities to cooperate (Buchsbaum and Buchsbaum, 1934; Shendure et al., 2005) or through evolution from originally parasitic associations (Fiegna

et al., 2006; Jeon, 1972). We were interested in constructing a synthetic cooperative system, in part to distinguish our work from these previous efforts, but largely to have a system where it would be easy to study constraints on viability.

Our system, which we have termed CoSMO (for *Co*operation that is *S*ynthetic and *M*utually Obligatory), consists of a pair of non-mating yeast strains, each supplying an essential metabolite to the other strain.

5.2 Results

5.2.1 Construction of CoSMO

As the initial step, we genetically modified the yeast *S. cerevisiae* to obtain two non-mating strains with different metabolic capabilities (section 2.1) so that they behave essentially as two different species. Specifically, the $R^{\leftarrow A}$ strain, labeled with red-fluorescent protein (DsRed), synthesizes lysine at normal levels but requires adenine to grow; and the $Y^{\leftarrow L}$ strain, labeled with yellow-fluorescent protein (YFP), synthesizes adenine at normal levels but requires lysine to grow. $R^{\leftarrow A}$ and $Y^{\leftarrow L}$ can be propagated in mono-cultures in the presence of adenine and lysine supplements, respectively. When the two strains were washed free of supplements and subsequently mixed to form a co-culture, both strains initially underwent residual growth using stored metabolites (Messenguy et al., 1980; Nagy, 1979) but eventually died off (Figure 15A). Thus, even though the two populations together have the required enzymes to synthesize both adenine and lysine, their co-culture failed to achieve sustained growth.

To create cooperation, we introduced an additional mutation in each strain by replacing the first enzyme in adenine or lysine biosynthetic pathway with an overproduction mutant that is no longer sensitive to end-product feedback inhibition (Armitt and Woods, 1970; Feller et al., 1999). Consequently, $R^{\leftarrow A}$ and $Y^{\leftarrow L}$ were respectively transformed into $R^{\leftarrow A}_{\rightarrow L}$, which requires adenine to grow and overproduces lysine, and $Y^{\leftarrow L}_{\rightarrow A}$, which requires lysine to grow and overproduces adenine .

Cooperation can indeed exist between $R^{\leftarrow A}_{\rightarrow L}$ and $Y^{\leftarrow L}_{\rightarrow A}$, as verified through the viability of their co-cultures. We defined co-culture viability as the ability to attain saturation density (~5×10^7 total cells/ml) in the absence of adenine and lysine supplements. We found that co-cultures initiated at low density (~10^5 total cells/ml) can be viable (Figure 15B) and that viability of cooperation requires both adenine- and lysine-overproduction mutations (Figure 15C). Together, $R^{\leftarrow A}_{\rightarrow L}$ and $Y^{\leftarrow L}_{\rightarrow A}$ form a cooperative system termed CoSMO (*Co*operation that is *S*ynthetic and *M*utually *O*bligatory), which mimics two-species obligate mutualistic systems in which cooperation is essential for the survival of both species (Cook and Rasplus, 2003; Kroon and van Ginkel, 2001; Nurmikko, 1956; Pellmyr and Huth, 1994; Stams et al., 2006; Zientz et al., 2004). The final design of CoSMO is depicted in Figure 16.

5.2.2 Behavior of CoSMO strains in monoculture and deduction of CoSMO growth pattern

To better understand the properties of CoSMO, we performed monocultures of the two strains in the absence of adenine and lysine supplements. After washout of the essential adenine or lysine supplement, each strain initially underwent residual growth using stored

metabolites (Messenguy et al., 1980; Nagy, 1979) until time T_I ~10 hours (Figure 17A). Immediately afterwards, $Y_{\rightarrow A}^{\leftarrow L}$ cells entered the death phase characterized by a decrease in the number of live cells (Figure 17, green stars) and an increase in the number of dead cells (Figure 17B, grey squares). $R_{\rightarrow L}^{\leftarrow A}$ cells, in contrast, did not enter death phase until time T_R ~70 hours (Figure 17A, red stars and Figure 17B, grey circles). The release of the overproduced metabolites into the medium was associated with cell death (Figure 17B). Consequently, the onset of lysine release by $R_{\rightarrow L}^{\leftarrow A}$ was significantly delayed until time T_R when the majority of $Y_{\rightarrow A}^{\leftarrow L}$ population already lost viability (Figure 17B). Thus, the two strains in CoSMO are not equivalent, and there is asymmetric starvation tolerance.

The properties of the two strains under monoculture can be used to construct a schematic diagram of the initial stages of CoSMO growth (Figure 17C) as well as to derive constraints on the viability of the system (section 5.2.3). In particular, the total cell density takes on a pattern of "rise-plateau-rise," with each rise resulting from net growth of at least one partner (Figure 17C).

5.2.3 Cosmo viability requirements

We used the individual characteristics of the two strains (Figure 17) to compute viability conditions for CoSMO.

Supply-consumption requirement

The supply of metabolites must be sufficiently high to sustain net growth of both components. Let A_s (L_s) be the total amount of adenine (lysine) supplied per $Y_{\rightarrow A}^{\leftarrow L}$ ($R_{\rightarrow L}^{\leftarrow A}$) cell until its death, and A_c (L_c) be the amount of adenine (lysine) consumed to make a new $R_{\rightarrow L}^{\leftarrow A}$ ($Y_{\rightarrow A}^{\leftarrow L}$) cell. Assuming that all released metabolites are completely consumed, changes (Δ) in population densities of live $R_{\rightarrow L}^{\leftarrow A}$ and $Y_{\rightarrow A}^{\leftarrow L}$, denoted R and Y, and of the corresponding dead cells, denoted $\tilde{R}$ and $\tilde{Y}$, are related through

$$\Delta R = \Delta\tilde{Y}\frac{A_s}{A_c} - \Delta\tilde{R} \quad \text{and} \quad \Delta Y = \Delta\tilde{R}\frac{L_s}{L_c} - \Delta\tilde{Y}. \tag{1}$$

Positive growth of both components requires $\Delta\tilde{Y}\frac{A_s}{A_c} > \Delta\tilde{R}$ and $\Delta\tilde{R}\frac{L_s}{L_c} > \Delta\tilde{Y}$, which leads to $A_sL_s / A_cL_c > 1$. This condition is analogous to those derived in mathematical models of obligate mutually cross-feeding systems in chemostats at steady state (Meyer and Tsuchiya, 1975). For CoSMO, experimentally measured values (see Appendix C) lead to $A_sL_s / A_cL_c \approx 22$, implying that CoSMO significantly exceeds this fundamental supply-consumption requirement.

The supply-consumption requirement is a fundamental constraint on the strain properties. It is not, however, a constraint on the initial conditions of the system. Even if the supply-consumption requirement is met, the system can fail to be viable, if a released metabolite is too dilute and its uptake rate is too slow to keep its consumer alive, or if any one strain goes extinct before its partner strain has a chance to release a substantial amount of metabolite. These two failure modes lead to constraints on the initial cell densities and initial cell numbers as described below.

Minimum initial cell density requirement

The growth rate of $Y_{\rightarrow A}^{\leftarrow L}$, G_Y, must exceed the death rate D_{YLate} at a finite time τ after the initiation of lysine release from dying $R_{\rightarrow L}^{\leftarrow A}$ at time ~T_R (Figure 17C). If each $Y_{\rightarrow A}^{\leftarrow L}$ cell uptakes lysine at concentration L in the medium following Michaelis-Menten kinetics with half-saturation constant K_{mL} and maximum rate V_{maxL}, and produces a new cell after acquiring a quantity L_c of lysine, we obtain

$$D_{YLate} < G_Y = \frac{1}{L_c}\frac{V_{\max L}}{K_{mL}+L}L \approx \frac{1}{L_c}\frac{V_{\max L}}{K_{mL}}L. \tag{2}$$

Note that measured L is small compared to K_{mL}. L is given by

$$L = R_{\max}(1-e^{-D_R\cdot\tau})L_s, \tag{3}$$

where R_{max} is the population density of $R_{\rightarrow L}^{\leftarrow A}$ at time T_R, and $(1-e^{-D_R\cdot\tau})$ is the fraction of $R_{\rightarrow L}^{\leftarrow A}$ cells that have died from time T_R to $T_R+\tau$. R_{max} is related to R_0 and Y_0, the initial population densities of the two partners, through

$$R_{\max} \approx I_R R_0 + I_Y Y_0 \frac{A_s}{A_c}, \tag{4}$$

accounting for increase in R resulting first from I_R-fold residual growth from R_0 and then from adenine released upon the death of almost the entire $Y_{\rightarrow A}^{\leftarrow L}$ population which has undergone I_Y-fold residual growth from Y_0. From inequality 2, equation 3, and the measured parameters (Appendix A), we obtain the minimal R_{max} required for CoSMO viability as

$$R_{\max}^{*} = \frac{D_{YLate}K_{mL}L_c}{V_{\max L}L_s} \approx 6\times10^4 \text{ cells/ml}. \tag{5}$$

Minimum initial cell number requirement

For a co-culture of volume V, the initial number of $R_{\rightarrow L}^{\leftarrow A}$ cells must be at least 1:

$$R_0 V \geq 1. \tag{6}$$

In addition, there must be at least one $Y_{\rightarrow A}^{\leftarrow L}$ cell alive at time $T_R + \tau$:

$$I_Y Y_0 V e^{-D_Y (T_R - T_I) - D_{YLate} \times \tau} \geq 1. \tag{7}$$

From inequalities 2 and 7 and equations 3-5, we obtain the condition

$$Y_0 V > \frac{e^{(T_R - T_I) D_Y}}{I_Y} \left(1 - \frac{R^*_{\max}}{R_{\max}}\right)^{\frac{-D_{YLate}}{D_R}} \approx \frac{e^{(T_R - T_I) D_Y}}{I_Y} \left(1 - \frac{R^*_{\max}}{I_R R_0 + I_Y Y_0 \, A_s / A_c}\right)^{\frac{-D_{YLate}}{D_R}}. \tag{8}$$

The minimum initial number of $Y_{\rightarrow A}^{\leftarrow L}$ cells required for CoSMO viability is obtained after setting R_0 in inequality 8 to the saturation density 5×10^7 cells/ml:

$$Y_0 V \geq 9. \tag{8a}$$

The initial cell density and cell number requirements can be combined to define the viability and inviability domains of CoSMO as a function of the initial densities of the two strains at a given volume. The two domains can be represented in a phase diagram (Figure 18), which has been drawn using parameter values detailed in Appendix C.

5.2.4 Experimental verification of viability phase diagram

As mentioned in section 5.2.3, the initial cell density and cell number requirements can be used to delineate viability and inviability domains of CoSMO in a phase diagram (Figure 18). We proceeded to verify whether the calculations of viability and inviability domains are accurate.

For initial conditions well within the calculated inviable domain (Figure 18, broken circles), replicate CoSMO cultures are never viable (time series not shown). In contrast, for initial conditions well within the calculated viable domain, replicate CoSMO cultures are always viable (Figure 18, filled circles). Specifically, when both cell-density and cell-number requirements were exceeded by at least ~10-fold (*e.g.* Figure 18, purple filled circles), CoSMO cultures initiated at $R_{\rightarrow L}^{\leftarrow A}$: $Y_{\rightarrow A}^{\leftarrow L}$ ratios spanning 9 orders of magnitude from 10^{-5} to 10^{4} achieved 100% viability (Figure 19, panels II-V). The inherent ability to survive a wide range of partner ratios is important for natural cooperative systems, because such wide ranges would be expected either as a result of initial encounters of partners at different population sizes or through intrinsic system dynamics.

For initial conditions close to the boundary that separates the viable and inviable domains (black and grey curves in Figure 18), the behavior of CoSMO is stochastic (Figure 18, open circles), leading replicate cultures non-deterministically to either viability or inviability. For instance, when the initial-density requirement was significantly exceeded and the initial-number requirement for either strain was barely satisfied (Figure 18, purple open circles), only a fraction of replicate CoSMO cultures were viable (Figure 19A, panels I and VI). Similarly, when the initial-density requirement was barely satisfied and the initial-number requirements were significantly exceeded (*e.g.* Figure 18, brown open circle), CoSMO was not viable in one case (Figure 19B, panel I) while it reached saturation in the other two (Figure 19B, panels II and III). These results confirm the viability and inviability domains calculated in section 5.2.3 and depicted in Figure 18.

5.2.5 Long-term population dynamics of CoSMO

Properties of CoSMO components can be used not only to determine system viability, but also to elucidate certain features of CoSMO dynamics. In particular, upon long-term culturing, the wide range of initial population ratios compatible with CoSMO viability converges to a narrow range. CoSMO cultures were seeded at $R_{\rightarrow L}^{\leftarrow A}$: $Y_{\rightarrow A}^{\leftarrow L}$ ratio of 10^3, 1, and 10^{-3} (Figure 20A, panels I, II, and III, respectively) and maintained at low density through monitoring of culture turbidities and performing dilutions at a fixed frequency (once per day or twice per day). Even though population ratios initially spanned 6 orders of magnitude, they underwent several oscillations and eventually settled into a narrow range between 1:5 and 5:1 (Figure 20A). In a similar experiment where dilutions were performed at high cell density, oscillating population ratio converges to the same range (Figure 20B).

Calculation of the steady state population ratio

The stabilized ratio can be computed from the supply and consumption of adenine and lysine. When a finite non-zero steady state ratio is achieved, $R_{\rightarrow L}^{\leftarrow A}$ and $Y_{\rightarrow A}^{\leftarrow L}$ grow with the same rate $\bar{G}$. Furthermore, let $\bar{D}_R$ and $\bar{D}_Y$ represent the death rates of $R_{\rightarrow L}^{\leftarrow A}$ and $Y_{\rightarrow A}^{\leftarrow L}$ at this stage, respectively.

Since $\frac{\Delta\tilde{R}}{\Delta R} = \frac{\bar{D}_R R \Delta t}{\bar{G} R \Delta t}$ and $\frac{\Delta\tilde{Y}}{\Delta Y} = \frac{\bar{D}_Y Y \Delta t}{\bar{G} Y \Delta t}$, equation 1 in section 5.2.3 becomes

$$\Delta R = \frac{\bar{D}_Y}{\bar{G}} \Delta Y \frac{A_s}{A_c} - \frac{\bar{D}_R}{\bar{G}} \Delta R \quad \text{and} \quad \Delta Y = \frac{\bar{D}_R}{\bar{G}} \Delta R \frac{L_s}{L_c} - \frac{\bar{D}_Y}{\bar{G}} \Delta Y.$$

Solving for $\frac{\Delta R}{\Delta Y}$ after replacing $\bar{G}$, we obtain:

$$\frac{\Delta R}{\Delta Y} = \frac{L_c}{2L_s}\left[\frac{\bar{D}_Y}{\bar{D}_R} - 1 + \sqrt{4\frac{\bar{D}_Y A_s L_s}{\bar{D}_R A_c L_c} + (\frac{\bar{D}_Y}{\bar{D}_R} - 1)^2}\right].$$

If we assume $\frac{\bar{D}_Y}{\bar{D}_R} = \frac{D_{YLate}}{D_R}$, then $\frac{\Delta R}{\Delta Y} \sim 1$ for CoSMO (parameter values are detailed in Appendix C). $\frac{R}{Y} = \frac{R_0 + \Delta R}{Y_0 + \Delta Y}$ tends to $\frac{\Delta R}{\Delta Y}$ when t is large because R_0 and Y_0 are small compared to ΔR and ΔY. Therefore, $\frac{R}{Y}$ is on the order of 1 for CoSMO. In CoSMO, $\frac{\bar{D}_Y}{\bar{D}_R} - 1$ is small compared to $\sqrt{4\frac{\bar{D}_Y A_s L_s}{\bar{D}_R A_c L_c}}$, in which case $\frac{R}{Y}$ can be simplified to $\sqrt{\frac{\bar{D}_Y A_s L_c}{\bar{D}_R L_s A_c}}$, a function of adenine and lysine supply rates ($\bar{D}_Y A_s$ and $\bar{D}_R L_s$) and consumption (A_c and L_c).

5.2.6 Changes in cell-density requirement upon long-term culture

An intriguing aspect of CoSMO is that upon long-term culturing, the cell density requirement for viability can undergo drastic reduction. The density requirement was estimated by performing a series of dilutions of a viable CoSMO culture and evaluating the minimum density at which viability was retained. Such an experiment is a laboratory analog of a natural system recovering from population bottlenecks, a commonly occurring perturbation.

Five CoSMO cultures were initiated, grown to near-saturation (Round-0) and subjected to ten rounds of dilution-and-regrowth, ending in Round-10 cultures (Figure 21A). The population density of both Round-0 and Round-10 cultures was on the order of 10^7 total cells/ml. The Round-0 cultures typically tolerated 10^3-10^4 - fold dilution (Figure 21B, left), and therefore a total population density on the order of 10^3-10^4 cells/ml was required for the viability of a diluted CoSMO culture. In contrast, the Round-10 cultures typically tolerated 10^5-10^6-fold dilution (Figure 21B, right), and therefore a total population density on the order of 10^1-10^2 cells/ml was sufficient for viability. Thus, even though the initial requirements for viable cooperation can be accurately predicted from properties of components (Figure 18), the density requirement underwent 100-fold relaxation over a relatively short period of time (~70 generations). This phenomenon may result from changes in one or both strains that aid the survival of the strain itself (*e.g.* through increased starvation tolerance) or the survival of its partner (*e.g.* through increased overproduction or expedited release of metabolites).

5.3 Summary

We have constructed a synthetic obligatory cooperative system, termed CoSMO, that consists of a pair of non-mating yeast strains, each supplying an essential metabolite to the other strain. Our results show that persistent cooperation between two populations can be created *de novo* through a small set of targeted genetic modifications. The behavior of the two strains in isolation however revealed unintended constraints that restrict cooperation, such as asymmetry in starvation tolerance and delays in nutrient release until near cell death. This monoculture behavior was used to derive constraints on the viability

of the system. In spite of such constraints, CoSMO is viable over a wide range of initial conditions, with the population ratio converging to a value predicted by nutrient supply and consumption. Unexpectedly, even in the absence of explicitly engineered mechanisms to stabilize cooperation, CoSMO can consistently develop increased ability to survive population bottlenecks.

Figure 15. Viability of CoSMO requires both adenine- and lysine- overproduction mutations. At time zero, mono-cultures of indicated strains grown in synthetic dextrose medium (SD) with the required adenine or lysine supplement (Guthrie and Fink, 1991) were washed free of supplements and mixed. Plots show population dynamics of fluorescent live R (red), fluorescent live Y (green), non-fluorescent dead (grey), and total (black) cells of the coculture as measured by flow cytometry (section 2.1). (A) CoSMO is not viable in the absence of mutant strains which overproduce adenine and lysine. (B) CoSMO cultures can be viable if both overproduction mutants are present, but not if only one is present (C). In panel B, data from three replicate cultures are superimposed.

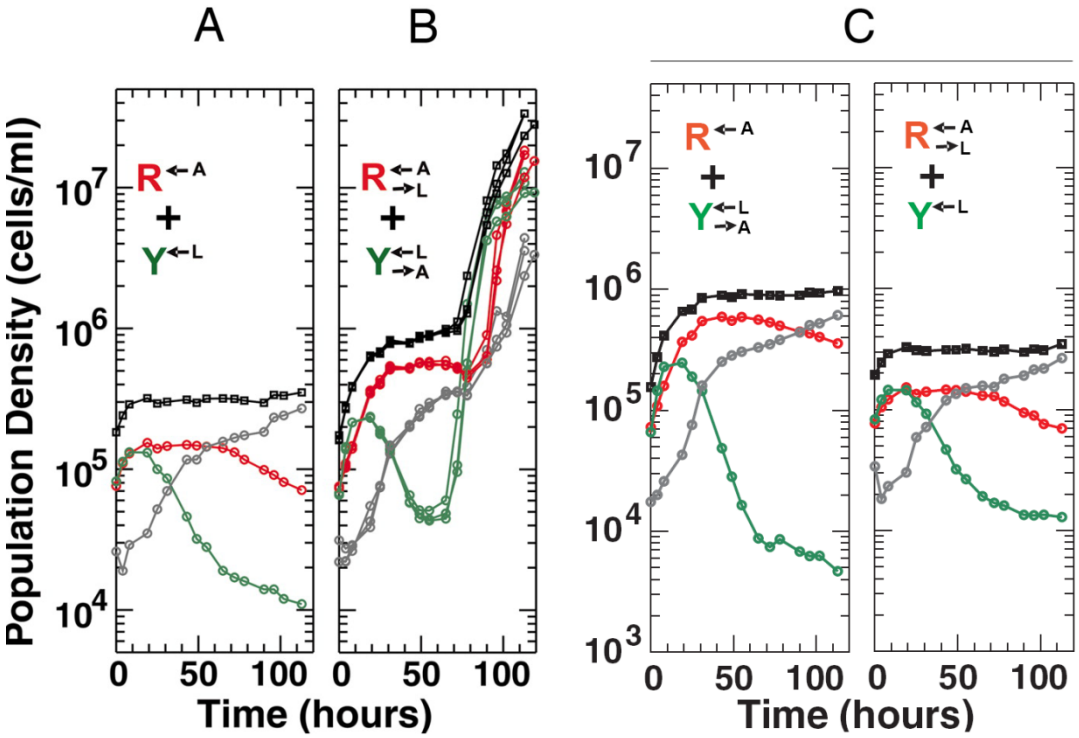

Figure 15. Viability of CoSMO requires both adenine- and lysine- overproduction mutations.

Figure 16. The "wiring" diagram of CoSMO. CoSMO consists of two yeast strains: $R^{\leftarrow A}_{\rightarrow L}$ which lacks Ade8 enzyme and harbors Lys21^{op} enzyme and $Y^{\leftarrow L}_{\rightarrow A}$ which lacks Lys2 enzyme and harbors Ade4^{op} enzyme. Cells lacking Ade8 (Lys2) cannot synthesize adenine (lysine) and therefore require intake ($\leftarrow$) of the corresponding metabolite. Ade4op and Lys21op are no longer sensitive to end-product feed-back inhibition and consequently overproduce (op) the corresponding metabolite which is eventually released ($\rightarrow$) into the medium (Armitt and Woods, 1970; Feller et al., 1999). Crosses represent genetic inactivation; yellow bars and arrows represent losses and gains in metabolite synthesis, respectively.

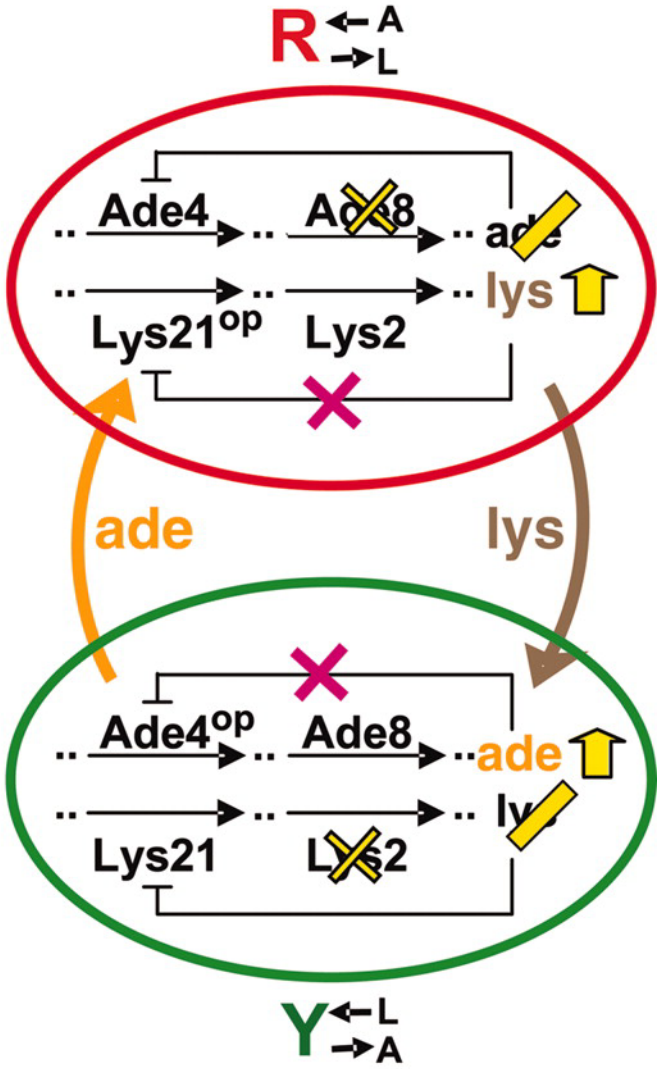

Figure 16. The "wiring" diagram of CoSMO.

Figure 17. Characterization of individual strains in mono-cultures and deduction of CoSMO growth pattern. (A, B) Asymmetry in starvation tolerance between two strains and delayed metabolite release. At time zero, mono-cultures of the two strains grown in the presence of the required supplement were washed free of the supplement. (A) shows live population density over time for an initial population density of ~$3x10^5$ cells/ml. (B) shows dead population density (top panel) and the concentration of lysine or adenine released into the medium over time (bottom panel) as measured by a bioassay (section 2.1) for an initial population density of ~$6x10^6$ cells/ml. The left and the right scales are for experiments on $Y_{\rightarrow A}^{\leftarrow L}$ (squares) and $R_{\rightarrow L}^{\leftarrow A}$ (circles), respectively. Grey vertical lines mark the time T_I when residual growth ends and the time T_R when $R_{\rightarrow L}^{\leftarrow A}$ enters death phase and releases lysine. (C) A schematic diagram of the initial stage of CoSMO growth deduced from (A) and (B). R and Y denote live population densities of $R_{\rightarrow L}^{\leftarrow A}$ and $Y_{\rightarrow A}^{\leftarrow L}$, respectively. Their initial values R_0 and Y_0 increase I_R- and I_Y- fold respectively during residual growth until time T_I. After T_I, adenine released from dying $Y_{\rightarrow A}^{\leftarrow L}$ enables growth of $R_{\rightarrow L}^{\leftarrow A}$. By time ~$T_R$, most of the $Y_{\rightarrow A}^{\leftarrow L}$ population has died and R is at a local maximum R_{max}. Lysine is subsequently released from dying $R_{\rightarrow L}^{\leftarrow A}$, and at some time τ after T_R, results in an increase in Y under conditions that permit CoSMO viability. The death rate for $R_{\rightarrow L}^{\leftarrow A}$ after T_R is D_R, and for $Y_{\rightarrow A}^{\leftarrow L}$ is D_Y from T_I to T_R and D_{YLate} from T_R onward. The total cell density, which is the sum of R, Y, and dead populations, consequently takes on a pattern of "rise-plateau-rise", with each rise resulting from net growth of at least one partner.

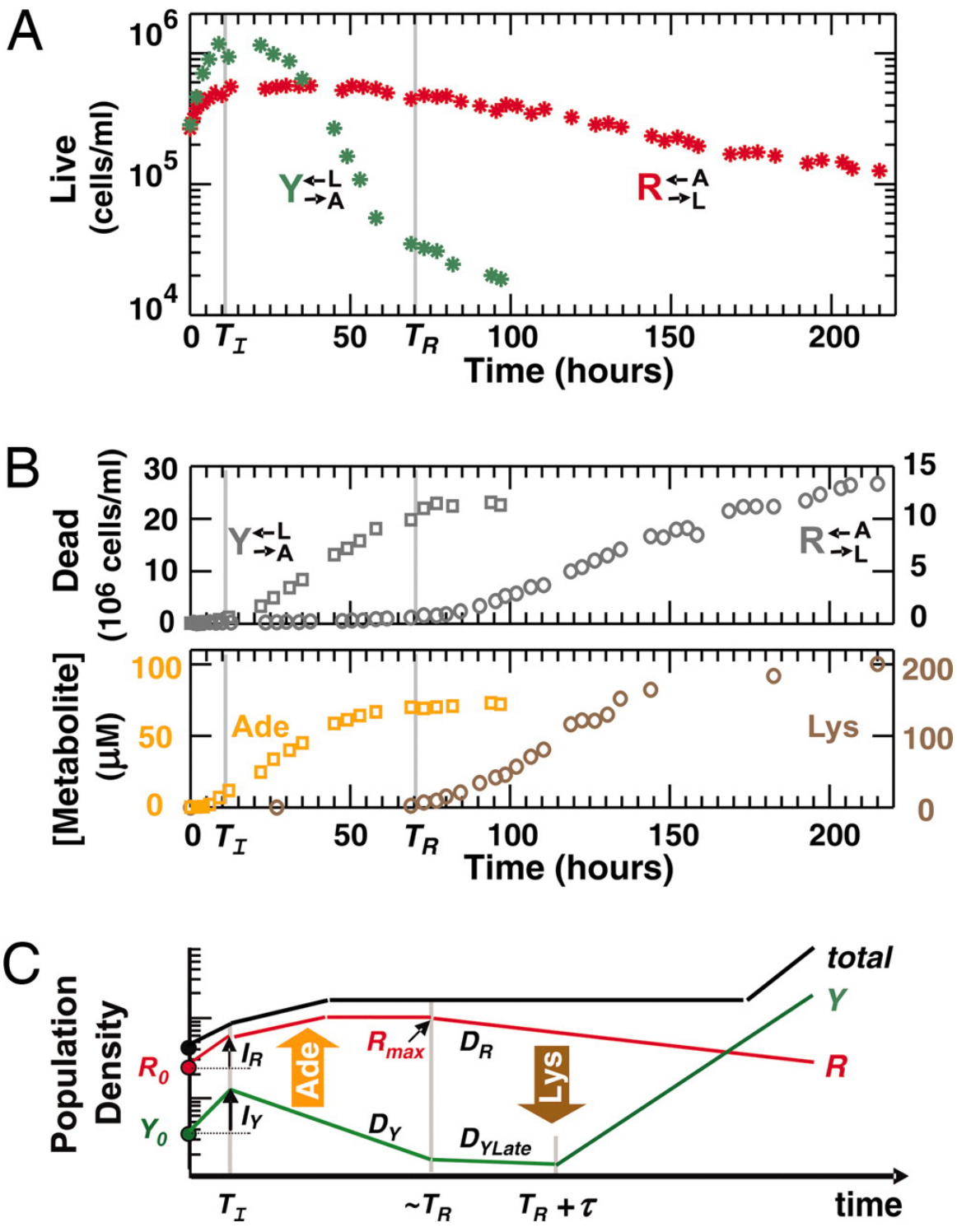

Figure 17. Characterization of individual strains in mono-cultures and deduction of CoSMO growth pattern.

Figure 18. Phase diagram for CoSMO viability. The domain of viability for CoSMO at volume V of 2.6 ml is bounded by a black vertical line (single-arrowhead, section 5.1, Inequality 6) and grey curves (section 5.1, Inequality 8, with I_Y set to different values in the experimentally observed range from 2 to 4). The shoulder represents the viability threshold imposed by the density requirement alone (section 5.1, Equations 4 and 5) and is therefore not affected by the culture volume. Different volumes affect only the black vertical line (single-arrowhead) and the horizontal asymptote (double-arrowhead), which shift along the R_0 and Y_0 axis according to the initial-number requirements expressed in inequalities 6 and 8a of section 5.1, respectively. Circles indicate values of (R_0, Y_0) corresponding to different experiments (orange for Figure 15 panel II; purple from top left to bottom right for Figure 19A panels I to VI; and brown for Figure 19B). In experiment marked with cyan, 1 out of 5 replicate cultures was viable (time series not shown); in experiments marked with black, 0 out of 4 or 5 replicate cultures was viable (time series not shown). Overall, the viability-inviability outcome of replicate CoSMO cultures close to the calculated boundary is highly variable (open circles), while cultures significantly above and below the boundary show 100% viability (filled circles) and 0% viability (broken circles), respectively.

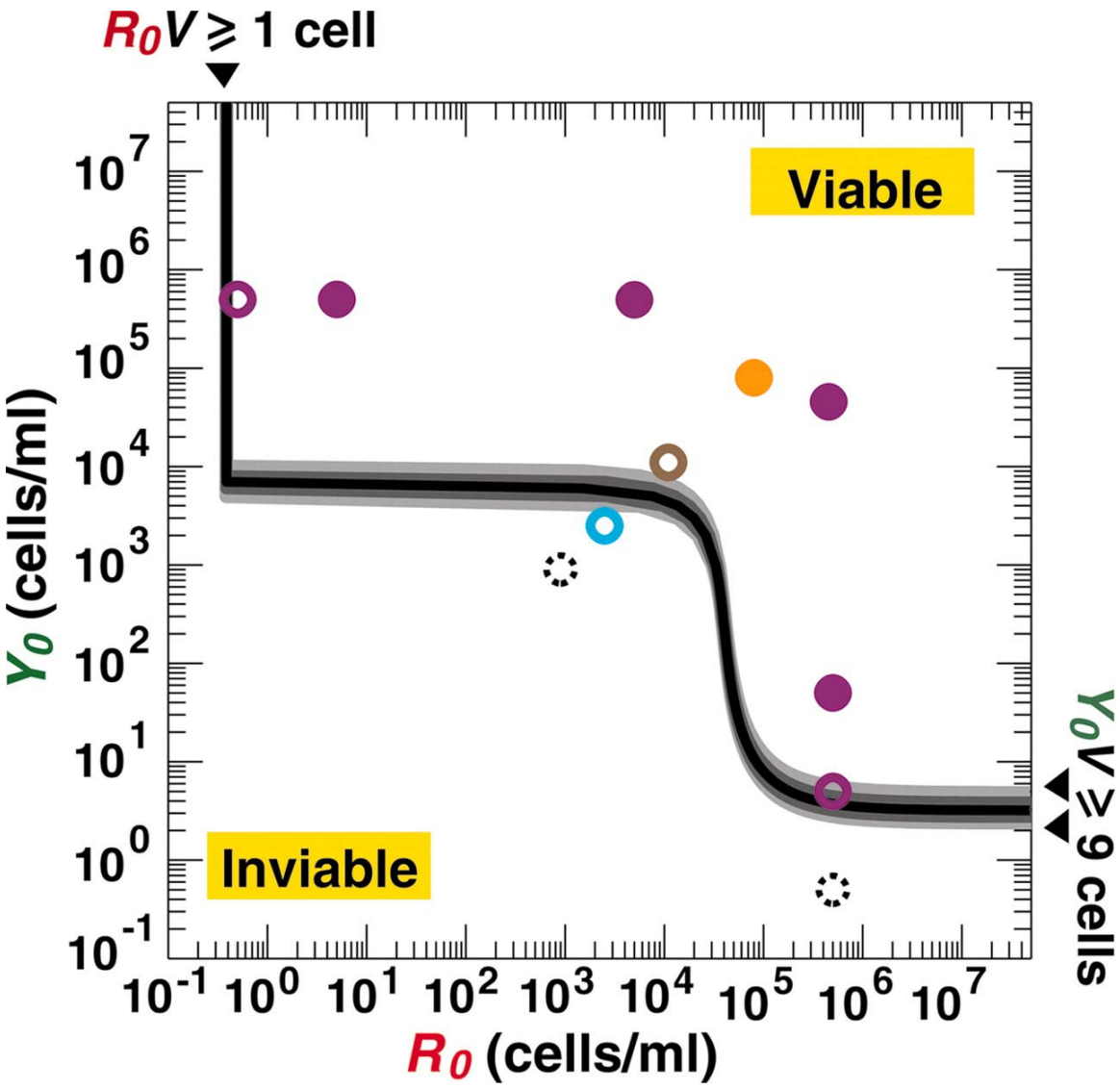

Figure 18. Phase diagram for CoSMO viability.

Figure 19. Viability of CoSMO. Mono-cultures of the two strains were washed free of adenine and lysine, and mixed at time zero. (A) CoSMO is viable under a wide range of initial partner ratios. The two strains were mixed at the indicated $R_{\rightarrow L}^{\leftarrow A}$:$Y_{\rightarrow A}^{\leftarrow L}$ ratios (R_0:Y_0) and at the same total initial cell density and culture volume (~5×10^5 cells/ml × 2.6 ml=1.3×10^6 cells/culture, four replicate cultures per condition). Plots show culture turbidity in OD_{600} (optical density at 600nm) over time. OD_{600} of 1 corresponds to a population density from 1×10^7 to 5×10^7 cells/ml depending on the cell size. (B) Stochastic CoSMO behavior close to the initial-density requirement. Three replicate cultures (≥20 ml) were set up at $1.1\text{x}10^4$ cells/ml/strain. Plots show the dynamics of live $R_{\rightarrow L}^{\leftarrow A}$(red), live $Y_{\rightarrow A}^{\leftarrow L}$ (green), dead (grey), and total (black) cell densities. One of the cultures was inviable (I) while the other two were viable (II and III).

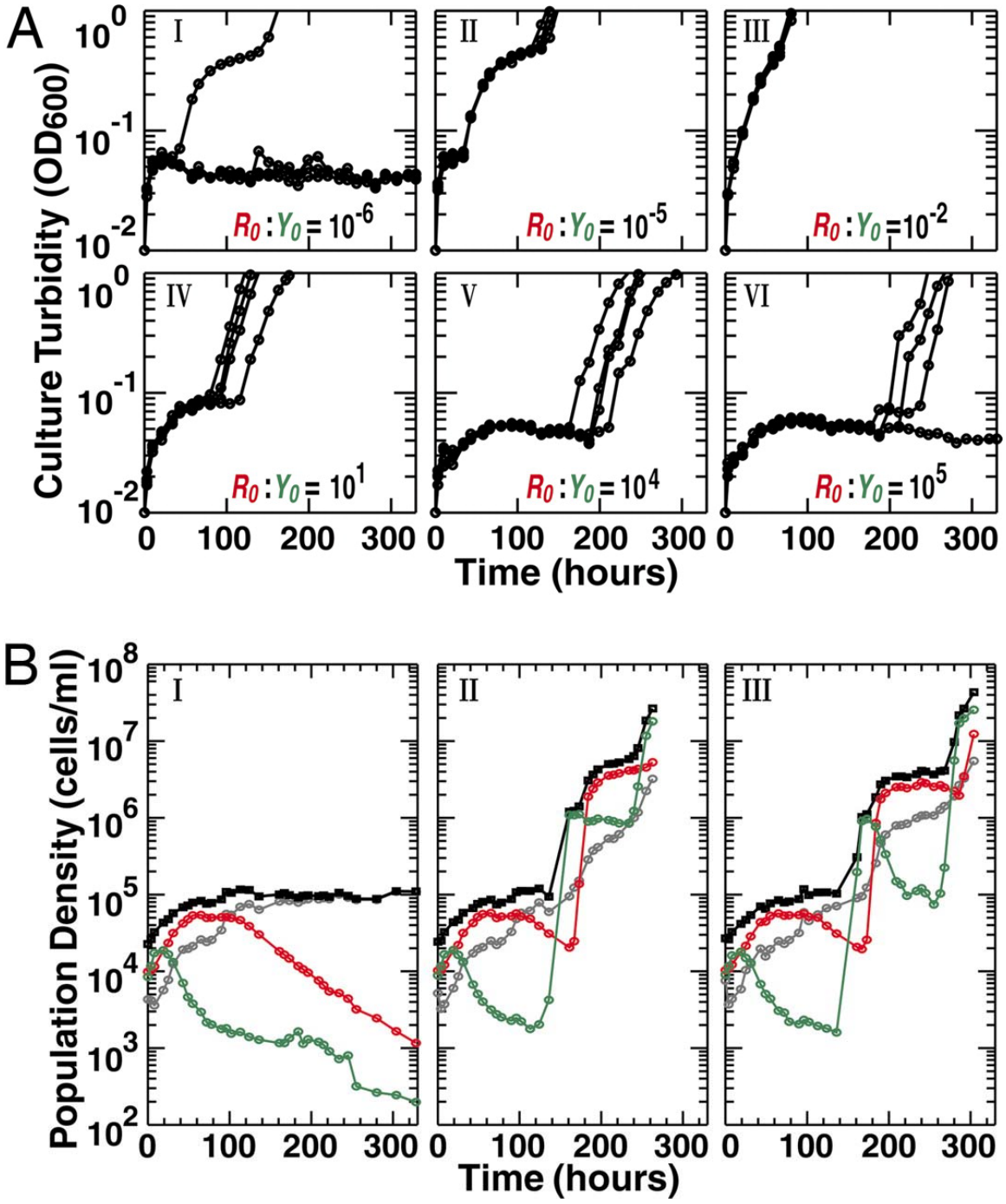

Figure 19. Viability of CoSMO.

Figure 20. Long-term population dynamics in CoSMO. (A) At time zero, duplicate CoSMO cultures (brown and blue) were initiated at OD_{600} of 0.01 ($4.7x10^5$ total cells/ml) and $R^{\leftarrow A}_{\rightarrow L}$:$Y^{\leftarrow L}_{\rightarrow A}$ ratios of 10^3 (I), 1 (II), and 10^{-3} (III). When OD_{600} exceeded the set point of 0.06 for the first time, two 3ml-samples were taken from each culture (brown and magenta from the brown; blue and cyan from the blue), and thereafter diluted once per day (magenta and cyan) or twice per day (brown and blue) to the set point. A low set point was chosen so that nutrients other than adenine and lysine were not limiting. Plots show $R^{\leftarrow A}_{\rightarrow L}$:$Y^{\leftarrow L}_{\rightarrow A}$ ratios over time, with triangles marking points of dilution. (B) Duplicate CoSMO cultures, in which partners were mixed at $R^{\leftarrow A}_{\rightarrow L}$: $Y^{\leftarrow L}_{\rightarrow A}$ =10^3 (magenta), 1 (cyan), and 10^{-3} (blue) to OD_{600} of 0.01, were initiated at time zero. Whenever the cultures reached the near-saturation set point of OD_{600}=0.4-1, they were diluted to OD_{600} of ~ 0.008. At various time points, population densities of DsRed-positive and YFP-positive cells were measured twice by flow cytometry. The average $R^{\leftarrow A}_{\rightarrow L}$:$Y^{\leftarrow L}_{\rightarrow A}$ ratio is shown with a vertical bar indicating the range. Triangles mark points of dilution.

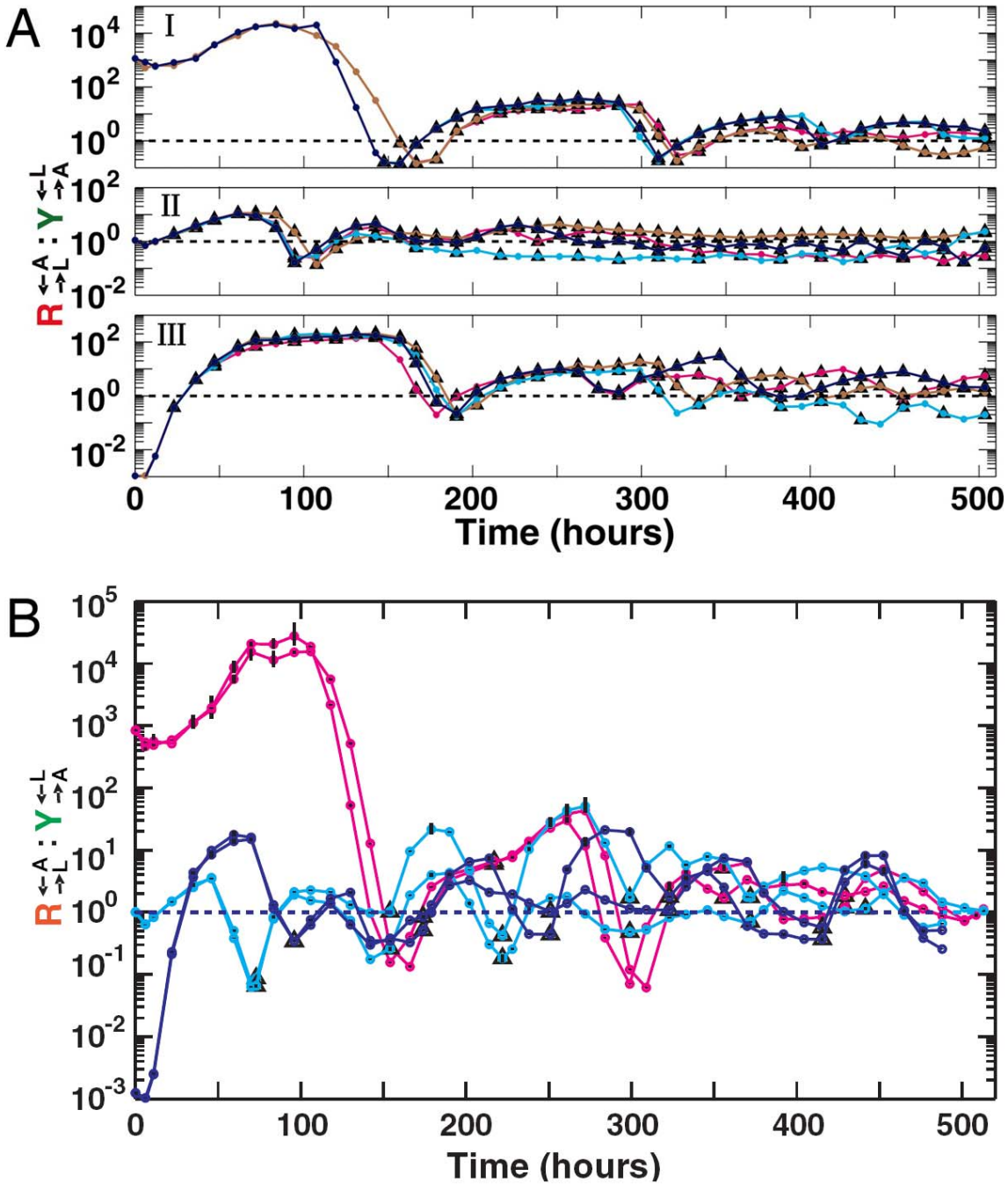

Figure 20. Long-term population dynamics in CoSMO.

Figure 21. Long-term increase in the ability to survive reductions in population density. (A) *A schematic diagram of the experimental protocol.* Five 2.6 ml-CoSMO cultures, initiated at different partner ratios, were grown to near-saturation and used as Round-0 cultures for five independent series. Each Round-0 culture was subjected to 10-fold serial dilutions with three replicate cultures per dilution so that density requirement of the culture, expressed in the number of cultures (out of 3) that are viable at various dilutions, could be measured. Out of the diluted cultures that were able to grow, one near-saturation culture was randomly chosen and subjected to 10-fold serial dilutions. This procedure was repeated ten times, spanning a total of ~70 generations. The last near-saturation culture chosen was the Round-10 culture, and its density requirement was determined in a manner similar to Round-0 cultures. (B) *Increased ability to survive reductions in population density.* Each row corresponds to a particular series and depicts the number of tubes (out of 3) that were viable at indicated dilutions for Round-0 (left) and Round-10 (right) cultures. Population densities of $R_{\rightarrow L}^{\leftarrow A}$ (red) and $Y_{\rightarrow A}^{\leftarrow L}$ (green) in million cells/ml for Round-0 and Round-10 cultures are shown in the inset.

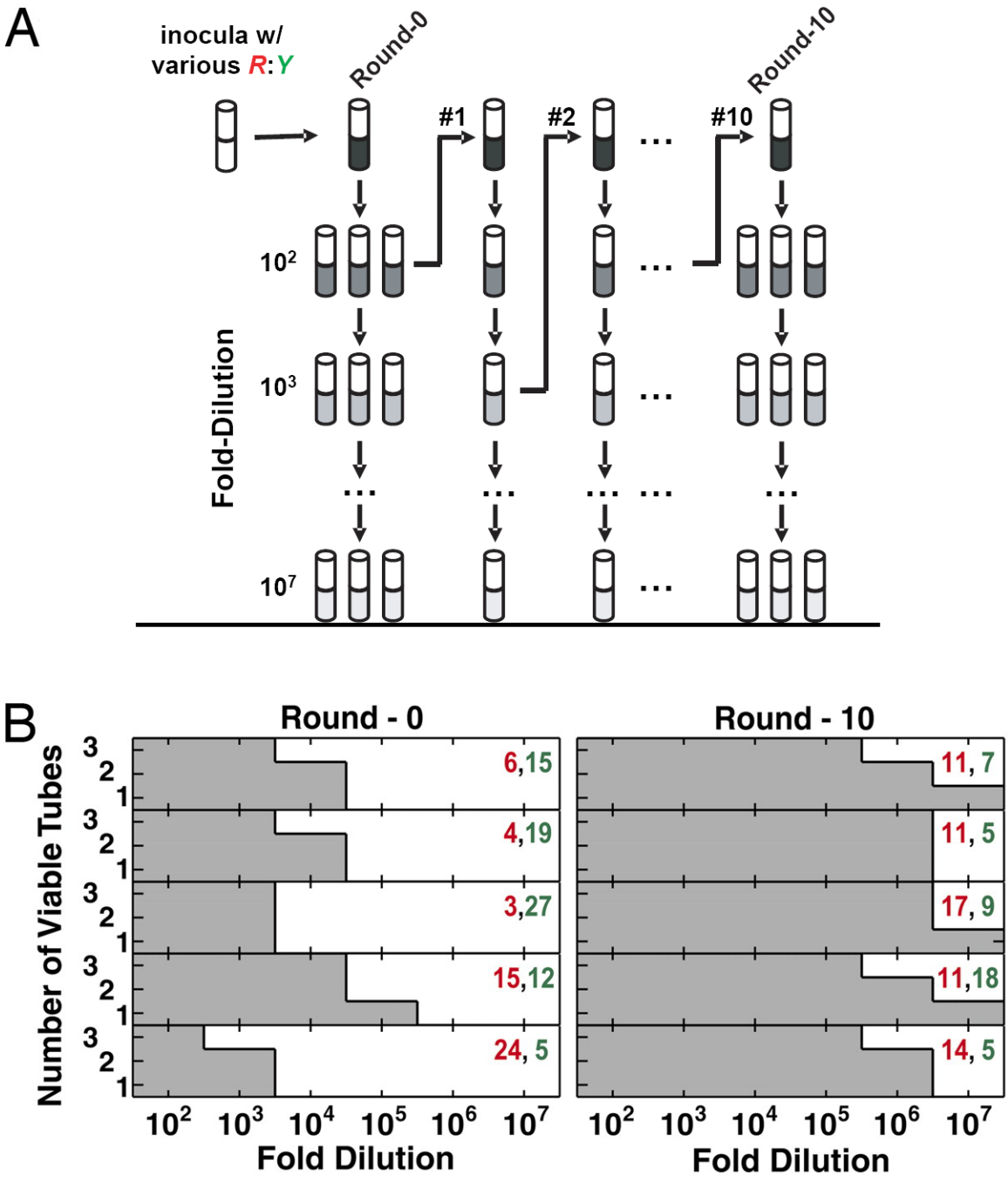

Figure 21. Long-term increase in the ability to survive reductions in population density.

Chapter 6. Discussion

6.1 Mutation Accumulation in Large Asexual Populations

The mutation rate of wild-type *E. coli* strains is estimated to be around 3×10^{-3} per genome per genome replication (Drake, 1991). More strikingly, as reviewed in section 1.1.1, this genomic mutation rate is typical of many DNA-based microbes and viruses. Many laboratory experiments (section 1.3.2), however, have shown that mutator strains outcompete their wild-type counterparts, and therefore have at least a short-term advantage. Theoretical work suggests that this should only be a transient phenomenon, and that eventually the wild-type mutation rate should be restored (section 1.3.3). In other words, mutators have a *long-term* cost, which results in their eventual downfall. What is the nature of this *long-term* cost? This question is particularly relevant for large asexual populations as there is little experimental evidence for *long-term* costs of high mutation rates in such populations (cf. section 1.3.2).

In Chapter 3, we used simulations to explore the possibility that the *long-term* cost involves deleterious mutations being fixed when rare beneficial mutations in large populations. At high mutation rates (mutator strength ~200), at least one deleterious mutation was fixed in around 60% of the simulation runs. The fitness consequences of the fixation of deleterious mutations, however, was quite small (~1%). The small effects are consistent with the observation that large populations of mutators do not suffer an

obvious fitness disadvantage in long-term evolution experiments (Sniegowski et al., 1997).

Our results suggest that high mutation rates are not a *perfect* strategy for climbing fitness peaks in the presence of rare beneficial mutations with large effects, i.e., they can lead to accumulation of deleterious mutations, and that the top of the fitness peak may never be reached. Most theoretical work on evolution in asexual populations does not consider the fixation of deleterious mutations. The primary emphasis is on the speed of adaptation, i.e., the rate of increase in mean fitness, and the effect of deleterious mutations in reducing the speed of adaptation (cf. section 1.2.1). To the best of our knowledge, there has not been any previous work directly examining mutation accumulation in large populations through the fixing of rare beneficial mutations.

Although mutation accumulation can be seen in simulations, it would be quite challenging to demonstrate it experimentally in view of the small effects involved. Deleterious effects would be most pronounced and manifested in the fewest number of generations if one used strong mutators ($M \sim 200$). Even with strong mutators, the experimental recording of mean fitness trajectories as in Figure 5 would require the ability to measure fitness of large populations ($\sim 10^9$) with high precision (~1%), high frequency (~1 fitness measurement/generation) and over long times (500-1000 generations).

6.2 Bioluminescence-based High Precision Growth Rate Measurements

In Chapter 4, we described a bioluminescence-based apparatus which allows recording of growth rate trajectories with a precision of 2.7% and a time resolution of 3.5 generations. The precision of measurements is sufficient to allow detection of changes in doubling time of as small as ~20 seconds as is the case between growth curves recorded at temperatures 0.3°C apart in Figure 8. We have improved upon the previously described technique of bioluminescence based growth rate measurements which achieved a precision of 5% (Kishony and Leibler, 2003). It is difficult to compare the precision of our measurements with other techniques as we are not aware of any studies which measure growth rates over such short time periods (~26 minutes) as we do. In some cases, the precision of measurements exceeds 5%, but the ability to make large number of replicate measurements is exploited to achieve an accuracy of less than 1% (Dekel and Alon, 2005). For experiments such as those involving measurement of fitness trajectories (cf. section 3.3), replicate measurements are not feasible as they would require sampling of the system, which would then limit the frequency of measurement.

Our work has some general bearing on making precise growth rate measurements of *E. coli*. First, we strongly recommend bioluminescence as a fast and precise method for measuring growth rates at low densities. Second, assuming that the observed temperature sensitivity of ~5.8%/˚C is typical (Figure 8), any technique should aim for a temperature stability of 0.1˚C or better to make sure that temperature fluctuations contribute at most

0.6% to the precision. Third, we find that growth curves in rich media (LB) are more reproducible than those in minimal media (Figure 6).

We identified a narrow operating region in growth curves in LB which is amenable to high precision measurement of growth rates (Figure 7). Measuring growth rates over a small operating range has several advantages: (a) the growth curves are well-described as straight lines (linear correlation coefficient $r > 0.9998$), (b) the time for a single measurement is small (~1.4 generations), and therefore not an impediment for high measurement frequency, (c) the operating range corresponds to culture densities where resource limitations are thought to be absent and cells are likely to be in the same physiological state (Baev et al., 2006), and (d) the small region ensures that intracellular physiological changes are likely to be small, thereby avoiding complications arising from changes in cellular luminescence, which is quite sensitive to physiological changes.

In order to achieve the same levels of precision in long-term cultures as in batch cultures, we had to devise an optimal dilution protocol. We find that rapid serial dilution protocols induce unacceptable temperature fluctuations in the culture (Figures 10B and 12A). This is probably an issue which is very specific to our apparatus. There is, however, a slight chance that the poor performance of rapid serial dilutions is not the direct result of the temperature fluctuations it induces (Figure 12A). In the temperature regime that we operate out apparatus, growth rates increase monotonically with temperature (Figure 8D). The temperature is expected to decrease by ~0.3°C during the growth phase of the rapid serial dilution protocol, and therefore one would expect growth rates to monotonically

decrease. Instead growth curves with the rapid serial dilution protocol (Figure 12B) have points of inflection, i.e. growth rate changes are non-monotonic. To avoid problems with temperature fluctuations, we devised a multiphase dilution protocol (Figure 13A), which maintains temperatures within 0.03°C (Figure 13B). Because there are multiple dilution phases, some of which are slow, the protocol sets the measurement frequency to around once every 3.5 generations.

Intrinsic measurement precision (0.3%, see Appendix B) can only account for a small fraction of the observed precision (2.7%). Growth rate reproducibility may be limited by fluctuations in environmental factors such as temperature, pH, dissolved oxygen concentration, and the chemical composition of the medium. Given the measured temperature sensitivity of ~5.8%/˚C (Figure 8D) and the temperature stability of 0.05˚C, we can rule out temperature as a factor limiting reproducibility. We also found that addition of pH buffers did not improve reproducibility. Medium composition is one factor that we have identified as a source of variation. There is clearly an effect on growth rate upon using different lots of medium (Figures 7B and 7D), although this cannot be the only relevant factor. For instance, the spread in generation times obtained with the first reservoir in Figure 14B (till 16.2 hours after inoculation) is ~1.3%, again more than the expected 0.3%, even though all these measurements are made with the same lot of medium. There could be some leaching of chemicals from the peristaltic pump tubing, but we do not see any systematic decrease in growth rates over time. Besides, this effect would be absent in batch cultures, even though the reproducibility in batch cultures is worse than 0.3%.

Our device is not without its limitations. First, it can only be used to measure growth rates of luminescent organisms. Long-term cultures also require the use of non-adherent strains. These two considerations would limit the range of microorganisms that can be potentially cultured in our device. Second, the operating region that we have identified is probably specific to our strain and medium. As such, this region would have to be determined afresh for each new strain. Third, bioluminescence is quite sensitive to intracellular physiology. The narrow operating region minimizes the chances of changes in light intensity per cell in that region, thereby ensuring that growth rate measurements are still valid. The operating region, however, is defined by the luminescence signal. If luminescence per cell changes, the operating region would correspond to different cell densities. Thus, it is possible that over the course of an evolutionary experiment, the operating region corresponds to different culture densities, and therefore growth rate measurements would be performed at slightly different densities. Nevertheless, given the possibility of high frequency, high precision measurements of growth rate over long-term, it is well-suited for laboratory evolution experiments.

6.3 Synthetic Cooperative System

In Chapter 5, we described the construction of a synthetic obligatory cooperative system, termed CoSMO, that consists of a pair of non-mating yeast strains, each supplying an essential metabolite to the other strain. Our system falls in the broad class of metabolically coupled microbes (Dean-Raymond and Alexander, 1977; Nurmikko, 1956; Stams et al., 2006) and provides a solution to several challenges that are present in

performing quantitative measurements on natural cooperative systems. By engineering the metabolic dependency, we know the exact nature of interaction between the two cooperating entities. In contrast, in natural systems, there are difficulties in measuring beneficial exchanges and population dynamics (Boucher, 1985). Population dynamics are easy to measure as the two CoSMO strains are marked by different fluorescent proteins.

In order to generate viable cooperative systems, we had to engineer mutations that overproduce metabolites in addition to the original auxotrophic mutation that creates the metabolic dependency (Figures 15, 16). Our results show that persistent cooperation between two populations can be created *de novo* through a small set of targeted genetic modifications. In fact, persistent cooperation is obtained in our system under a wide range of initial conditions (Figures 18,19A)

We then characterized the behavior of the two strains in isolation (Figure 17). The monoculture behavior revealed unintended constraints that restrict cooperation, such as asymmetry in starvation tolerance and delays in nutrient release until near cell death. These constraints were used to derive the requirements for the viability of the system which could be summarized as a phase diagram (Figure 18). This highlights the importance of the synthetic approach to studying cooperation. Because population dynamics could be measured easily, and the nature of the cooperative exchange was known, we were able to compute constraints on the viability of the system and verify the existence of these constraints experimentally.

Long-term population dynamics of CoSMO involves the collapse of the wide range of initial population ratios compatible with system viability to a value predicted by nutrient supply and consumption (Figure 20). Stabilization of population ratio irrespective of the starting ratio and the dilution regime suggests that CoSMO may be regarded as a single cooperative entity with the two partners serving as mutually dependent components. The relative quantities of components are self-adjusted to achieve a stoichiometric balance between nutrient supply and nutrient consumption. Ratio convergence has been observed in other cooperative systems (Rai et al., 2000; Yeoh et al., 1968) and it is possible that similar mechanisms are important in the evolution of multicellularity where proportions of different cooperating cell types are regulated (Mohanty and Firtel, 1999).

Unexpectedly, even in the absence of explicitly engineered mechanisms to stabilize cooperation, CoSMO can consistently develop increased ability to survive population bottlenecks (Figure 21). This phenomenon may result from changes in one or both strains that aid the survival of the strain itself (*e.g.* through increased starvation tolerance) or the survival of its partner (*e.g.* through increased overproduction or expedited release of metabolites). Unlike natural systems in which partner coevolution has rendered the evolutionary history of cooperation difficult to retrace (Cook and Rasplus, 2003), multiple CoSMO cultures can be initiated and their evolutionary trajectories compared. Uncovering the nature of these changes will elucidate the adaptation pathways of cooperation and the diversity in adaptive strategies (Shendure et al., 2005).

Despite its artificial origin, CoSMO closely mimics aspects of naturally occurring cooperative systems such as exchange of essential nutrients between partners (Kroon and van Ginkel, 2001; Nurmikko, 1956; Zientz et al., 2004), death of a fraction of one partner population to support the reproduction of the other partner (Cook and Rasplus, 2003; Pellmyr and Huth, 1994), and delayed reward for a particular investment. It is therefore a useful system to study the evolution of cooperation, especially given the ease with which replicate CoSMO cultures can be set up and monitored.

6.4 Future Directions

We are now poised to use the apparatus described in Chapter 4 to measure mean fitness trajectories with strong mutators (cf. section 3.3) and to potentially quantify the deleterious effects of mutation accumulation in large populations. In the immediate future, we will use the apparatus for long-term cultures with the NS2 strain (wild-type mutation rate) for a period of ~1000 generations, and verify that sweeps corresponding to beneficial mutations of large effect occur.

We also have some preliminary promising results with long-term cultures in lactose minimal media, which also appear to have a precision of~2%, even though independent batch cultures show a much higher spread (~4%, Figure 6B). We would like to see whether this is a general phenomenon, i.e., the spread in growth rate measurements in long-term cultures in minimal media is smaller than the spread obtained by setting up independent batch cultures with the same lot of medium.

We are currently in the process of constructing non-adherent mutator strains of *E. coli* as described in section 2.3. Once this process is complete, we will focus our efforts on the strongest mutator. We will first evaluate the reproducibility of growth rates in batch cultures followed by recording of mean fitness trajectories in long-term cultures. Our initial measurements will be used to verify that independent experiments charting mean fitness trajectories are reproducible in the sense that they correspond to successive sweeps of beneficial mutations of identical effect in the same order. This reproducibility has been documented in glucose-limited chemostats with large populations (Wick et al., 2002), but it may break down if measurements are made with greater precision and frequency. We will then try and align mean fitness trajectories to see if the variability is indeed higher in the case of strong mutators.

Appendix A. Temperature Sensitivity of Growth Rates

The temperature dependence of the growth rate (λ) of *E. coli* over the normal range (21˚C to 37˚C) can be described by an Arrhenius-type relationship (Ingraham and Marr, 1996):

$$\lambda(T) = \exp(-\mu/RT) \tag{1}$$

where T is the absolute temperature, R is the universal gas constant and μ is the so-called temperature characteristic. Typical values of μ range between 54,000 J/mol and 59,000 J/mol. The temperature sensitivity of growth rate (TS_λ) can then be calculated as:

$$TS_\lambda \equiv \frac{1}{\lambda}\frac{d\lambda}{dT} = \frac{\mu}{RT^2} \tag{2}$$

Extrapolating equation 1 to the temperature range used in Figure 8 and using $\mu = 56{,}500$ J/mol and $T = 311.5$ K (38.3˚C), we estimate the temperature sensitivity at 38.3˚C to be 0.07 /˚C or 7%/˚C.

Square-root models describe the temperature dependence of growth rate as follows:

$$\sqrt{\lambda(T)} = b(T - T_0) \tag{3}$$

where b and T_0 are parameters obtained by fitting the above equation to growth rate data. They are better descriptors of growth rate dependence than Arrhenius-type models over a broader range of temperatures (Ratkowsky et al., 1982). Values of T_0 for *E. coli* range from 277K to 280K. Here, the temperature sensitivity of growth rate (TS_λ) is simply:

$$TS_{\lambda} \equiv \frac{1}{\lambda}\frac{d\lambda}{dT} = \frac{2}{T - T_0} \tag{4}$$

Using $T = 311.5\,\mathrm{K}$ (38.3˚C) and $T_0 = 278.5\,\mathrm{K}$, we estimate the temperature sensitivity at 38.3˚C to be $0.06\,/^{\circ}\mathrm{C}$ or 6%/˚C.

Appendix B. Intrinsic Measurement Precision of Growth Rate Measurements

B.1 Estimating the contribution of intrinsic measurement precision to growth rate observations

Intrinsic measurement precision refers to the precision with which population size is measured. In our apparatus, this translates to the precision of measurement of bioluminescence. We adopt a conservative approach in estimating intrinsic measurement errors as our claim is that the precision in growth rate measurements is not limited by these errors.

The raw signal recorded by the multimeter, $L_{raw}(i)$, can be viewed as a random variable and written as

$$L_{raw}(i) = L_{true}(i) + B + \varepsilon(i) \quad (1)$$

where $L_{true}(i)$ is the true luminescence signal (a fixed value), B is the background signal (a fixed value), and $\varepsilon(i)$ is the intrinsic measurement error (a random variable). Since the background signal can be measured during the pre-inoculation phase, we concern ourselves with errors in the transformed signal, $L_{tr}(i) = L_{true}(i) + \varepsilon(i)$. In order to estimate statistical properties of $\varepsilon(i)$, we divide the data into contiguous, non-overlapping blocks of size $N_E = 150$ points. Assuming that the dynamics of $X_{true}(i) = \ln(L_{true}(i))$ is a linear function of time $t(i)$ in each block, we get for each block

$$X_{true}(i) = \lambda_{Blk} t(i) + \beta_{Blk} \quad (2)$$

The subscript Blk is used to denote that these are block-specific parameters. We estimate λ_{Blk} and β_{Blk} using linear least square regression of $X_{tr}(i) = \ln(L_{tr}(i))$ against $t(i)$. The estimated intrinsic error in each point then becomes

$$\varepsilon(i) = L_{tr}(i) - \exp(\lambda_{Blk} t(i) + \beta_{Blk}) \tag{3}$$

Denoting the mean block error as μ_{Blk} , variance of block error as σ^2_{Blk} , and the geometric mean of the luminescence signal in the block as $L_{Blk} = \exp\left(\frac{1}{N_E}\sum_{i\in Blk} X_{tr}(i)\right)$, we find that to a first approximation (Figures 22 and 23),

$$\mu_{Blk} = \frac{1}{N_E}\sum_{i\in Blk}\varepsilon(i) \approx 0 \tag{4a}$$

$$\sigma^2_{Blk} = \frac{1}{N_E - 1}\sum_{i\in Blk}\left(\varepsilon(i) - \mu_{Blk}\right)^2 \approx C^2 L_{Blk},\ C \approx 9\,\mu V/(mV)^{1/2} \tag{4b}$$

We therefore posit that $\varepsilon(i)$'s are independent random variables with mean $\mu_\varepsilon(i) = 0$ and variance $\sigma^2_\varepsilon(i) = C^2 L_{true}(i)$, which would be the case if the error was dominated by shot noise in the detection of photons by the PMT. We shall refer to this assumption as our intrinsic error model.

We now compute the contribution of intrinsic errors to slopes calculated from blocks of size N_S. Assuming that intrinsic errors are small, the mean $\left(\mu_X(i)\right)$ and the variance $\left(\sigma^2_X(i)\right)$ of $X_{tr}(i) = \ln(L_{tr}(i))$ can be approximated as

$$\mu_X(i) \approx \ln\left(L_{true}(i)\right) \tag{5a}$$

$$\sigma^2_X(i) \approx \frac{1}{\left(L_{true}(i)\right)^2}\sigma^2_\varepsilon(i) \approx \frac{C^2}{L_{tr}(i)} \tag{5b}$$

Once the error in individual data points in the linear regression is known, one can estimate the variance in the slope computation $\left(\sigma_{slp}^2\right)$ using standard procedures (Press et al., 1992) as:

$$\sigma_{slp}^2 = \frac{C^2\left(\sum_{i=I}^{I+N_S-1} L_{tr}(i)\right)}{\left(\sum_{i=I}^{I+N_S-1} L_{tr}(i)\right)\left(\sum_{i=I}^{I+N_S-1} t^2(i)L_{tr}(i)\right)-\left(\sum_{i=I}^{I+N_S-1} t(i)L_{tr}(i)\right)^2} \tag{6}$$

Based on simulations performed with the intrinsic error model presented above, we find that the true slope value is within $\pm 2\sigma_{slp}$ in about 95% of the cases (see section 0). We therefore use $4\sigma_{slp}$ as an estimate of the expected spread in growth rate measurements resulting from intrinsic measurement errors. Figure 25C shows how the expected spread varies as a function of geometric mean luminescence for a block size of $N_S = 250$ points, the block size used in Figures 6B, 6D, 6F,7B, and 8B. The observed spread is larger than the estimated value, implying that growth rate measurement precision is not limited by intrinsic measurement errors. In the case of Figures 7D, 8D and 14B, where at least 450 points were used to compute the generation time, the spread expected from intrinsic measurement errors is 0.3%, while the observed spread in Figure 14B is 2%, and the overall precision is ~2.7%.

B.2 Simulated Growth Curves

In order to verify the estimation procedure for intrinsic errors, we generated synthetic growth curve data using simulations which followed the intrinsic error model presented above. In the simulations,

$$L_{true}(i) = L_0 2^{t(i)/t_{gen}}, t(i) = i \cdot \tau, 0 \le i \le 3001 \quad (7)$$

where $L_{true}(i)$ is the true luminescence signal at time $t(i)$, $L_0 = 0.1$ mV is the luminescence signal at time $t(0) = 0$, $t_{gen} = 18.5$ min is the generation time and $\tau = 3.4$ s is the measurement sampling interval. These parameters were chosen as they are representative of the growth curves presented in Figure 7. Simulated growth curves were generated according to the following equation:

$$L_{tr}(i) = (1-C)L_{true}(i) + C \cdot Poiss\left(L_{true}(i)\right) \quad (8)$$

where $L_{tr}(i)$ is the measured luminescence signal, $C = 9\,\mu V/(mV)^{1/2}$ is defined in equation 4, and $Poiss(L)$ is an independent deviate drawn from a Poisson distribution with mean L. Consequently, the intrinsic measurement error in the i^{th} data point is $\varepsilon(i) = C\left(Poiss\left(L_{true}(i)\right) - L_{true}(i)\right)$ and its mean and variance are $\mu_\varepsilon(i) = 0$ and $\sigma_\varepsilon^2(i) = C^2 L_{true}(i)$ respectively.

A total of 500 simulated growth curves were generated. For each simulated growth curve, we first performed the procedure for estimating the statistics of $\varepsilon(i)$ as explained in section B.1. The luminescence time series $L_{tr}(i)$ was divided into non-overlapping blocks of size $N_E = 150$ points, and the parameters μ_{Blk} (mean block error) and σ_{Blk} (standard

deviation of block error) as defined in equation 4 were computed for each block. σ_{Blk} was fitted to a power law of L_{Blk} (the geometric mean of the luminescence signal in the block) as follows:

$$\ln(\sigma_{Blk}) \equiv \alpha \cdot \ln(L_{Blk}) + \ln C \tag{9}$$

and the parameters α and C were estimated by linear least squares regression.

Figure 24 shows the distribution of the relative error in the estimated parameters C and α in the 500 simulated growth curves. Relative error is defined as (Estimated Parameter Value – True Parameter Value)/(True Parameter Value). We find that both parameters are estimated with an accuracy of $\sim 8\%$, implying that if the intrinsic error model is taken to be true, then the estimation procedure described in section B.1 yields reasonable values for the two parameters.

We also used the simulated growth curves to evaluate the contribution of intrinsic errors to the measurement of growth rates. For this, we computed slope curves as described in section 2.1 by dividing the time series into overlapping blocks of size $N_S = 250$ points with $N_{Slide} = 25$ points. Since the true generation time is given by t_{gen}, we can compute the difference between the estimated (λ_{Blk}) and true slope $(\ln(2)/t_{gen})$. In Figure 25A, the relative error (difference between estimated and true value scaled to the true value) is plotted. Using equation 6, we can estimate the contribution of intrinsic measurement errors to slope computations (σ^2_{slp}).Figure 25B shows that the difference between the estimated and true slopes $(\lambda_{Blk} - \ln(2)/t_{gen})$ lies within $\pm 2\sigma_{slp}$ in $\sim 95\%$ of the cases

across the entire range of the luminescence signal. $4\sigma_{slp}$ is therefore a good estimate of the expected spread in the growth rate measurements resulting from intrinsic measurement errors. Finally, in Figure 25C, the expected relative spread (estimated spread in slope measurement scaled to the true value of the slope, i.e., $4\sigma_{slp}/\left(\ln(2)/t_{gen}\right)$) is plotted as a function of geometric mean luminescence $\left(L_{Blk}\right)$. This curve gives an estimate of the spread in growth rate measurements that should be observed across multiple growth curves on account of intrinsic measurement errors for a block size of $N_S = 250$ points.

Figure 22. Estimating means of intrinsic measurement errors. Growth curves depicted in Figure 7 were divided into non-overlapping blocks of size $N_E = 150$ points, and mean block error (μ_{Blk}) was plotted as a function of L_{Blk}, the geometric mean of the luminescence of the block (see section B.1). Colors used in this plot are the same as those used in Figure 7 and indicate different lots of media used. The horizontal, dashed, black line indicates a mean of zero.

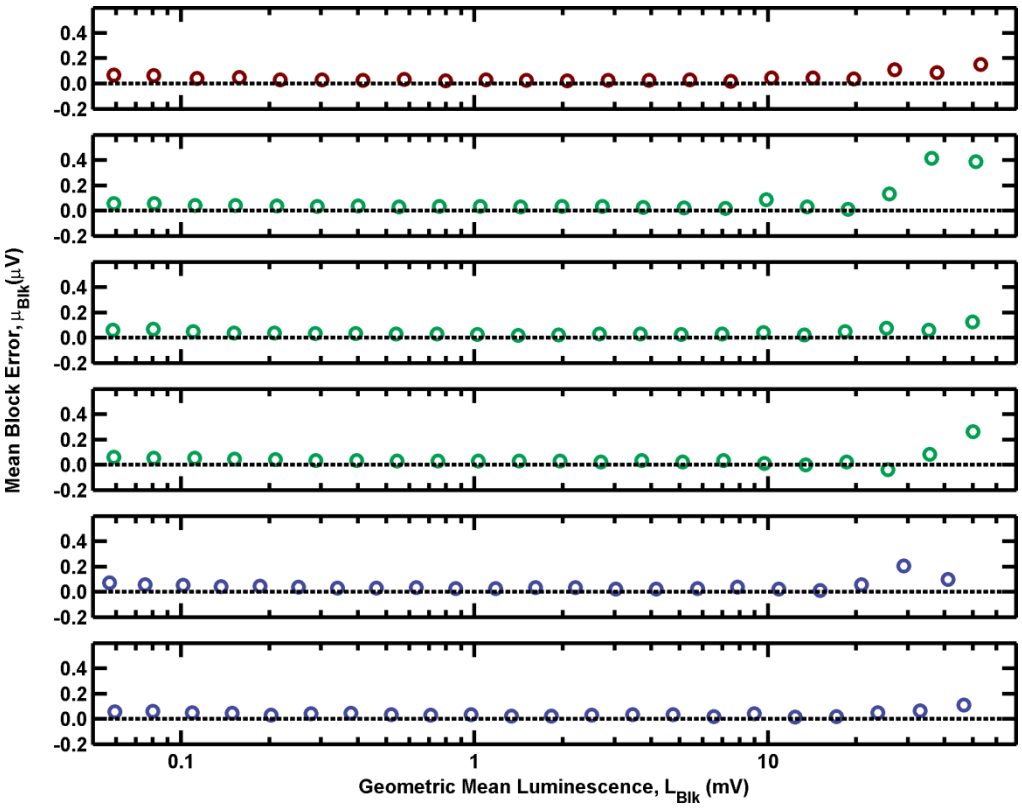

Figure 22. Estimating means of intrinsic measurement errors.

Figure 23. Estimating standard deviations of intrinsic measurement errors. Growth curves depicted in Figure 7 were divided into non-overlapping blocks of size $N_E = 150$ points, and the standard deviation of block error (σ_{Blk}) was plotted as a function of L_{Blk}, the geometric mean of the luminescence of the block (see section B.1). Open circles represent computed block parameters, whereas solid lines are power law fits as indicated in each panel. Colors used in this plot are the same as those used in Figure 7 and indicate different lots of media used.

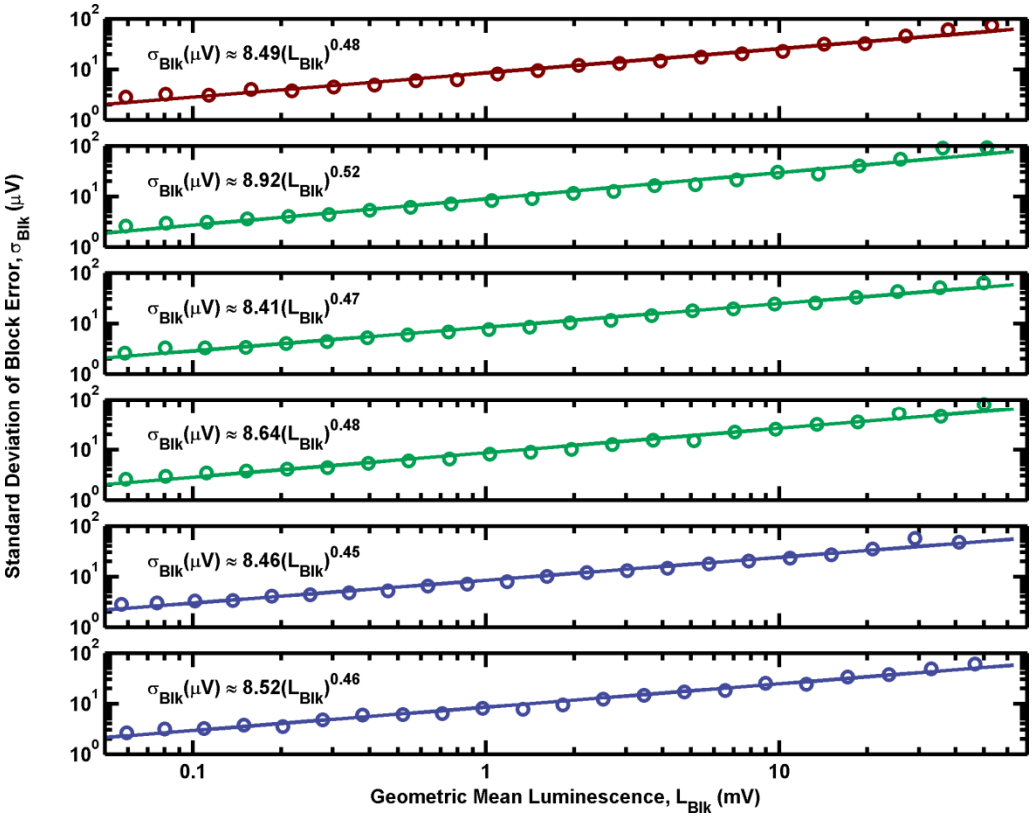

Figure 23. Estimating standard deviations of intrinsic measurement errors.

Figure 24. Accuracy of estimation of parameters *C* and α in simulated growth curves. Simulated growth curves were generated as described in section 0, and divided into non-overlapping blocks of size $N_E = 150$ points. For each simulated curve, the standard deviation of block error (σ_{Blk}) was fitted to the power law, $\ln(\sigma_{Blk}) \equiv \alpha \cdot \ln(L_{Blk}) + \ln C$. The estimated values of C and α were compared to their true values ($9\,\mu V/(mV)^{1/2}$ and 0.5 respectively) and the histogram of the relative error across all simulated growth curves is depicted. For both parameters, the accuracy of the estimation process is around 8%.

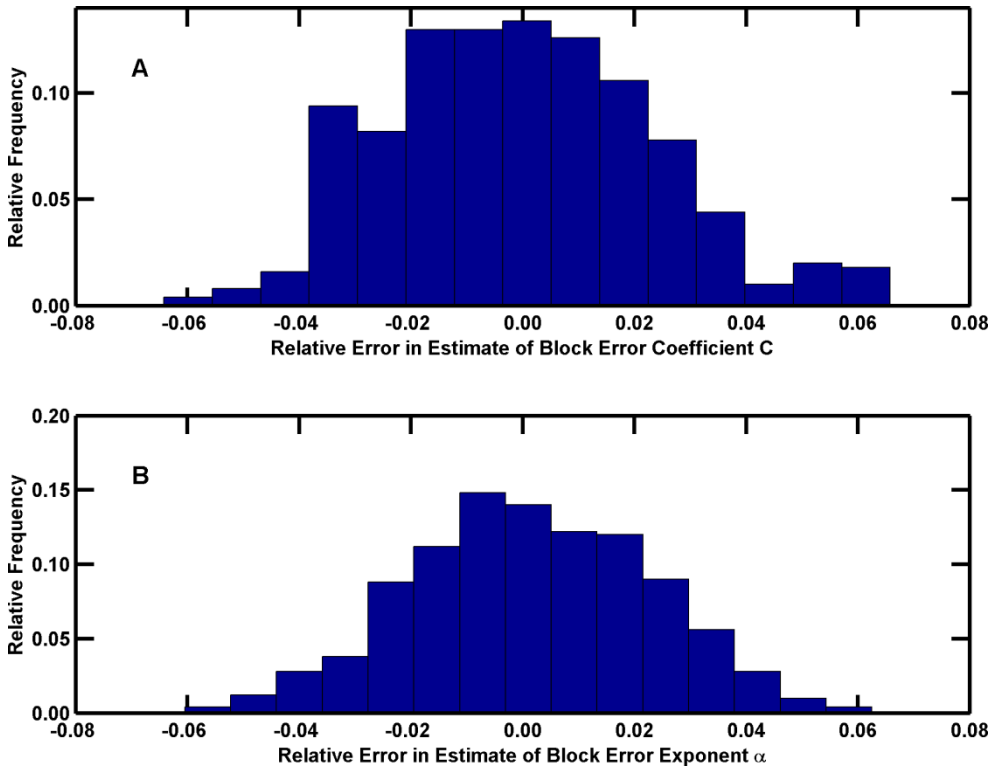

Figure 24. Accuracy of estimation of parameters C and α in simulated growth curves.

Figure 25. Intrinsic measurement error in simulated growth curves. Simulated growth curves were generated as described in section 0, and divided into overlapping blocks of size $N_S = 250$ points with $N_{Slide} = 25$ points. Slope curves were computed for each simulated growth curve as described in section 2.1. Observed error is the difference between the estimated slope (λ_{Blk}) and the true slope $(\ln(2)/t_{gen})$. (a) Relative error (ratio of observed error to true value) plotted as a function of geometric mean luminescence, L_{Blk}. (b) Ratio of observed error and estimated standard deviation in slope measurements (σ_{slp}) as a function of geometric mean luminescence. The solid horizontal black lines represent scaled deviations of ± 2. Around 95% of the slope estimates fall within these two lines. (c) Estimated spread scaled to the true slope value $(4\sigma_{slp}/(\ln(2)/t_{gen}))$ as a function of geometric mean luminescence (L_{Blk}). This curve gives an estimate of the spread in growth rate measurements that should be observed across multiple growth curves on account of intrinsic measurement errors for a block size of $N_S = 250$ points.

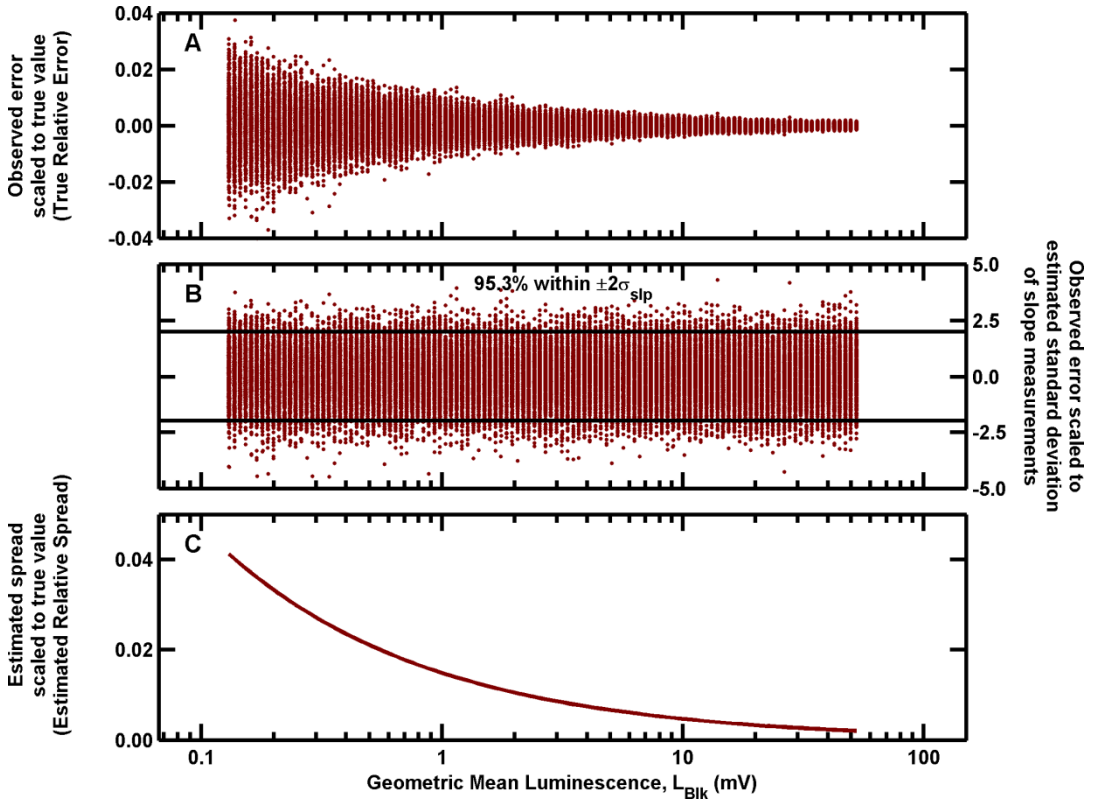

Figure 25. Intrinsic measurement error in simulated growth curves.

Appendix C. Definitions and Experimental Values of Parameters Used in Chapter 5

Symbol	Definition	Value Range (Experimental)	Value*
T_I [i]	Time of the end of residual growth	10 hours	10
T_R [i]	Delay in $R_{\rightarrow L}^{\leftarrow A}$'s entry into death phase after the onset of starvation	60-80 hours	70
D_R [ii]	Death rate of $R_{\rightarrow L}^{\leftarrow A}$ in the absence of adenine after time T_R	0.007-0.04/hour	0.01
D_Y [ii]	Death rate of $Y_{\rightarrow A}^{\leftarrow L}$ in the absence of lysine averaged from time T_I to T_R	0.054/hour	0.054
D_{YLate} [ii]	Death rate of $Y_{\rightarrow A}^{\leftarrow L}$ in the absence of lysine after time T_R	0.02/hour	0.02
A_s [iii]	Adenine supplied per $Y_{\rightarrow A}^{\leftarrow L}$ cell upon death	3 fmole/cell	3
L_s [iii]	Lysine supplied per $R_{\rightarrow L}^{\leftarrow A}$ cell upon death	15 fmole/cell	15
G_{maxY} [iv]	Maximum growth rate of $Y_{\rightarrow A}^{\leftarrow L}$ when lysine is in excess	0.31/hour	0.31
V_{maxL} [iv]	Maximum lysine uptake rate per $Y_{\rightarrow A}^{\leftarrow L}$ cell when lysine is in excess	2.4 fmole/cell/hr	2.4
$A_{c\text{-}fed}$ [v]	Adenine consumed to produce a fed $R_{\rightarrow L}^{\leftarrow A}$ cell when adenine is in excess	1 fmole/cell	
$L_{c\text{-}fed}$ [v]	Lysine consumed to produce a fed $Y_{\rightarrow A}^{\leftarrow L}$ cell when lysine is in excess	5.4 fmole/cell	
I_R	Fold-increase in cell density during residual growth of $R_{\rightarrow L}^{\leftarrow A}$	1-2	1.5
I_Y	Fold-increase in cell density during residual growth of $Y_{\rightarrow A}^{\leftarrow L}$	2-4	3
A_c [vi]	Adenine consumed in order to produce a starving $R_{\rightarrow L}^{\leftarrow A}$ cell	0.5-1 fmole/cell	1
L_c [vi]	Lysine consumed in order to produce a starving $Y_{\rightarrow A}^{\leftarrow L}$ cell	1.4-2.7 fmole/cell	2
K_{mL} [vii]	Michaelis-Menten half-saturation constant of lysine transporter	20-80 μM	50

Table 2. Parameter values used in Chapter 5.

*: Values used in calculations.

[i] Data from Figure 17.

[ii] Death rates were measured during the specified time windows, and were found to be density-dependent. D_R=0.01 is the average of 0.007, 0.009, and 0.018/hour, obtained over a range of initial cell densities varying from 0.05 to 1.1×10^6 cells/ml. D_Y and D_{YLate} were obtained at initial cell densities ranging from 0.28 to 1.2×10^6 cells/ml.

[iii] The kinetics of metabolite release approximately coincided with that of cell death (Figure 17B). Thus, we assume that a starving cell releases a fixed amount of the overproduced metabolite into the medium upon death. Metabolite supplied per dead cell was estimated from Figure 17B by dividing the final concentration of released metabolite by the final population density of dead cells.

[iv] Figure 26.

[v] When adenine was present in excess, the maximum uptake rate of adenine V_{maxA} was 0.5 fmole/cell/hr and the maximum growth rate of $R_{\rightarrow L}^{\leftarrow A}$ cells was G_{maxR} = 0.37/hr (methods of measurement similar to those in Figure 26). Thus, it took $A_{c\text{-}fed} = V_{maxA}$ X (ln2/ G_{maxR}) ~1 fmole adenine to produce a fed $R_{\rightarrow L}^{\leftarrow A}$ cell, where ln2/ G_{maxR} was the doubling time of $R_{\rightarrow L}^{\leftarrow A}$. Similarly, it took $L_{c\text{-}fed} = V_{maxL}$ X (ln2/ G_{maxY})= 5.4 fmole lysine to produce a fed $Y_{\rightarrow A}^{\leftarrow L}$ cell.

[vi] Since one fed $Y_{\rightarrow A}^{\leftarrow L}$ cell gave rise to I_Y lysine-starved $Y_{\rightarrow A}^{\leftarrow L}$ cells during residual growth, it took $L_c = L_{c\text{-}fed}/I_Y$ amount of lysine to produce a starving $Y_{\rightarrow A}^{\leftarrow L}$ cell. Similarly, it took $A_c = A_{c\text{-}fed}/I_R$ amount of adenine to produce an adenine-starved $R_{\rightarrow L}^{\leftarrow A}$ cell.

[vii] (Garcia and Kotyk, 1988; Sychrova and Chevallier, 1993).

Figure 26. Measurements of G_{maxY} and V_{maxL}. $Y_{\rightarrow A}^{\leftarrow L}$ cells were grown in SD supplemented with lysine. Time zero was arbitrarily chosen in early exponential phase. Plots show the population density of $Y_{\rightarrow A}^{\leftarrow L}$ (left panel, green circles) and the concentration of lysine remaining in the medium (right panel, brown circles) over time. The least-square-fitting equation for the left panel is $Y = Y_0 e^{t \cdot G_{maxY}}$ (dotted line) and yields the initial population density Y_0 and the maximum growth rate G_{maxY}. The least-square-fitting equation for the right panel is $L = L_0 + V_{maxL} Y_0 (1 - e^{t \cdot G_{maxY}}) / G_{maxY}$ (dotted line), which is the solution to the differential equation $\frac{dL}{dt} = -V_{maxL} Y = -V_{maxL} Y_0 e^{t \cdot G_{maxY}}$, and yields the initial lysine concentration L_0 and the maximum lysine uptake rate per cell V_{maxL}.

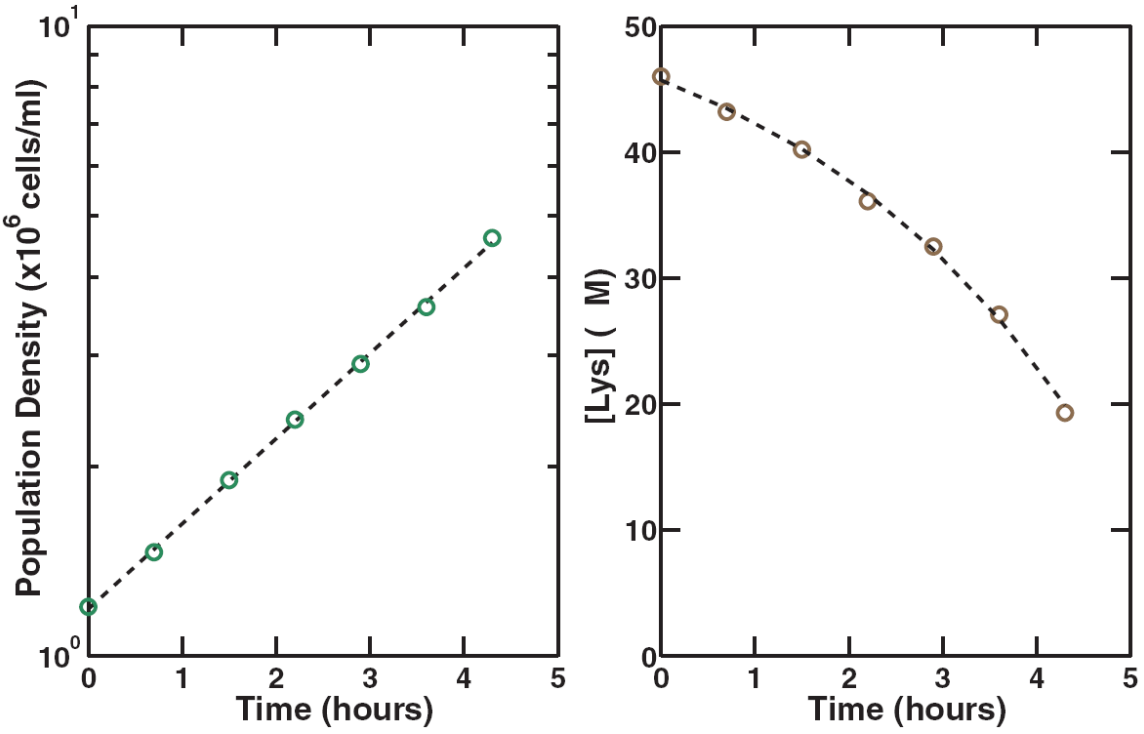

Figure 26. Measurements of G_{maxY} and V_{maxL}.

References

Anderson, P.A. (1953) Automatic recording of the growth rates of continuously cultured microorganisms. *Journal of General Physiology* **36**: 733-737.

André, J.B., and Godelle, B. (2006) The evolution of mutation rate in finite asexual populations. *Genetics* **172**: 611-626.

Armitt, S., and Woods, R.A. (1970) Purine-excreting mutants of *Saccharomyces cerevisiae*. I. Isolation and genetic analysis. *Genetical Research* **15**: 7-17.

Baba, T., Ara, T., Hasegawa, M., Takai, Y., Okumura, Y., Baba, M., Datsenko, K.A., Tomita, M., Wanner, B.L., and Mori, H. (2006) Construction of *Escherichia coli* K-12 in-frame, single-gene knockout mutants: The Keio collection. *Molecular Systems Biology* **2**: 2006.0008.

Baev, M.V., Baev, D., Radek, A.J., and Campbell, J.W. (2006) Growth of *Escherichia coli* MG1655 on LB medium: Determining metabolic strategy with transcriptional microarrays. *Applied Microbiology and Biotechnology* **71**: 323-328.

Balagadde, F.K., You, L.C., Hansen, C.L., Arnold, F.H., and Quake, S.R. (2005) Long-term monitoring of bacteria undergoing programmed population control in a microchemostat. *Science* **309**: 137-140.

Baquero, M.R., Nilsson, A.I., del Carmen Turrientes, M., Sandvang, D., Galan, J.C., Martinez, J.L., Frimodt-Moller, N., Baquero, F., and Andersson, D.I. (2004) Polymorphic mutation frequencies in *Escherichia coli*: Emergence of weak mutators in clinical isolates. *Journal of Bacteriology* **186**: 5538-5542.

Baquero, M.R., Galan, J.C., Turrientes, M.D., Canton, R., Coque, T.M., Martinez, J.L., and Baquero, F. (2005) Increased mutation frequencies in *Escherichia coli* isolates harboring extended-spectrum beta-lactamases. *Antimicrobial Agents and Chemotherapy* **49**: 4754-4756.

Bergstrom, C.T., Bronstein, J.L., Bshary, R., Connor, R.C., Daly, M., Frank, S.A., Gintis, H., Keller, L., Leimar, O., Noe, R., and Queller, D.C. (2002) Group report: Interspecific mutualism - puzzles and predictions. In *Genetic and cultural evolution of cooperation*. Hammerstein, P. (ed): The MIT Press.

Bevis, B.J., and Glick, B.S. (2002) Rapidly maturing variants of the *Discosoma* red fluorescent protein (dsred). *Nature Biotechnology* **20**: 83-87.

Blázquez, J. (2003) Hypermutation as a factor contributing to the acquisition of antimicrobial resistance. *Clinical Infectious Diseases* **37**: 1201-1209.

Boe, L., Danielsen, M., Knudsen, S., Petersen, J.B., Maymann, J., and Jensen, P.R. (2000) The frequency of mutators in populations of *Escherichia coli*. *Mutation Research-Fundamental and Molecular Mechanisms of Mutagenesis* **448**: 47-55.

Boucher, D.H. (1985) *The biology of mutualism: Ecology and evolution.* New York: Oxford University Press.

Brachmann, C.B., Davies, A., Cost, G.J., Caputo, E., Li, J., Hieter, P., and Boeke, J.D. (1998) Designer deletion strains derived from *Saccharomyces cerevisiae* S288C: A useful set of strains and plasmids for PCR-mediated gene disruption and other applications. *Yeast* **14**: 115-132.

Bronstein, J.L., and Hossaert-McKey, M. (1995) Hurricane Andrew and a Florida fig pollination mutualism: Resilience of an obligate interaction. *Biotropica* **27**: 373-381.

Buchsbaum, R., and Buchsbaum, M. (1934) An artificial symbiosis. *Science* **80**: 408-409.

Campos, P.R.A., and De Oliveira, V.M. (2004) Mutational effects on the clonal interference phenomenon. *Evolution* **58**: 932-937.

Chao, L., and Cox, E.C. (1983) Competition between high and low mutating strains of *Escherichia coli*. *Evolution* **37**: 125-134.

Cherepanov, P.P., and Wackernagel, W. (1995) Gene disruption in *Escherichia coli*: Tc^R and Km^R cassettes with the option of Flp-catalyzed excision of the antibiotic-resistance determinant. *Gene* **158**: 9-14.

Chopra, I., O'Neill, A.J., and Miller, K. (2003) The role of mutators in the emergence of antibiotic-resistant bacteria. *Drug Resistance Updates* **6**: 137-145.

Cook, J.M., and Rasplus, J.Y. (2003) Mutualists with attitude: Coevolving fig wasps and figs. *Trends in Ecology & Evolution* **18**: 241-248.

Cooper, T.F., Rozen, D.E., and Lenski, R.E. (2003) Parallel changes in qene expression after 20,000 generations of evolution in *Escherichia coli*. *Proceedings of the National Academy of Sciences of the United States of America* **100**: 1072-1077.

Cooper, V.S., and Lenski, R.E. (2000) The population genetics of ecological specialization in evolving *Escherichia coli* populations. *Nature* **407**: 736-739.

Cox, E.C., and Gibson, T.C. (1974) Selection for high mutation rates in chemostats. *Genetics* **77**: 169-184.

Cox, E.C. (1976) Bacterial mutator genes and the control of spontaneous mutation. *Annual Review of Genetics* **10**: 135-156.

Darwin, C. (1859) *On the origin of species by means of natural selection, or the preservation of favoured races in the struggle for life.* London: John Murray.

Datsenko, K.A., and Wanner, B.L. (2000) One-step inactivation of chromosomal genes in *Escherichia coli* K-12 using PCR products. *Proceedings of the National Academy of Sciences of the United States of America* **97**: 6640-6645.

Daurel, C., Prunier, A.L., Chau, F., Garry, L., Leclercq, R., and Fantin, B. (2007) Role of hypermutability on bacterial fitness and emergence of resistance in experimental osteomyelitis due to *Staphylococcus aureus*. *FEMS Immunology and Medical Microbiology* **51**: 344-349.

de Visser, J.A.G.M., Zeyl, C.W., Gerrish, P.J., Blanchard, J.L., and Lenski, R.E. (1999) Diminishing returns from mutation supply rate in asexual populations. *Science* **283**: 404-406.

de Visser, J.A.G.M., and Rozen, D.E. (2006) Clonal interference and the periodic selection of new beneficial mutations in *Escherichia coli*. *Genetics* **172**: 2093-2100.

Dean-Raymond, D., and Alexander, M. (1977) Bacterial metabolism of quaternary ammonium-compounds. *Applied and Environmental Microbiology* **33**: 1037-1041.

Dekel, E., and Alon, U. (2005) Optimality and evolutionary tuning of the expression level of a protein. *Nature* **436**: 588-592.

Denamur, E., Tenaillon, O., Deschamps, C., Skurnik, D., Ronco, E., Gaillard, J.L., Picard, B., Branger, C., and Matic, I. (2005) Intermediate mutation frequencies favor evolution of multidrug resistance in *Escherichia coli*. *Genetics* **171**: 825-827.

Desai, M.M., and Fisher, D.S. (2007) Beneficial mutation selection balance and the effect of linkage on positive selection. *Genetics* **176**: 1759-1798.

Desai, M.M., Fisher, D.S., and Murray, A.W. (2007) The speed of evolution and maintenance of variation in asexual populations. *Current Biology* **17**: 385-394.

Drake, J.W. (1991) A constant rate of spontaneous mutation in DNA-based microbes. *Proceedings of the National Academy of Sciences of the United States of America* **88**: 7160-7164.

Drake, J.W., Charlesworth, B., Charlesworth, D., and Crow, J.F. (1998) Rates of spontaneous mutation. *Genetics* **148**: 1667-1686.

Drake, J.W. (1999) The distribution of rates of spontaneous mutation over viruses, prokaryotes, and eukaryotes. *Annals of the New York Academy of Sciences* **870**: 100-107.

Dykhuizen, D.E., and Hartl, D.L. (1983) Selection in chemostats. *Microbiological Reviews* **47**: 150-168.

Elena, S.F., and Lenski, R.E. (2003) Evolution experiments with microorganisms: The dynamics and genetic bases of adaptation. *Nature Reviews Genetics* **4**: 457-469.

Feller, A., Ramos, F., Pierard, A., and Dubois, E. (1999) In *Saccharomyces cerevisae*, feedback inhibition of homocitrate synthase isoenzymes by lysine modulates the activation of LYS gene expression by Lys14p. *European Journal of Biochemistry* **261**: 163-170.

Fiegna, F., Yu, Y.T.N., Kadam, S.V., and Velicer, G.J. (2006) Evolution of an obligate social cheater to a superior cooperator. *Nature* **441**: 310-314.

Fisher, R.A. (1930) *The genetical theory of natural selection.* Oxford: Oxford University Press.

Funchain, P., Yeung, A., Stewart, J.L., Lin, R., Slupska, M.M., and Miller, J.H. (2000) The consequences of growth of a mutator strain of *Escherichia coli* as measured by loss of function among multiple gene targets and loss of fitness. *Genetics* **154**: 959-970.

Garcia, J.C., and Kotyk, A. (1988) Uptake of L-lysine by a double mutant of *Saccharomyces cerevisiae*. *Folia Microbiologica* **33**: 285-291.

Garibyan, L., Huang, T., Kim, M., Wolff, E., Nguyen, A., Nguyen, T., Diep, A., Hu, K., Iverson, A., and Yang, H. (2003) Use of the *rpoB* gene to determine the specificity of base substitution mutations on the *Escherichia coli* chromosome. *DNA Repair* **2**: 593-608.

Gerrish, P.J., and Lenski, R.E. (1998) The fate of competing beneficial mutations in an asexual population. *Genetica* **102**: 127-144.

Gibson, T.C., Scheppe, M.L., and Cox, E.C. (1970) Fitness of an *Escherichia coli* mutator gene. *Science* **169**: 686-688.

Giraud, A., Matic, I., Tenaillon, O., Clara, A., Radman, M., Fons, M., and Taddei, F. (2001) Costs and benefits of high mutation rates: Adaptive evolution of bacteria in the mouse gut. *Science* **291**: 2606-2608.

Gordo, I., and Charlesworth, B. (2000) The degeneration of asexual haploid populations and the speed of Muller's ratchet. *Genetics* **154**: 1379-1387.

Gray, G.S., and Bhattacharjee, J.K. (1976) Biosynthesis of lysine in *Saccharomyces cerevisiae*: Regulation of homocitrate synthase in analogue-resistant mutants. *Journal of General Microbiology* **97**: 117-120.

Guthrie, C., and Fink, G.R. (1991) *Guide to yeast genetics and molecular biology.* San Diego: Academic Press.

Hagen, D.C., McCaffrey, G., and Sprague, G.F., Jr. (1986) Evidence the yeast STE3 gene encodes a receptor for the peptide pheromone a factor: Gene sequence and implications for the structure of the presumed receptor. *Proceedings of the National Academy of Sciences of the United States of America* **83**: 1418-1422.

Haigh, J. (1978) Accumulation of deleterious genes in a population - Muller's ratchet. *Theoretical Population Biology* **14**: 251-267.

Hall, L.M.C., and Henderson-Begg, S.K. (2006) Hypermutable bacteria isolated from humans - a critical analysis. *Microbiology* **152**: 2505-2514.

Hanahan, D., and Folkman, J. (1996) Patterns and emerging mechanisms of the angiogenic switch during tumorigenesis. *Cell* **86**: 353-364.

Hegreness, M., Shoresh, N., Hartl, D., and Kishony, R. (2006) An equivalence principle for the incorporation of favorable mutations in asexual populations. *Science* **311**: 1615-1617.

Horst, J.P., Wu, T.H., and Marinus, M.G. (1999) *Escherichia coli* mutator genes. *Trends in Microbiology* **7**: 29-36.

Hoskisson, P.A., and Hobbs, G. (2005) Continuous culture - making a comeback? *Microbiology* **151**: 3153-3159.

Humayun, M.Z. (1998) SOS and mayday: Multiple inducible mutagenic pathways in *Escherichia coli*. *Molecular Microbiology* **30**: 905-910.

Imhof, M., and Schlötterer, C. (2001) Fitness effects of advantageous mutations in evolving *Escherichia coli* populations. *Proceedings of the National Academy of Sciences of the United States of America* **98**: 1113-1117.

Ingraham, J.L., and Marr, A.G. (1996) Effects of temperature, pressure, pH, and osmotic stress on growth. In *Escherichia coli and Salmonella: Cellular and molecular biology*. Umbarger, H.E. (ed). Washington, D.C.: ASM Press, pp. 1570-1578.

Jeon, K.W. (1972) Development of cellular dependence on infective organisms: Micrurgical studies in amoebas. *Science* **176**: 1122-1123.

Johnson, T. (1999) The approach to mutation-selection balance in an infinite asexual population, and the evolution of mutation rates. *Proceedings of the Royal Society of London. Series B: Biological Sciences* **266**: 2389-2397.

Johnson, T., and Barton, N.H. (2002) The effect of deleterious alleles on adaptation in asexual populations. *Genetics* **162**: 395-411.

Kessler, D.A., and Levine, H. (1998) Mutator dynamics on a smooth evolutionary landscape. *Physical Review Letters* **80**: 2012-2015.

Kibota, T.T., and Lynch, M. (1996) Estimate of the genomic mutation rate deleterious to overall fitness in *E. coli*. *Nature* **381**: 694-696.

Kimura, M. (1967) On the evolutionary adjustment of spontaneous mutation rates. *Genetical Research* **9**: 23-34.

Kimura, M. (1983) *The neutral theory of molecular evolution.* Cambridge: Cambridge University Press.

Kishony, R., and Leibler, S. (2003) Environmental stresses can alleviate the average deleterious effect of mutations. *Journal of Biology* **2**: 14.

Kjargaard, K., Schembri, M.A., Hasman, H., and Klemm, P. (2000) Antigen 43 from *Escherichia coli* induces inter- and intraspecies cell aggregation and changes in colony morphology of *Pseudomonas fluorescens*. *Journal of Bacteriology* **182**: 4789-4796.

Kroon, A.G.M., and van Ginkel, C.G. (2001) Complete mineralization of dodecyldimethylamine using a two-membered bacterial culture. *Environmental Microbiology* **3**: 131-136.

Kussell, E., and Leibler, S. (2005) Phenotypic diversity, population growth, and information in fluctuating environments. *Science* **309**: 2075-2078.

Le Chat, L., Fons, M., and Taddei, F. (2006) *Escherichia coli* mutators: Selection criteria and migration effect. *Microbiology* **152**: 67-73.

LeClerc, J.E., Li, B., Payne, W.L., and Cebula, T.A. (1996) High mutation frequencies among *Escherichia coli* and *Salmonella* pathogens. *Science* **274**: 1208.

Lehmann, L., and Keller, L. (2006) The evolution of cooperation and altruism - a general framework and a classification of models. *Journal of Evolutionary Biology* **19**: 1365-1376.

Leigh, E.G. (1970) Natural selection and mutability. *American Naturalist* **104**: 301-&.

Leimar, O., and Hammerstein, P. (2006) Facing the facts. *Journal of Evolutionary Biology* **19**: 1403-1405.

Lenski, R.E. (1988) Experimental studies of pleiotropy and epistasis in *Escherichia coli*. I. Variation in competitive fitness among mutants resistant to virus T4. *Evolution* **42**: 425-432.

Lenski, R.E., Rose, M.R., Simpson, S.C., and Tadler, S.C. (1991) Long-term experimental evolution in *Escherichia coli*. I. Adaptation and divergence during 2,000 generations. *American Naturalist* **138**: 1315-1341.

Lenski, R.E., and Travisano, M. (1994) Dynamics of adaptation and diversification: A 10,000-generation experiment with bacterial populations. *Proceedings of the National Academy of Sciences of the United States of America* **91**: 6808-6814.

Maharjan, R., Seeto, S., Notley-McRobb, L., and Ferenci, T. (2006) Clonal adaptive radiation in a constant environment. *Science* **313**: 514-517.

Maki, H. (2002) Origins of spontaneous mutations: Specificity and directionality of base-substitution, frameshift, and sequence-substitution mutageneses. *Annual Review of Genetics* **36**: 279-303.

Mao, E.F., Lane, L., Lee, J., and Miller, J.H. (1997) Proliferation of mutators in a cell population. *Journal of Bacteriology* **179**: 417.

Marincs, F. (2000) On-line monitoring of growth of *Escherichia coli* in batch cultures by bioluminescence. *Applied Microbiology and Biotechnology* **53**: 536-541.

Markx, G.H., Davey, C.L., and Kell, D.B. (1991) The permittistat - a novel type of turbidostat. *Journal of General Microbiology* **137**: 735-743.

Matic, I., Radman, M., Taddei, F., Picard, B., Doit, C., Bingen, E., Denamur, E., and Elion, J. (1997) Highly variable mutation rates in commensal and pathogenic *Escherichia coli*. *Science* **277**: 1833-1834.

Meighen, E.A. (1993) Bacterial bioluminescence: Organization, regulation, and application of the *lux* genes. *FASEB Journal* **7**: 1016-1022.

Messenguy, F., Colin, D., and ten Have, J.P. (1980) Regulation of compartmentation of amino acid pools in *Saccharomyces cerevisiae* and its effects on metabolic control. *European Journal of Biochemistry* **108**: 439-447.

Metzgar, D., and Wills, C. (2000) Evidence for the adaptive evolution of mutation rates. *Cell* **101**: 581-584.

Meyer, J.S., and Tsuchiya, H.M. (1975) Dynamics of mixed populations having complementary metabolism. *Biotechnology and Bioengineering* **17**: 1065-1081.

Miller, J.H. (1992) *A short course in bacterial genetics : A laboratory manual and handbook for Escherichia coli and related bacteria.* Plainview, N.Y.: Cold Spring Harbor Laboratory Press.

Miller, J.H. (1996) Spontaneous mutators in bacteria: Insights into pathways of mutagenesis and repair. *Annual Review of Microbiology* **50**: 625-643.

Miller, J.H. (1998) Mutators in *Escherichia coli*. *Mutation Research* **409**: 99-106.

Miller, J.H., Suthar, A., Tai, J., Yeung, A., Truong, C., and Stewart, J.L. (1999) Direct selection for mutators in *Escherichia coli*. *Journal of Bacteriology* **181**: 1576-1584.

Miller, K., O'Neill, A.J., and Chopra, I. (2004) *Escherichia coli* mutators present an enhanced risk for emergence of antibiotic resistance during urinary tract infections. *Antimicrobial Agents and Chemotherapy* **48**: 23-29.

Mohanty, S., and Firtel, R.A. (1999) Control of spatial patterning and cell-type proportioning in *Dictyostelium*. *Seminars in Cell and Developmental Biology* **10**: 597-607.

Monod, J. (1949) The growth of bacterial cultures. *Annual Review of Microbiology* **3**: 371-394.

Monod, J. (1950) La technique de culture continue théorie et applications. *Annales de l Institut Pasteur* **79**: 390-410.

Moxon, E.R., Rainey, P.B., Nowak, M.A., and Lenski, R.E. (1994) Adaptive evolution of highly mutable loci in pathogenic bacteria. *Current Biology* **4**: 24-33.

Munson, R.J. (1970) Turbidostats. *Methods in Microbiology* **2**: 349-376.

Nagy, M. (1979) Studies on purine transport and on purine content in vacuoles isolated from *Saccharomyces cerevisiae*. *Biochimica et Biophysica Acta* **558**: 221-232.

Nestmann, E.R., and Hill, R.F. (1973) Population changes in continuously growing mutator cultures of *Escherichia coli*. *Genetics* **73**: 41-44.

Nohmi, T. (2006) Environmental stress and lesion-bypass DNA polymerases. *Annual Review of Microbiology* **60**: 231-253.

Notley-McRobb, L., Pinto, R., Seeto, S., and Ferenci, T. (2002a) Regulation of *mutY* and nature of mutator mutations in *Escherichia coli* populations under nutrient limitation. *Journal of Bacteriology* **184**: 739-745.

Notley-McRobb, L., Seeto, S., and Ferenci, T. (2002b) Enrichment and elimination of *mutY* mutators in *Escherichia coli* populations. *Genetics* **162**: 1055-1062.

Notley-McRobb, L., Seeto, S., and Ferenci, T. (2003) The influence of cellular physiology on the initiation of mutational pathways in *Escherichia coli* populations. *Proceedings of the Royal Society of London. Series B: Biological Sciences* **270**: 843-848.

Novick, A., and Szilard, L. (1950a) Experiments with the chemostat on spontaneous mutations of bacteria. *Proceedings of the National Academy of Sciences of the United States of America* **36**: 708-719.

Novick, A., and Szilard, L. (1950b) Description of the chemostat. *Science* **112**: 715-716.

Nurmikko, V. (1956) Biochemical factors affecting symbiosis among bacteria. *Experientia* **12**: 245-249.

Örlén, H., and Hughes, D. (2006) Weak mutators can drive the evolution of fluoroquinolone resistance in *Escherichia coli*. *Antimicrobial Agents and Chemotherapy* **50**: 3454-3456.

Orr, H.A. (2000) The rate of adaptation in asexuals. *Genetics* **155**: 961-968.

Palmer, M.E., and Lipsitch, M. (2006) The influence of hitchhiking and deleterious mutation upon asexual mutation rates. *Genetics* **173**: 461-472.

Park, H., Berzin, I., De Luis, J., and Vunjak-Novakovic, G. (2005) Evaluation of silicone tubing toxicity using tobacco BY2 culture. *In Vitro Cellular and Developmental Biology. Plant* **41**: 555-560.

Peck, J.R. (1994) A ruby in the rubbish - beneficial mutations, deleterious mutations and the evolution of sex. *Genetics* **137**: 597-606.

Pellmyr, O., and Huth, C.J. (1994) Evolutionary stability of mutualism between yuccas and yucca moths. *Nature* **372**: 257-260.

Pellmyr, O., and Leebens-Mack, J. (1999) Forty million years of mutualism: Evidence for eocene origin of the yucca-yucca moth association. *Proceedings of the National Academy of Sciences of the United States of America* **96**: 9178-9183.

Perfeito, L., Fernandes, L., Mota, C., and Gordo, I. (2007) Adaptive mutations in bacteria: High rate and small effects. *Science* **317**: 813-815.

Picart, P., Bendriaa, L., Daniel, P., Horry, H., Durand, M.J., Jouvanneau, L., and Thouand, G. (2004) New bioreactor for *in situ* simultaneous measurement of bioluminescence and cell density. *Review of Scientific Instruments* **75**: 747-755.

Pooley, D.T., Larsson, J., Jones, G., Rayner-Brandes, M.H., Lloyd, D., Gibson, C., and Stewart, W.R. (2004) Continuous culture of photobacterium. *Biosensors and Bioelectronics* **19**: 1457-1463.

Press, W.H., Teukolsky, S.A., Vetterling, W.T., and Flannery, B.P. (1992) *Numerical recipes in c : The art of scientific computing.* Cambridge: Cambridge University Press.

Rai, A.N., Soderback, E., and Bergman, B. (2000) Cyanobacterium-plant symbioses. *New Phytologist* **147**: 449-481.

Rainey, P.B., and Rainey, K. (2003) Evolution of cooperation and conflict in experimental bacterial populations. *Nature* **425**: 72-74.

Ratkowsky, D.A., Olley, J., McMeekin, T.A., and Ball, A. (1982) Relationship between temperature and growth-rate of bacterial cultures. *Journal of Bacteriology* **149**: 1-5.

Roda, A., Pasini, P., Mirasoli, M., Michelini, E., and Guardigli, M. (2004) Biotechnological applications of bioluminescence and chemiluminescence. *Trends in Biotechnology* **22**: 295-303.

Rouzine, I.M., Wakeley, J., and Coffin, J.M. (2003) The solitary wave of asexual evolution. *Proceedings of the National Academy of Sciences of the United States of America* **100**: 587-592.

Rouzine, I.M., Brunet, E., and Wilke, C.O. (2008) The traveling-wave approach to asexual evolution: Muller's ratchet and speed of adaptation. *Theoretical Population Biology* **73**: 24-46.

Rowan, R., Knowlton, N., Baker, A., and Jara, J. (1997) Landscape ecology of algal symbionts creates variation in episodes of coral bleaching. *Nature* **388**: 265-269.

Sektas, M., Gregorowicz, M., and Szybalski, W. (1999) Transient conversion to $RecA^{+}$ phenotype to permit P1 transduction in any *Escherichia coli recA*$^{-}$ strains. *Biotechniques* **27**: 911-914.

Shaver, A.C., Dombrowski, P.G., Sweeney, J.Y., Treis, T., Zappala, R.M., and Sniegowski, P.D. (2002) Fitness evolution and the rise of mutator alleles in experimental *Escherichia coli* populations. *Genetics* **162**: 557-566.

Shendure, J., Porreca, G.J., Reppas, N.B., Lin, X.X., McCutcheon, J.P., Rosenbaum, A.M., Wang, M.D., Zhang, K., Mitra, R.D., and Church, G.M. (2005) Accurate multiplex polony sequencing of an evolved bacterial genome. *Science* **309**: 1728-1732.

Shou, W.Y., Ram, S., and Vilar, J.M.G. (2007) Synthetic cooperation in engineered yeast populations. *Proceedings of the National Academy of Sciences of the United States of America* **104**: 1877-1882.

Sniegowski, P.D., Gerrish, P.J., and Lenski, R.E. (1997) Evolution of high mutation rates in experimental populations of *E. coli*. *Nature* **387**: 659-661.

Stade, K., Ford, C.S., Guthrie, C., and Weis, K. (1997) Exportin 1 (Crm1p) is an essential nuclear export factor. *Cell* **90**: 1041-1050.

Stams, A.J.M., de Bok, F.A.M., Plugge, C.M., van Eekert, M.H.A., Dolfing, J., and Schraa, G. (2006) Exocellular electron transfer in anaerobic microbial communities. *Environmental Microbiology* **8**: 371-382.

Stewart, E.J., Madden, R., Paul, G., and Taddei, F. (2005) Aging and death in an organism that reproduces by morphologically symmetric division. *PLoS Biology* **3**: 295-300.

Sundin, G.W., and Weigand, M.R. (2007) The microbiology of mutability. *FEMS Microbiology Letters* **277**: 11-20.

Sychrova, H., and Chevallier, M.R. (1993) Cloning and sequencing of the *Saccharomyces cerevisiae* gene LYP1 coding for a lysine-specific permease. *Yeast* **9**: 771-782.

Taddei, F., Radman, M., Maynard-Smith, J., Toupance, B., Gouyon, P., and Godelle, B. (1997) Role of mutator alleles in adaptive evolution. *Nature* **387**: 659-661.

Tanaka, M.M., Bergstrom, C.T., and Levin, B.R. (2003) The evolution of mutator genes in bacterial populations: The roles of environmental change and timing. *Genetics* **164**: 843-854.

Tempest, D.W. (1970) The continuous cultivation of microorganisms. I. Theory of the chemostat. *Methods in Microbiology* **2**: 259-276.

Tenaillon, O., Toupance, B., Le Nagard, H., Taddei, F., and Godelle, B. (1999) Mutators, population size, adaptive landscape and the adaptation of asexual populations of bacteria. *Genetics* **152**: 485-493.

Tenaillon, O., Taddei, F., Radman, M., and Matic, I. (2001) Second-order selection in bacterial evolution: Selection acting on mutation and recombination rates in the course of adaptation. *Research in Microbiology* **152**: 11-16.

Tomlin, G.C., Wixon, J.L., Bolotin-Fukuhara, M., and Oliver, S.G. (2001) A new family of yeast vectors and S288C-derived strains for the systematic analysis of gene function. *Yeast* **18**: 563-575.

Travis, J.M.J., and Travis, E.R. (2002) Mutator dynamics in fluctuating environments. *Proceedings of the Royal Society of London. Series B: Biological Sciences* **269**: 591-597.

Treffers, H.P., Spinelli, V., and Belser, N.O. (1954) A factor (or mutator gene) influencing mutation rates in *Escherichia coli*. *Proceedings of the National Academy of Sciences of the United States of America* **40**: 1064-1071.

Tröbner, W., and Piechocki, R. (1984a) Competition between isogenic *mutS* and *mut*$^{+}$ populations of *Escherichia coli K12* in continuously growing cultures. *Molecular and General Genetics* **198**: 175-176.

Tröbner, W., and Piechocki, R. (1984b) Selection against hypermutability in *Escherichia coli* during long term evolution. *Molecular and General Genetics* **198**: 177-178.

Tröbner, W., and Piechocki, R. (1985) Competition between the dam mutator and the isogenic wild-type of *Escherichia coli*. *Mutation Research* **144**: 145-149.

Tsimring, L.S., Levine, H., and Kessler, D.A. (1996) RNA virus evolution via a fitness-space model. *Physical Review Letters* **76**: 4440-4443.

Wernegreen, J.J. (2002) Genome evolution in bacterial endosymbionts of insects. *Nature Reviews Genetics* **3**: 850-861.

West, S.A., Griffin, A.S., and Gardner, A. (2007) Evolutionary explanations for cooperation. *Current Biology* **17**: R661-R672.

Wick, L.M., Weilenmann, H., and Egli, T. (2002) The apparent clock-like evolution of *Escherichia coli* in glucose-limited chemostats is reproducible at large but not at small population sizes and can be explained with Monod kinetics. *Microbiology* **148**: 2889-2902.

Wilke, C.O. (2004) The speed of adaptation in large asexual populations. *Genetics* **167**: 2045-2053.

Yeiser, B., Pepper, E.D., Goodman, M.F., and Finkel, S.E. (2002) SOS-induced DNA polymerases enhance long-term survival and evolutionary fitness. *Proceedings of the National Academy of Sciences of the United States of America* **99**: 8737-8741.

Yeoh, H.T., Bungay, H.R., and Krieg, N.R. (1968) A microbial interaction involving combined mutualism and inhibition. *Canadian Journal of Microbiology* **14**: 491-492.

Zientz, E., Dandekar, T., and Gross, R. (2004) Metabolic interdependence of obligate intracellular bacteria and their insect hosts. *Microbiology and Molecular Biology Reviews* **68**: 745-770.